

University of New Hampshire
University of New Hampshire Scholars' Repository

Master's Theses and Capstones

Student Scholarship

Spring 2009

The measurement of volatile organic compounds during ICARTT 2004 and experimental studies of chlorine atom reactions with alpha- and beta-pinene

Leif Carsten Nielsen

University of New Hampshire, Durham

Follow this and additional works at: <https://scholars.unh.edu/thesis>

Recommended Citation

Nielsen, Leif Carsten, "The measurement of volatile organic compounds during ICARTT 2004 and experimental studies of chlorine atom reactions with alpha- and beta-pinene" (2009). *Master's Theses and Capstones*. 453.
<https://scholars.unh.edu/thesis/453>

This Thesis is brought to you for free and open access by the Student Scholarship at University of New Hampshire Scholars' Repository. It has been accepted for inclusion in Master's Theses and Capstones by an authorized administrator of University of New Hampshire Scholars' Repository. For more information, please contact nicole.hentz@unh.edu.

THE MEASUREMENT OF VOLATILE ORGANIC COMPOUNDS
DURING ICARTT 2004 AND EXPERIMENTAL STUDIES OF
CHLORINE ATOM REACTIONS WITH α - AND β -PINENE

BY

LEIF CARSTEN NIELSEN

BA, Kalamazoo College, 1996

Thesis

Submitted to the University of New Hampshire

in Partial Fulfillment of

the Requirements for the Degree of

Master of Science

in

Chemistry

May, 2009

UMI Number: 1466945

INFORMATION TO USERS

The quality of this reproduction is dependent upon the quality of the copy submitted. Broken or indistinct print, colored or poor quality illustrations and photographs, print bleed-through, substandard margins, and improper alignment can adversely affect reproduction.

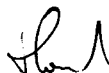
In the unlikely event that the author did not send a complete manuscript and there are missing pages, these will be noted. Also, if unauthorized copyright material had to be removed, a note will indicate the deletion.

UMI[®]

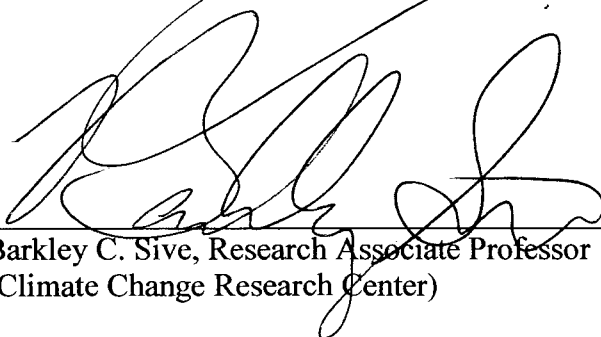
UMI Microform 1466945
Copyright 2009 by ProQuest LLC
All rights reserved. This microform edition is protected against
unauthorized copying under Title 17, United States Code.

ProQuest LLC
789 East Eisenhower Parkway
P.O. Box 1346
Ann Arbor, MI 48106-1346

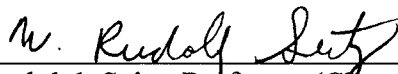
This thesis has been examined and approved.



Thesis Director, Howard R. Mayne, Professor (Chemistry)



Barkley C. Sive, Research Associate Professor
(Climate Change Research Center)



W. Rudolph Seitz, Professor (Chemistry)

Date

May 6, 2009

ACKNOWLEDGEMENTS

During graduate school I have been fortunate to gain the friendship of those whom I deeply respect. My friendship with Jonathan Briggs and Matthew Ronsheim has been, and continues to be, invaluable. The support and friendship of Sean Cleary, Andreas Athans, and Jennifer Terew has helped me far more than they know.

I have always admired the strengths and talents of Melinda Kalainoff, Mikhail Zhukovskiy, Gregory Bubnis, and Ryan Kopreski. In their own unique ways, they have given me a great deal of insight.

Without the support of the department faculty and staff, everything already difficult would have become impossible. I would like to specifically acknowledge the efforts and patience of Cindi Rohwer, Peg Torch, and Robert Constantine, whom have always been helpful, knowledgeable, and kind.

TABLE OF CONTENTS

ACKNOWLEDGEMENTS.....	iii
LIST OF FIGURES.....	viii
LIST OF TABLES.....	x
ABSTRACT.....	xii
CHAPTER 1: OXIDATION OF VOLATILE ORGANIC COMPOUNDS IN NEW ENGLAND.....	1
1.1 Tropospheric VOCs.....	1
1.1.1 Tropospheric Loss Processes.....	2
1.2 Halogenated Compounds in the Troposphere.....	2
1.3 Reactive Tropospheric Chlorine.....	4
1.3.1 Oxidation of VOCs.....	4
1.3.2 Sources of Chlorine Radical.....	5
1.4 Specific Aims.....	7
CHAPTER 2: PROTON TRANSFER REACTION – MASS SPECTROMETRY.....	9
2.1 Introduction.....	9
2.2 Experimental.....	12
2.2.1 Instrument Design and Operation.....	22
2.2.1.1 Proton Transfer Reaction.....	16
2.2.1.2 Cluster Formation and Ion Chemistry.....	20
2.2.1.3 Specificity of PTR-MS.....	22
2.2.2 Calibration and Limits of Detection.....	24
2.2.2.1 Calibrations.....	29

2.2.2.2 Determination of Sensitivity.....	29
2.2.2.3 Detection Limits.....	30
2.2.3 Field Measurement Sites.....	31
2.2.2.1 AIRMAP Continuous Monitoring at Thompson Farm.....	31
2.2.2.1 Appledore Island.....	33
2.3 Results and Discussion.....	34
2.3.1 Correlation between PTR-MS-ss and PTR-MS-hs.....	34
2.3.2 Correlation between Calculation and Calibration.....	35
2.3.3 Comparison to Other Instruments.....	38
2.4 Summary and Conclusions.....	41
2.5 Appendix.....	44
2.5.1 Calibration Standards.....	44

CHAPTER 3: MONITORING OF SELECT VOCS USING PTR-MS DURING ICARTT 2004: AVERAGE DIURNAL PROFILES, LOSS, AND DRY DEPOSITION.....	49
3.1 Introduction.....	49
3.1.2 Specific Aim.....	54
3.2 Experimental.....	55
3.3 Results and Discussion.....	56
3.3.1 Average VOC Mixing Ratios at TF and AI.....	56
3.3.1.1 Methanol.....	57
3.3.1.1 Acetaldehyde.....	57
3.3.1.1 Acetone.....	58
3.3.1.1 MEK.....	59

3.3.1.1 Monoterpenes.....	60
3.3.1.1 Isoprene.....	61
3.3.1.1 MVK+MACR.....	62
3.3.2 Average Diurnal Trends at TF and AI.....	63
3.3.2.1 Biogenic VOCs at TF and AI.....	63
3.3.2.2 VOC Oxidation Products at TF and AI.....	66
3.3.3 Deposition Velocities at TF.....	70
3.3.4 VOC Loss at AI.....	72
3.4 Summary and Conclusions.....	74
CHAPTER 4: OXIDATION OF α - AND β -PINENE BY CHLORINE ATOMS.....	77
4.1 Introduction.....	77
4.1.1 Environmental Chambers.....	77
4.1.2 Chlorine Reactions with Monoterpenes.....	78
4.1.3 Chlorine Reactions with Other Alkenes.....	79
4.1.4 Chlorine Reactions with Aldehydes/Ketones.....	81
4.1.5 Chlorine Reactions with Alkyl Peroxy Radicals.....	82
4.1.6 Specific Aims.....	83
4.2 Experimental.....	84
4.2.1 Chamber.....	84
4.2.2 PTR-MS-ss.....	86
4.2.2.1 Determining Mixing Ratios and Error.....	86
4.3 Results.....	89

4.3.1 Product Identification and Yields for The Cl Initiated Oxidation of α - and β -Pinene.....	89
4.3.1.1 Case 1: 130 ppbv α -pinene + 100 ppbv Cl ₂	89
4.3.1.2 Case 2: 400 ppbv α -pinene + 100 ppbv Cl ₂	91
4.3.1.3 Case 3a: 93 ppbv β -pinene + 100 ppbv Cl ₂	93
4.3.1.4 Case 3b: 80 ppbv β -pinene + 100 ppbv Cl ₂	94
4.4 Discussion.....	96
4.4.1 Comparison to OH/NO Oxidation of α - and β -Pinene.....	96
4.4.2 Chlorine Reaction Rate Coefficients.....	101
4.4.3 Deoxygenation of Peroxy Radicals.....	101
4.4.4 Proposed Chlorine Reaction Mechanisms.....	102
4.4.4.1 Alkyl Peroxy Hydrogen Abstraction Pathways.....	102
4.4.4.2 Criegee Intermediate Reaction Pathways.....	103
4.4.4.3 Proposed Mechanisms Leading to Pinonaldehyde...	103
4.4.4.4 Mechanisms Leading to Acetone and Acetic Acid.....	106
4.4.4.5 Mechanisms Leading to Nopinone.....	108
4.4.4.5 Mechanisms Leading to Acetone (β -Pinene).....	110
4.5 Summary and Conclusions.....	111
4.6 Appendix.....	114
REFERENCES.....	119

LIST OF FIGURES

<u>Number</u>	<u>Page</u>
2.1 PTR-MS components.....	12
2.2 Calibration schematic for PTR-MS.....	26
2.3 Calibration steps for MEK.....	28
2.4 Comparison of acetone mixing ratios between PTR-MS-ss and PTR-MS-hs.....	35
2.5 PTR-MS-hs comparisons to other PTR-MS measurements on AI.....	39
2.6 Toluene comparison by GC-MS and PTR-MS-hs.....	40
2.7 Benzene comparison by GC-MS and PTR-MS-hs.....	41
2.A1 Acetone calibrations for PTR-MS-ss and PTR-MS-hs.....	44
2.A2 Methanol calibrations for PTR-MS-ss and PTR-MS-hs.....	45
2.A3 MEK calibrations for PTR-MS-ss and PTR-MS-hs.....	45
2.A4 Acetaldehyde calibrations for PTR-MS-ss and PTR-MS-hs.....	45
2.A5 MVK+MACR calibrations for PTR-MS-ss and PTR-MS-hs.....	46
2.A6 Isoprene calibrations for PTR-MS-ss and PTR-MS-hs.....	46
2.A7 Monoterpene calibrations for PTR-MS-ss and PTR-MS-hs.....	46
2.A8 Acetonitrile calibrations for PTR-MS-ss and PTR-MS-hs.....	47
2.A9 Toluene calibrations for PTR-MS-ss and PTR-MS-hs.....	47
2.A10 Benzene(1) calibrations for PTR-MS-ss and PTR-MS-hs.....	47
2.A11 Benzene(2) calibrations for PTR-MS-ss and PTR-MS-hs.....	48
3.1 Average mixing ratios of select biogenics.....	65
3.2 Average mixing ratios of select oxygenated compounds.....	67
3.3 Average mixing ratios of acetaldehyde and MEK.....	68

3.8	Wind speed correlations.....	73
4.1	Schematic of environmental chamber.....	85
4.2	Products of Cl oxidation of α -pinene (Case 1).....	90
4.3	Acetic acid and acetaldehyde in the Cl oxidation of α -pinene (Case 1).....	91
4.4	Products of Cl oxidation of α -pinene (Case 2).....	92
4.5	Acetic acid and acetaldehyde in the Cl oxidation of α -pinene (Case 2).....	93
4.6	Products of Cl oxidation of β -pinene (Case 3a).....	94
4.7	Products of Cl oxidation of β -pinene (Case 3b).....	95
4.8	Pinonaldehyde formation via secondary radical.....	104
4.9	Reaction pathways for α -pinene tertiary radical.....	105
4.10	Acetone formation from α -pinene.....	106
4.11	Acetic acid formation from α -pinene.....	107
4.12	Formation of nopinone from β -pinene.....	109
4.13	Acetone formation from β -pinene.....	111
4.A1	Output spectrum for UV source.....	117

LIST OF TABLES

<u>Number</u>	<u>Page</u>
2.1 Ion reactions in the hollow cathode discharge.....	13
2.2 Proton transfer reaction rate constants for select VOCs.....	18
2.3 Sensitivity of PTR-MS-ss and PTR-MS-hs.....	29
2.4 Limits of detection for PTR-MS-ss and PTR-MS-hs.....	30
2.5 Protonated masses measured during ICARTT.....	32
2.6 Correlation between PTR-MS-ss and PTR-MS-hs.....	34
2.7 Comparison between calculation method and calibration.....	36
2.A1 Calibration standard VOCs and instrument parameters.....	44
3.1 Statistics of VOC mixing ratios during ICARTT 2004.....	56
3.2 TF deposition velocities from hourly averaged diurnal profiles.....	70
3.3 TF deposition velocities from sorted hourly average diurnal profiles.....	70
3.4 Comparison of TF deposition velocities.....	72
4.1 LODs calculated for chamber study.....	88
4.2 Molar yields of products from Cl oxidation of monoterpenes.....	96
4.3 Molar yields of products from the OH/NO oxidation of α -pinene.....	98
4.3 Molar yields of products from the OH/NO oxidation of β -pinene.....	99
4.A1 Summary early reactions and rate constants.....	114
4.A2 Summary intermediate reactions and rate constants.....	114

4.A3	Masses and fragments observed.....	115
4.A4	Mixing ratio and rate constant conversions.....	116

CHAPTER 1

OXIDATION OF VOLATILE ORGANIC COMPOUNDS IN NEW ENGLAND

1.1 Tropospheric Volatile Organic Compounds

Tropospheric volatile organic compounds (VOCs) are produced via numerous pathways. Natural processes include emission of these gases from vegetation, livestock, and biomass burning.¹⁻⁴ Industrial complexes, fossil fuel burning, and agricultural practices constitute the major anthropogenic sources.^{5,6} Some gases (such as methanol) may be attributed to both anthropogenic and natural sources.^{7,8} Others are distinct markers for natural processes (*e.g.* monoterpenes from plants)⁹⁻¹² or anthropogenic sources (*e.g.* hexanes from automobiles).¹³⁻¹⁵

Anthropogenic VOCs are emitted from industry, various modes of transportation, and agricultural practices. These emissions occur primarily in the industrialized northern hemisphere, with the main source of pollutants being incomplete combustion from automobile exhaust.¹⁶ Anthropogenic pollutant emissions encompass a huge class of compounds including, but not limited to: alcohols, alkanes, aromatics, esters, ethers, peroxides, acids, halocarbons, and aldehydes.¹⁶ Besides being reactive, many of these compounds (*e.g.* benzene) cause human health problems.¹⁷

1.1.1 Tropospheric Loss Processes

The atmospheric lifetime of a VOC is determined by its chemical reaction, primarily with atmospheric oxidants, its photolysis rate, and how quickly it deposits to the Earth's surface (both solid and liquid) and to water in the atmosphere.¹⁸ The physical removal process of gases to the surface, dry deposition, of longer lived VOCs is introduced and discussed in Chapter 3. For gas phase chemical transformations, hydroxyl radical is considered to be the primary daytime oxidant, although halogen compounds also contribute to tropospheric oxidation of VOCs. Other oxidants include ozone, and night-time gas phase chemistry is dominated by the nitrate radical.

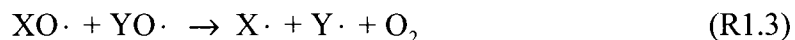
1.2 Halogenated Compounds in the Troposphere

Halogen chemistry was suspected in the unexpected ozone depletion in the polar regions at the surface.^{19,20} Of the numerous sources of halogenated compounds, the relevant emission sources are derived from both marine and continental sources. According to Khalil et al.,²¹ reactive chlorinated gases are generally described as gases that have lifetimes of less than 2 years. Cox et al.²² note that hydrogen containing chlorohydrocarbons are moderately reactive in the troposphere with lifetimes less than one year.

The most abundant halogenated compound in the atmosphere is the organohalogen CH_3Cl with an average mixing ratio of ~600 pptv in the northern hemisphere.²³ Organohalogenes are those molecules that have a halogen bound to at least one carbon atom. Besides organohalogenes, inorganic sources of halogens in the

atmosphere include compounds like HCl, HOCl, ClONO₂, ClO, and corresponding brominated and iodinated compounds.²⁴ Recent studies have indicated that halogens and their various oxides are important tropospheric trace gases, specifically in the Arctic regions and coastal areas.²⁵ In these areas of higher organohalogen and inorganic halogen loadings, significant impacts on ozone regulation and aerosol formation have been observed.^{24,26-35} The most important reactions for the formation of chlorine radical and its subsequent chemistry are discussed in Section 1.3.2.

In non-polluted areas in the troposphere, halogens have been shown to participate in ozone destruction.³⁶ The cycle for ozone destruction (particularly by reactive bromine and iodine) in the marine boundary layer (MBL) has been proposed to consist of at least two cycles.³⁷⁻³⁹ Cycle 1 is the formation of a halogen oxide and O₂ from the reaction of a halogen radical with ozone,



where X and Y may be the same or different halogens.

Halogens participate in dual roles in ozone regulation. Levels of halogen oxide between 20 and 30 pptv have been shown to decrease ozone concentrations in the troposphere significantly.⁴⁰ While this decrease in tropospheric ozone is pertinent in areas with small amounts of NO_x (less than 20 pptv) and VOCs, it has been shown that urban polluted areas show a net increase in ozone because of chlorine radical chemistry.⁴¹⁻⁴⁷

Formation of ozone in these areas is initiated by photolysis of photochemically labile chlorine compounds (*e.g.* Cl₂ and HOCl) and subsequent reactions.



As seen in (R1.7), chlorine abstraction results in formation of alkyl radical, similar to what is observed in OH radical chemistry.

Halogen radicals are strong oxidants, with rate constants generally 1-2 orders of magnitude greater than hydroxyl radical.⁴⁸ This oxidizing potential may be important in coastal regions, where strong terrestrial sources of VOCs mix with reactive halogen compounds.⁴¹⁻⁴³ One important class of halogenated compounds is reactive chlorine containing compounds.

1.3 Reactive Tropospheric Chlorine

1.3.1 Oxidation of VOCs

Recently it has been shown that chlorine atom concentrations in the Northeast are relatively large in the early morning hours ($2-6 \times 10^4$ molecules cm⁻³)⁴⁶ and may be competitive to hydroxyl radical oxidation chemistry. This is consistent with other studies that estimate the Cl atom concentration between 10^3-10^5 molecules cm⁻³.^{49,50} A recent modeling study by Pechtl et al.⁵¹ concluded that noon-time concentrations of Cl radical were $\sim 10^5$ molecules cm⁻³ for polluted air masses, and $\sim 10^4$ for clean air masses. High

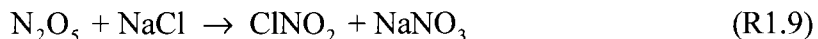
chlorine radical concentrations suggest that chlorine atoms contribute significantly to oxidation of VOCs in polluted or marine atmospheres.

1.3.2 Sources of Chlorine Radical

The source of chlorine radical is photolysis of chlorine containing compounds in the troposphere, either continental or marine derived. The dominant source of marine derived chlorine containing compounds is sea salt.⁵² The availability of sea salt to participate in heterogeneous chemistry is derived specifically from wave breaking processes that emit sea salt aerosol into the marine boundary layer. This is a continuing area of research and has been reviewed by Finlayson-Pitts.⁵³ Proposed pathways particularly important in polluted coastal areas are the reaction of nitrogen dioxide with sea salt to form nitrosyl chloride,



or the reaction of nitrogen pentoxide with sea salt to form nitryl chloride



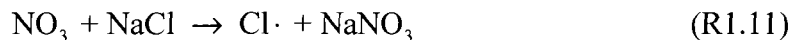
where both nitrosyl chloride and nitryl chloride are photolyzed to release chlorine atoms.

Besides being photolyzed, ClNO_2 may also be available for nighttime reactions with sea salt⁵⁴

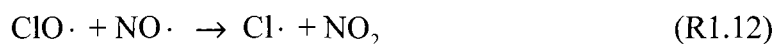


to form molecular chlorine which would be photolyzed in the daylight.

Another nighttime reaction in polluted areas is reaction of NO_3 with sea salt to form sodium nitrate and chlorine radical,



Photolysis of XO (R1.1) is a source of Br and I atoms but is of minor importance for generation of chlorine atoms.²⁵ However, in polluted areas, reaction of nitric oxide with chlorine oxide is another source of chlorine atoms via the reaction,

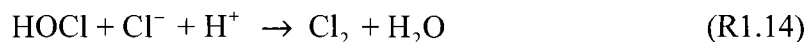


In highly polluted regions, atmospheric acids (*e.g.* HNO₃, H₂SO₄) are thought to displace the chloride ions of sea salt aerosols and partition to gas phase HCl.⁵⁵ Chlorine atoms may be subsequently formed by reaction of hydrochloric acid with hydroxyl radical via the relatively slow reaction³³

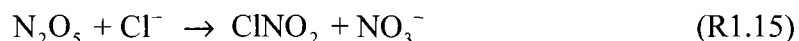


but may contribute significantly to chlorine atom concentrations over the MBL.⁵¹

Sea salt is emitted to the marine boundary layer primarily in aerosol form. This complicates the understanding of sea salt reactions listed above by having to account for aqueous-phase chemistry.^{53,56,57} Currently, the understanding is that compounds like HOCl may be taken up by sea salt aerosol to form molecular chlorine through the reaction^{53,58,59}



And at nighttime, reaction between N₂O₅ and chloride ion may form nitryl chloride,



which may again be photolyzed to form chlorine atom in the daylight hours. Therefore, reactions of aqueous salt solutions have an impact on the oxidizing capacity of the troposphere.

1.4 Specific Aims

This work focuses on quantifying VOCs using PTR-MS to gain a better understanding of physical and chemical processes in the troposphere. Specifically, insight into the transport and transformation of these molecules is gained. VOCs covered in this work are the broad class of alkenes and oxygenated compounds produced from biogenic and anthropogenic sources. The ultimate fate of these molecules, via photochemical oxidation and physical processes, is covered.

Detection of VOCs via PTR-MS is discussed in Chapter 2. Issues of detection limits, calibrations, interferences, and intercomparisons with other methods and other PTR-MS measurements are covered.

Chapter 3 covers diurnal trends and deposition processes observed during ICARTT at two locations in the Northeast. The focus is on nighttime deposition of longer lived oxygenated volatile organic compounds, and how these deposition measurements compare with other published data. It further emphasizes the distinct difference in air masses observed in a rural continental site, and a remote marine site off the coast of New England.

Oxidation of α - and β - pinene by chlorine atoms is discussed in Chapter 4. Unique chlorine atom oxidation products may be used as markers to identify when this

chemistry occurs. To investigate oxidation products, environmental chamber studies were performed and oxidation products were identified by PTR-MS. These products are compared to OH/NO oxidation mechanisms, kinetics, and products.

CHAPTER 2

PROTON TRANSFER REACTION – MASS SPECTROMETRY

2.1 Introduction

Quantification of VOCs in the atmosphere has largely been done using gas chromatographic (GC) methods often coupled with mass spectrometry (MS). Such methods offer benefits of detection limits at the sub-pptv level and an ability to distinguish between hundreds of different compounds. In general, GC measurements require several minutes for sampling or rely on collection of canister samples which are analyzed later in the laboratory. Often, large dewars of cryogenics are also necessary, although cryogen free instrumentation has recently been developed.⁶⁰ For canister samples, reliability of measurements is largely dependent upon the stability of the VOC between collection time and analysis. Fairly recent development⁶¹⁻⁶³ and availability of proton transfer reaction-mass spectrometers (PTR-MS) has allowed for measurement of VOCs with high time resolution and offers other operational benefits.^{61,63} The proton transfer reaction is a soft (non-dissociative) ionization method, whereby a proton is transferred to an analyte (*i.e.* VOC) allowing for detection of parent ions with little fragmentation. While other trace gas detection methods require substantial processing of air prior to analysis, PTR-MS air is continuously sampled directly from the pumping stream and directed into the reaction chamber without constituent modification (pre-treatment of samples). This eliminates the necessity for cylinders of buffer gases,

allowing for direct transport of atmospheric trace gases directly into the instrument. While PTR-MS does not resolve as many compounds as GC methods, it does allow a very high time resolution (seconds) and detection limits on the order of tens of pptv. Additional components are generally few, making the operational PTR-MS both compact and portable.

Because of these advantages, PTR-MS has seen extensive use in atmospheric field deployments, quantifying atmospheric trace gases in rural, remote, and urban environments. Because of high time resolution, PTR-MS has been successfully implemented for eddy covariance studies⁶⁴⁻⁶⁸ and on platforms including aircraft⁶⁹⁻⁷² and vehicles.^{73,74} Laboratory studies using PTR-MS include the measurement of products from oxidation of VOCs.⁷⁵⁻⁷⁷ More recently, efforts have been made to detail performance characteristics of the instrument and validate VOC measurements.⁷⁸⁻⁸² Detailed comparisons between PTR-MS and other techniques have shown that PTR-MS measurement and quantification of VOCs is generally in excellent agreement with the more established methods.^{78,83,84}

PTR-MS signals are converted to mixing ratios by two different methods. When available, calibration standards may be used to generate instrument response curves at different VOC mixing ratios. This method is dependent upon the stability, quality, and components of the gas standard while also being dependent on stability of the instrument response over time. If no calibration standards are available, PTR-MS signals may be converted to mixing ratios by equations relating gas kinetic parameters and operational settings of the instrument. Since PTR-MS distinguishes components solely based on

mass, isobaric and isomeric interferences may cause overestimations in mixing ratios of a VOC assigned to a particular mass. Studies have made progress in understanding and quantifying these interferences.^{64,79,85} Since calibration standards are not always available, the calculation method is a useful tool for quantifying VOC mixing ratios for those cases.

This chapter intends to cover the methods used to determine atmospheric mixing ratios of VOCs using PTR-MS. Integral to the methods are measurement and processing of signal data, calculation of mixing ratios, and calibration procedures. As PTR-MS is a mass spectrometric method, mass specificity is discussed. Details about the ion chemistry involved are covered as they are necessary for the quantification of VOCs. Calibrations, operating parameters, sensitivities and limits of detection are presented for a high sensitivity PTR-MS and a standard sensitivity PTR-MS. These two instruments were used during the International Consortium for Atmospheric Research on Transport and Transformation (ICARTT) to quantify a suite of VOCs at two locations in New England. VOC mixing ratios from the same sampled air are compared for the two instruments and physical differences between them are also addressed. Further, this chapter shows comparisons between the two different methods of determining mixing ratios in PTR-MS, and gives operational parameters at two field sites in New England. Data gleaned from the ICARTT 2004 field study are compared to GC measurements and other PTR-MS measurements.

2.2 Experimental

2.2.1 Instrument Design and Operation

While PTR-MS methodology and has been detailed elsewhere,⁶¹ important aspects of PTR-MS operation pertinent to this research are covered here. Components of a PTR-MS include a hollow cathode discharge, short drift tube (or source drift region), drift tube, and mass analyzer (Figure 2.1).

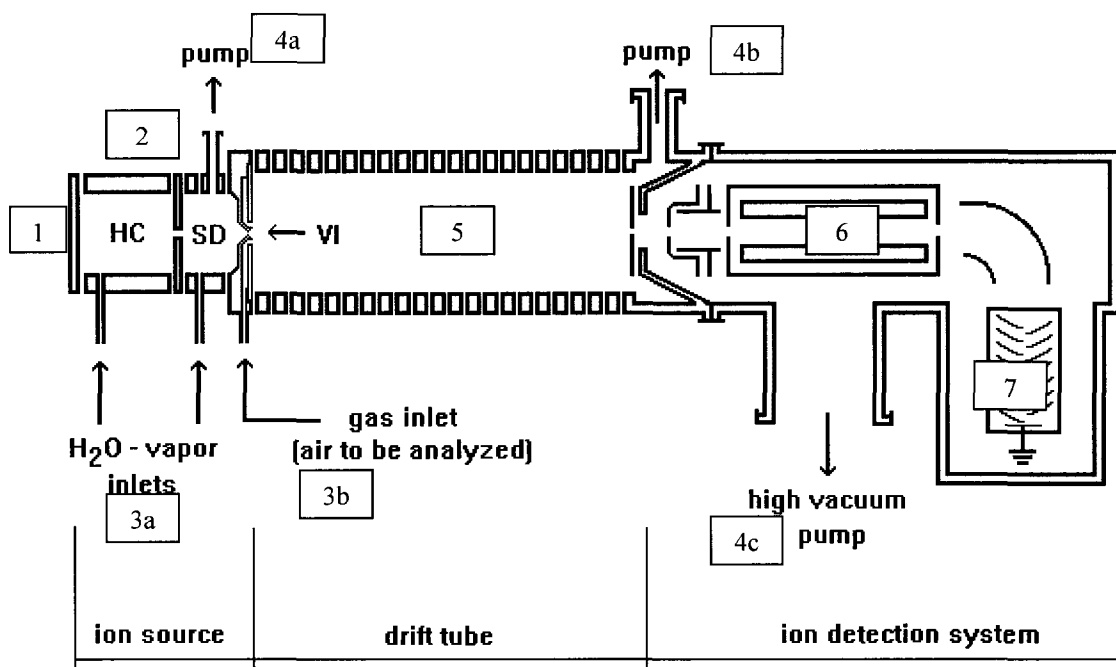


Figure 2.1: PTR-MS components^{61,86,87} 1: hollow cathode discharge (HC), 2: short drift tube, or source drift region, (SD), a Venturi-type inlet (VI), 3a: water vapor inlet, 3b: ambient air inlet, 4a-c: turbo molecular pumps, 5: drift tube, 6: mass analyzer (quadrupole), 7: ion detection and amplification (secondary electron multiplier).

The ambient air inlet (Figure 2.1, 1b) to the PTR-MS consists of 45 °C heated 1/8" Teflon tubing. This inlet to the drift tube sub-samples (~11 sccm) from the PTR-MS

adjustable air inlet (50-500 sccm) and is pumped by a Vacuubrand (MD4 or MZ2) membrane pump. Tubing is heated to limit adsorption of VOCs to tubing walls.

PTR-MS uses a cylindrical cathode (or hollow cathode) as the ion source. Hydronium ions (H_3O^+) are produced in large concentrations and purities (up to 99.5%)⁶¹ from the discharge of 6-11 standard cubic centimeters (sccm) of water vapor (Figure 2.1, 3a) from a stainless steel canister of water connected to the discharge (Figure 2.1, 1). Areas of the discharge include the low field region of the cathode (negative glow), which has a high density of electrons, followed by the cathode fall region, where electrons are accelerated and ionize water. Discharge voltages and current can be changed to increase hydronium ion concentrations, but are typically kept at 600 volts and 8 mA to minimize formation of reactive impurity ions of O_2^+ and NO^+ .⁸⁴ Products from the discharge react with water both in the hollow cathode and source drift region (Figure 2.1, 2) to produce H_3O^+ ions via reactions shown in Table 2.1. Rate constants are included to emphasize the efficiency of hydronium ion formation via use of a hollow cathode discharge.

Table 2.1: Ion reactions with water in the hollow cathode discharge and source drift region of PTR-MS for ultimate formation of hydronium ion⁶²

<u>Reaction</u>	<u>Rate Constant ($\times 10^{-9} \text{ cm}^3 \text{ s}^{-1}$)</u>
$\text{H}_2\text{O} + \text{O}^+ \rightarrow \text{H}_2\text{O}^+ + \text{O}$	2.6
$\text{H}_2\text{O} + \text{H}^+ \rightarrow \text{H}_2\text{O}^+ + \text{H}$	8.2
$\text{H}_2\text{O} + \text{OH}^+ \rightarrow \text{H}_2\text{O}^+ + \text{OH}$	1.8
$\text{H}_2\text{O} + \text{OH}^+ \rightarrow \text{H}_3\text{O}^+ + \text{O}$	1.3
$\text{H}_2\text{O} + \text{H}_2^+ \rightarrow \text{H}_3\text{O}^+ + \text{H}$	3.4
$\text{H}_2\text{O} + \text{H}_2^+ \rightarrow \text{H}_2\text{O}^+ + \text{H}_2$	3.7
$\text{H}_2\text{O} + \text{H}_2\text{O}^+ \rightarrow \text{H}_3\text{O}^+ + \text{OH}$	1.8

A constant discharge current above 5 mA assures high conversion to the hydronium ion in excess of VOC in the drift tube. High purity H_3O^+ created from the

discharge excludes the need for any sort of mass filter to preselect the hydronium ion prior to entering the drift tube. Count rates of H_3O^+ produced from the discharge ($\sim 10^6$ - 10^8 counts s^{-1}) are monitored and are many (>3) orders of magnitude greater than the trace gas counts.

Potential impurities from the ion source include O_2^+ and NO^+ which may arise from gas effusing from the drift region to the discharge. Both O_2^+ and NO^+ may undergo charge transfer reactions with VOCs. These charge transfer reactions can result in significantly more fragmentation than what is observed with proton transfer from H_3O^+ . Further, the molecules O_2^+ and NO^+ can react with alkanes, causing potential interference in mass spectral identification.⁸⁸ Positively charged oxygen is monitored, and is typically between 1-3% of the positively charged signal in the drift tube (mainly consisting of hydronium ion). Formation of these impurities is minimized by incorporation of a Venturi-type inlet (Figure 2.1, VI) which minimizes the back streaming of air from the drift tube (Figure 2.1, 5) and serves as the ambient air inlet for the drift tube.

The drift tube consists of electrically isolated sections connected to resistors in order to maintain a homogeneous electric field and serves the purpose of accelerating ions to the detection region while also limiting cluster formation. This region of the PTR-MS is kept at a pressure of 2.00(2) mbar and 600(5) volts and protons from the hydronium ion are transferred to the analyte (*i.e.* VOCs). The gases in the drift tube (including buffer gas, water, hydronium ion, VOCs, and protonated compounds) pass through ion lenses where they are focused. Charged products are mass selected at the

quadrupole (QuadStar 422) (Figure 2.1, 6) and are detected by a secondary electron multiplier (Pfeiffer SEV 217) (Figure 2.1, 7).

The quadrupole employed in both instruments has an operational range of m/z 1-512. The instruments discussed in this chapter were typically run in the multiple ion detect mode (MID), and occasionally in the scan bar-graph mode. In both of these modes, the user can specify the cycle time and resolution. In the MID mode (or peak picking mode), the user creates a file that specifies the masses to be monitored, and dwell times for each mass may be varied to give the best signal to noise ratio (S/N). VOCs that typically have larger atmospheric mixing ratios (*e.g.* acetone) are set to shorter dwell times than compounds with lower atmospheric mixing ratios (*e.g.* benzene). As one objective of research using PTR-MS is to generate data with a high time resolution and as the PTR-MS measures over twenty different atmospheric compounds, choice of appropriate dwell times is an important consideration for field experiments.

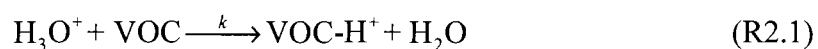
In the scan bar-graph mode, the instrument records all signals between two specified masses (*e.g.* 21-200 amu) at the user specified resolution (*e.g.* 1 amu) at a user specified time for the complete cycle. Individual mass dwell times cannot be changed in this operating mode, only the total cycle time and resolution. This particular method is used as a probe to determine which masses are present in a given air sample and was used only in our laboratory chamber work.

Different configurations of PTR-MS are available from Ionicon. This work uses the commercially available high sensitivity (PTR-MS-hs) and standard sensitivity (PTR-MS-ss) instruments (Ionicon Analytik GmbH, Innsbruck, Austria). PTR-MS-ss is

equipped with one turbo molecular pump for each pumping regime: the source drift region (Figure 2.1, 4a) and quadrupole (Figure 2.1, 4c). PTR-MS-hs has an additional turbo molecular pump (Figure 2.1, 4b) for the added differential pumping region for enhanced detection limits, as per the specifications from Ionicon, from ~30 pptv (PTR-MS-ss) to ~5 pptv (PTR-MS-hs).⁸⁹ However, as will be shown in Section 2.2.2.3, limits of detection are dependent on mass and background signal of the instrument. Since this work, the Sive group has upgraded PTR-MS-ss to a high sensitivity instrument from an upgrade kit available from Ionicon.

2.2.1.1 Proton Transfer Reaction.

Absolute mixing ratios without calibration standards can be determined through calculations based on proton transfer reactions in a buffer gas. In the case of analyzing ambient air samples containing VOCs, the buffer gas is 78% N₂ and 21% O₂, and the reactants in the drift tube are hydronium ion (H₃O⁺) and the VOCs. If the VOC of interest has a larger proton affinity than water, the proton transfer reaction is exothermic



and the rate of reaction is governed by the proton transfer reaction rate constant, k , and the concentration of hydronium ion and the VOC. Proton affinities for a large selection of molecules have been compiled elsewhere.⁹⁰

Rate of decay of the VOC may be determined by

$$-\frac{d[\text{VOC}]}{dt} = k[\text{VOC}][\text{H}_3\text{O}^+] \quad (2.1)$$

As the number density of hydronium ions in the drift tube is large compared to reactive molecules in the drift tube, hydronium ions are not significantly depleted by reactions in this region. The number density of hydronium ions at any time is assumed to be the same with or without reactive molecules present and to be much greater than the number density of VOC.

$$[\text{H}_3\text{O}^+]_0 \gg [\text{VOC}] \quad (2.2)$$

$$[\text{H}_3\text{O}^+] = [\text{H}_3\text{O}^+]_0 \quad (2.3)$$

Assumptions made in (2.2) and (2.3) allow the reaction to be treated as pseudo-first order. Following from (2.1), (2.2), and (2.3), VOC concentration may be calculated by

$$[\text{VOC}] = [\text{VOC}]_0 e^{-k[\text{H}_3\text{O}^+]_0 t} \quad (2.4)$$

Concentration of the protonated molecule $[\text{VOC-H}^+]$ can be related to $[\text{VOC}]$ by the equation

$$[\text{VOC-H}^+]_t = [\text{VOC}]_0 - [\text{VOC}]_t \quad (2.5)$$

The protonated VOC concentration is then related to the initial VOC concentration, hydronium ion concentration, the proton transfer reaction rate constant, and time (t) in the drift tube through the equation

$$[\text{VOC-H}^+]_t = [\text{VOC}]_0 (1 - e^{-k[\text{H}_3\text{O}^+]_0 t}) \approx [\text{VOC}]_0 [\text{H}_3\text{O}^+]_0 kt \quad (2.6)$$

As ion signals for both hydronium ion and VOC are proportional to their concentrations, the ultimate concentration of the VOC is determined by k , t , and the ratio of signals of hydronium ion and the protonated VOC. Because not all of the charged

compounds are detected, ratios of detected signals are used instead of absolute concentrations

$$[\text{VOC}] \approx \frac{i(\text{VOC-H}^+)}{i(\text{H}_3\text{O}^+)kt} \quad (2.7)$$

and may be used to calculate the concentration of VOC assuming that there is proportional detection efficiency for both $i(\text{VOC-H}^+)$ and $i(\text{H}_3\text{O}^+)$ and the proton transfer rate constants are known.

In the case of proton transfer, if a VOC has a large enough proton affinity to accept a proton, the rate constant may be approximated using the ion-molecule rate constant. This ion-molecule rate constant may be calculated for ions reacting with polar or non-polar molecules.⁹¹ A list of proton transfer reaction rate constants for select VOCs are shown in Table 2.2.⁹² These values generally have an associated error of ~20%.^{62,93}

Table 2.2: Proton transfer reaction rate constants for select VOCs

<u>Compound</u>	<u>Formula</u>	<u>$k_c (\times 10^{-9} \text{ cm}^3 \text{ s}^{-1})$</u>
methanol	CH ₃ OH	2.33
ethanol	C ₂ H ₅ OH	2.26
formaldehyde	CH ₂ O	2.92
acetaldehyde	C ₂ H ₄ O	3.36
acetone	C ₃ H ₆ O	3.00
methyl ethyl ketone (MEK)	C ₄ H ₈ O	3.48
isoprene	C ₅ H ₈	1.94
methyl vinyl ketone (MVK)	C ₄ H ₆ O	3.83
methacrolein (MACR)	C ₄ H ₆ O	3.55
α-pinene	C ₁₀ H ₁₆	2.44
β-pinene	C ₁₀ H ₁₆	2.50
d-limonene	C ₁₀ H ₁₆	2.54
acetonitrile	C ₂ H ₃ N	4.74
benzene	C ₆ H ₆	1.97
toluene	C ₇ H ₈	2.12
m-xylene	C ₈ H ₁₀	2.26
o-xylene	C ₈ H ₁₀	2.32
p-xylene	C ₈ H ₁₀	2.27

<u>Compound</u>	<u>Formula</u>	<u>$k_c (\times 10^{-9} \text{ cm}^3 \text{ s}^{-1})$</u>
ethylbenzene	C_8H_{10}	2.25
1,2,3 trimethylbenzene	C_9H_{12}	2.47
1,2,4 trimethylbenzene	C_9H_{12}	2.40
1,3,5 trimethylbenzene	C_9H_{12}	2.40
isopropylbenzene	C_9H_{12}	2.54
Dimethyl sulfide (DMS)	$\text{C}_2\text{H}_6\text{S}$	2.53
acetic acid	$\text{C}_2\text{H}_4\text{O}_2$	2.27

In determining VOC mixing ratios, (2.7) also assumes that all molecules are detected with the same efficiency, which is not the case in PTR-MS. Recently, Keck et al.⁹⁴ have included corrections accounting for ionic mobility of different protonated compounds. Protonated VOCs may be much larger, and thereby have smaller ion mobilities than hydronium ion.⁹⁴

Besides accounting for ionic mobility, the assumption in (2.7) is that detection efficiency for all charged molecules are equivalent. Further, it also assumes no loss of molecules moving from the drift tube to the quadrupole, and 100% transport efficiency of molecules through the quadrupole. All of these assumptions are usually lumped into the term ‘transmission’, and this effective transmission may be measured to correct for mass dependent losses. Determining transmission is typically done by introducing a large enough concentration of a specific gas such that a decrease in the hydronium ion signal is observed. This ratio is then incorporated into (2.7) to give the transmission corrected equation as

$$[\text{VOC}] \approx \frac{i(\text{VOC-H}^+) Tr_{\text{H}_3\text{O}^+}}{i(\text{H}_3\text{O}^+)kt Tr_{\text{VOC-H}^+}} \quad (2.8)$$

where Tr is the transmission factor for either hydronium ion or the protonated VOC.

Calculation of absolute mixing ratios is further dependent upon the time two reactive molecules (hydronium ion and VOC) have to react in the drift tube (2.8). Reaction time may either be measured directly by pulsing the source and measuring arrival time at the detector or by calculating the drift velocity from ionic mobility. Drift velocity (v) is

$$v = \mu \times E \quad (2.9)$$

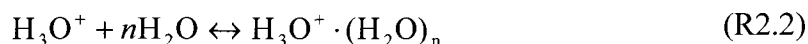
where μ is ionic mobility ($\text{cm}^2 \text{V}^{-1} \text{s}^{-1}$) and E is the electric field (V cm^{-1}), where ionic mobility is the average velocity at which an ion moves under the influence of a field of 1 V cm^{-1} . This drift velocity is proportional to the ratio of the electrostatic field strength to the number density of neutrals (E/N).^{85,95,96}

Although proton transfer from hydronium ion to VOC is the primary reaction in the drift tube there are other possible mechanisms for formation of protonated VOCs not accounted for in (2.8). These mechanisms generally involve proton transfer from cluster ions formed in the drift tube.

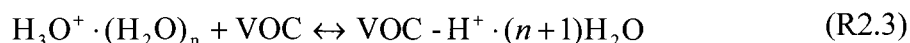
2.2.1.2 Cluster Formation and Ion Chemistry.

Typical clusters observed in the drift tube include $\text{H}_3\text{O}^+(\text{H}_2\text{O})_n$, where $n = 1, 2, 3$. These clusters are capable of undergoing proton transfer reactions with VOCs with large proton affinities at a rate similar to that of the proton transfer from H_3O^+ itself. For molecules with small polarities and small proton affinities, there is a competition in the proton transfer to $(\text{H}_2\text{O})_2$.⁹⁷ Clusters are monitored during operation of the PTR-MS with orders of magnitude smaller signals than H_3O^+ ion under standard operating conditions.

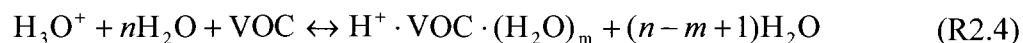
As hydronium ions and water vapor (from ambient air humidity) enter the drift tube region of the PTR-MS, clusters may form from the reversible reaction⁸⁴



The cluster observed in largest abundance in PTR-MS under normal operating conditions is typically $\text{H}_3\text{O}^+ \cdot (\text{H}_2\text{O})$, but cluster $\text{H}_3\text{O}^+ \cdot (\text{H}_2\text{O})_2$ is also present. Water clusters may interact with the VOC, transferring a proton through the reaction⁸⁴



Transfer of a proton from the water cluster to the VOC is more selective than transfer from hydronium ion due to larger proton affinity of the water cluster.⁸⁴ Compounds with small proton affinities (only slightly larger than water) will not react with the water cluster. It has been reported⁹⁷ that compounds that are nonpolar (*e.g.* benzene) or have small polarity (*e.g.* toluene) react with both hydronium ion and hydronium ion clusters. This dependence on humidity for detection of both benzene and toluene has been investigated.⁹⁷ Besides cluster formation of hydronium ions with water, clusters may form with the VOC through the reaction⁸⁴



Cluster formation with the VOC will result in an underestimation of the final mixing ratio of the VOC, especially for molecules with a large dipole moment. These cluster concentrations may be decreased by increasing kinetic energy of the reagent ions by increasing drift tube voltage. This however yields protonated ions with larger kinetic

energies, which in turn results in an increase in the fragmentation of those protonated ions. de Gouw et al.⁸⁴ have shown that when E/N is greater than 120 Td, H_3O^+ ions are the dominant signal. As drift tube voltage is decreased, larger fractions of clusters are present, with the largest fraction (80%) being $\text{H}_3\text{O}^+(\text{H}_2\text{O})$ at 500 V and E/N \sim 90. As drift tube voltage is decreased to below 350 V, the $\text{H}_3\text{O}^+(\text{H}_2\text{O})_2$ is the dominant signal (60%).

Throughout all field and laboratory studies, four masses (21, 37, 55, and 32) were monitored for calculation and diagnostic purposes. Masses 21, 37, 55, and 32 correspond to $\text{H}_3^{18}\text{O}^+$, $\text{H}_3\text{O}^+(\text{H}_2\text{O})$, $\text{H}_3\text{O}^+(\text{H}_2\text{O})_2$, and O_2^+ respectively. Mass 21 was used for the normalization of the signal from the VOC or for estimation of mixing ratios (2.8). Clusters and charged oxygen were monitored because these compounds may also react with monitored VOCs. The signal for the first hydronium ion cluster was typically less than 1% of the primary ion signal, and charged oxygen was constantly monitored and drift tube voltages were modified to keep this signal less than 3%. Dwell times for these masses were short (0.1 second, 20ms, 20ms, and 20ms respectively). Because of the large signal from the high number density of hydronium ion, a short dwell time for $\text{H}_3^{18}\text{O}^+$ was employed to preserve the secondary electron multiplier (SEM). The signal for $\text{H}_3^{18}\text{O}^+$ was multiplied by 489 to give the true H_3O^+ signal as the stable isotope ^{16}O comprises 99.7587% of the oxygen, and the abundance of the stable isotope ^{18}O is 0.2039%.

2.2.1.3 Specificity of PTR-MS.

Although the proton transfer reaction is a soft chemical ionization, fragmentation of some molecules does occur. Fragmentation to daughter ions is significant in at least a few VOCs commonly monitored by PTR-MS.

First, in the class of monoterpenes (*e.g.* α -pinene, β -pinene), a protonated parent ion signal ($C_{10}H_{16}H^+$) is observed at 137 amu. A correlated signal at mass 81 ($C_6H_8H^+$) represents a fragmentation of the parent ion. Over 99% of the monoterpene signal is observed at these two masses,^{98,99} but there is some evidence that mass 57 ($C_4H_8H^+$) is also correlated with monoterpenes.⁸¹ de Gouw et al.⁸¹ suggested that the signal at mass 57 was potentially due to butanes and methyl tertiary butyl ether (MTBE), but that the combined mixing ratio was too low to explain the PTR-MS signal.

Tani et al.⁹⁹ showed that, besides mass 81, other ions are produced from the fragmentation of the monoterpene molecular ion peak. In that study, α - and β -pinene, limonene, and 3-carene standards were used to determine fragmentation patterns with varied E/N drift tube conditions. Other masses due to fragmentation were 67 and 95 amu for α - and β -pinene and 3-carene, but the total contribution of these two masses was less than 2% of the total ion signal. In the case of limonene, mass 95 contributed to 5% of the total ion signal. The molecular ion peak at 137 amu was 43-49% of the total ion signal for α - and β -pinene and limonene. 3-carene had a total contribution of 57% at mass 137.

Another common fragmentation observed in PTR-MS is acetic acid (mass 61) fragmenting to acylium ion (CH_3CO^+ , mass 43) and water.¹⁰⁰

The major limitation in PTR-MS is the inability of the instrument to distinguish between molecules of the same mass (either isobars or isomers). Isobaric tropospheric compounds measured by PTR-MS have been recently summarized by de Gouw et al.⁸⁴ Interferences occur at 43 amu which may be attributed to acylium ion (from the

fragmentation shown above), propanol, fragments of peroxyacetyl nitrate (PAN), or hydrocarbons.

MVK and MACR are isomers observed at 71 amu. As these two molecules are the major oxidation products of isoprene, and no other interferences are observed at mass 71, they are reported as a sum. The oxidative precursor to MVK and MACR, isoprene, shows a some atmospheric interferences at mass 69. Potential interfering compounds include 2-methyl-butanal, 3-methyl butanal, and 1-penten-3-ol.^{101,102} Other interferences include furan from biomass burning and 2-methyl-3-buten-2-ol from vegetation.^{100,103}

On the other hand there are few atmospheric interferences in the measurement of acetone, methanol, and acetaldehyde. In the ambient measurement of acetone, potential interferences from propanal are small (<10%).⁷⁸ Interferences in the measurement of MEK include butanal, and the $\text{H}_3\text{O}^+(\text{H}_2\text{O})_3$ cluster which is dependent on humidity.⁸⁴ No significant interferences for detection of acetonitrile are observed. Although alkanes may react with positively charged oxygen to cause isobaric and isomeric interferences, the sensitivity of PTR-MS to these compounds is small, and the positively charged oxygen signal in the instrument is also small.⁷⁸

2.2.2 Calibration and Limits of Detection

2.2.2.1 Calibrations.

Use of calibration gases is a more accurate way of determining instrument response to different mixing ratios of atmospheric compounds than the calculation method. Furthermore, it allows for quantification of VOC mixing ratios without needing to account for fragmentation.

Three different high pressure cylinders (Apel-Reimer Environmental, Inc., Denver, CO) containing synthetic blends of non-methane hydrocarbons (NMHCs) and oxygenated VOCs (OVOCs) in the ppbv range were used for calibrations. Contents and mixing ratios of gases used from these standards are given in the Appendix (Table 2.A1). Using volume dilution methods, gas standards were diluted to atmospheric mixing ratios (ppbv to pptv levels) with whole air passed through a catalytic converter (0.5% Pd on alumina at 450 °C) to scrub all VOCs and maintain the same humidity as the sampled air. A schematic of the setup for the calibration of the PTR-MS is shown in Figure 2.2. Flow from the calibration cylinder was typically controlled by a 50 or 20 sccm Mass Flo[®] controller (MKS Instruments, Andover, MA). Catalytically converted air was controlled by a needle valve with a downstream 2000 sccm Mass Flo[®] meter (MKS Instruments, Andover, MA). After the calibration cylinder, a substantial amount (feet) of 1/4" Teflon tubing allowed for proper mixing of catalytically converted air with the calibration standard mixture. Flow was generated by a diaphragm pump (Vacuubrand MZ2) and the PTR-MS sub-sampled from that flow.

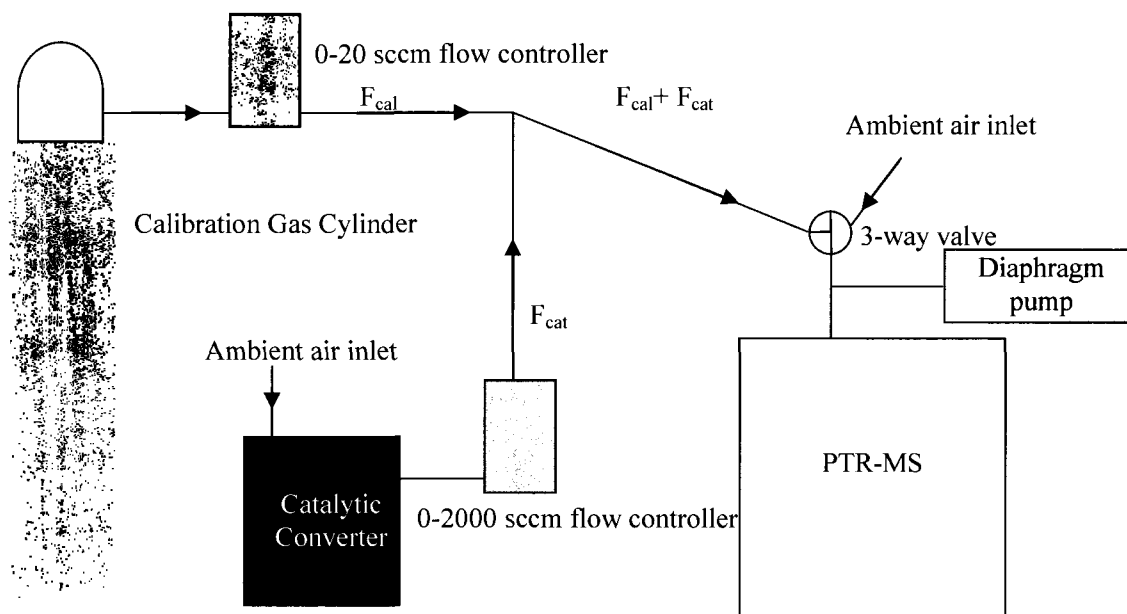


Figure 2.2: Schematic for introduction of ambient air and calibration gases to the PTR-MS.

For calibration, air was run through the catalytic converter at a flow between 0.5 and 2.0 liters per minutes (LPM). Catalytically converted air was used to determine background signals once stable signals were achieved (after at least 10 cycles) followed by introduction of the calibration gas into the sample stream. Generally, when the VOC signal had a constant zero slope for at least 10 cycles, calibration gas flow was increased to the next flow controller setting. After completion of the calibration curve, absolute mixing ratios for each compound were calculated by

$$[\text{VOC}]_{\text{ppbv}} = \frac{[\text{VOC}]_{\text{cal ppbv}} \times F_{\text{cal}}}{(F_{\text{cat}} + F_{\text{cal}})} \quad (2.10)$$

where $[\text{VOC}]_{\text{cal ppbv}}$ is concentration (ppbv) of the VOC in the calibration cylinder, F_{cal} is flow from the calibration cylinder to the sample stream (sccm), and F_{cat} is flow rate of the sample stream before the calibration cylinder.

To determine the signal corresponding to the absolute mixing ratio of VOC, the PTR-MS signal in counts per second (cps) was converted to normalized counts per second (ncps), as the counts of the VOC signal are determined by the availability of hydronium ions (2.8). The normalized signal is determined by

$$i(\text{VOC-H}^+)_{norm} = \frac{i(\text{VOC-H}^+)_{cps}}{\text{H}_3\text{O}^+_{cps}} \times 10^6 \quad (2.11)$$

where $i(\text{VOC-H}^+)_{cps}$ is the signal for the mass of interest, $\text{H}_3\text{O}^+_{cps}$ is the hydronium ion signal, and 10^6 is used as a normalization factor. An average of the normalized background counts was subtracted from the average signal at each calibration flow setting. Unweighted linear least squares fits were used to generate calibration curves with mixing ratio on the abscissa and ncps on the ordinate to determine calibration factors. Abscissa error bars result from the propagation of error associated with the two mass flow controllers (1% of flow rate setting) and the mixing ratio errors associated with the calibration gases. Associated ordinate error is 2σ of the normalized ion signal for each mass flow controller setting. Calibration factors based on unweighted linear least squares fits are given in Table 2.3 as sensitivities.

A full set of calibrations was performed before and after field studies and typically once during field studies. Starting in the summer of 2005, a one point calibration for each mass was done once per week on both instruments.

Typical calibration curves for PTR-MS-ss over the range of tens of pptv to ppbv are shown in the Appendix (Figures 2.A1-2.A11) for a compounds quantified in Table 2.3. These calibrations do not account for the proton transfer of the $(\text{H}_3\text{O}^+\text{H}_2\text{O})$ cluster at

37 amu to the VOC because the signal from this cluster is generally two orders of magnitude smaller than the signal attributed to the hydronium ion.

Figure 2.3 shows raw data generated from monitoring MEK signal (ncps) versus cycle number. Each step in the data series indicates a different mass flow controller setting and corresponding mixing ratios are shown at each step. The average signal was taken at each mass flow controller setting to determine the calibration curve.

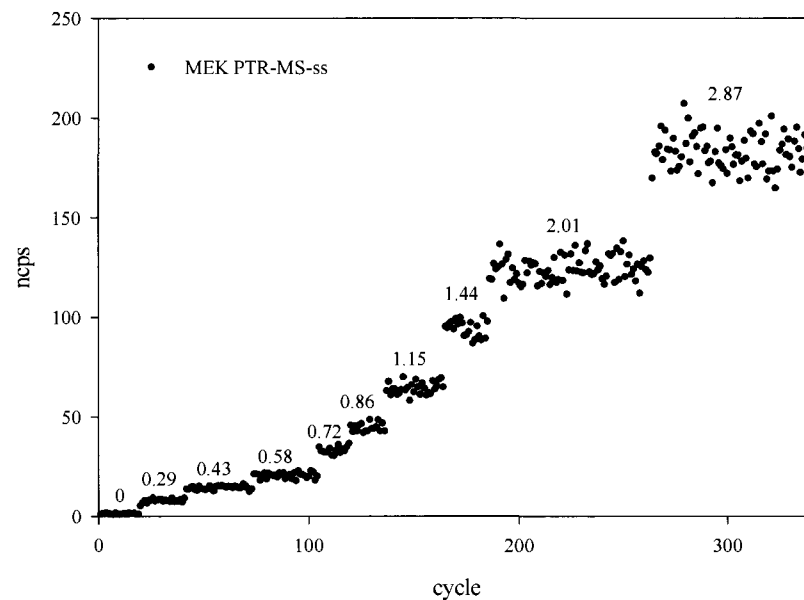


Figure 2.3: Calibration steps for the PTR-MS-ss detection of MEK with steps indicating the mixing ratios of MEK.

Details of the following calibrations are based on those done in May 2005. During this period, both instruments were located in a laboratory environment and a comprehensive set of calibrations were completed. All of these calibrations were done flowing 1760 sccm of ambient air through the catalytic converter. A 50 sccm mass flow controller was used to control the flow from the calibration cylinders.

2.2.2.2 Determination of Sensitivity.

Sensitivity and limit of detection calculations are used to determine the smallest VOC mixing ratios that may be reliably measured (Table 2.2). Sensitivity may be determined by relating kinetic and operational parameters.⁸⁴ This method of determining sensitivity is hampered in part by error associated with the rate constant and transmission.

Consequently, sensitivity may also be calculated by calibrating the instrument using gas standards (Section 2.2.2.1). With known amounts of a gas introduced into the PTR-MS, sensitivity is simply determined by a plot of ncps versus the known mixing ratio from the calibration standards. Calculated sensitivities are shown in Table 2.3.

Table 2.3: Sensitivity of PTR-MS-ss and PTR-MS-hs from calibration standards

<u>Compound</u>	<u>PTR-MS-ss</u> <u>Sensitivity (ncps ppbv⁻¹)</u>	<u>PTR-MS-hs</u> <u>Sensitivity (ncps ppbv⁻¹)</u>
methanol	13.6(3)	11.8(4)
acetaldehyde	13.6(3)	16.3(2)
acetone	22.0(2)	17.0(3)
methyl ethyl ketone (MEK)	20.2(2)	13.3(2)
isoprene	14.8(1)	6.3(2)
methyl vinyl ketone + methacrolein (MVK+MACR)	18.5(2)	9.9(3)
monoterpenes	5.36(8)	1.34(2)
acetonitrile	17.1(2)	16.4(3)
benzene(1)	12.6(1)	10.3(2)
benzene(2)	11.0(1)	6.8(2)
toluene	15.1(2)	9.2(1)

The sensitivities from both PTR-MS-ss and PTR-MS-hs may then be used to convert the ratio of the ion signal for the protonated VOC and hydronium ion to mixing ratios.

2.2.2.3 Detection Limits.

Sensitivity is necessary for calculation of the limit of detection (LOD) which is calculated as

$$LOD = 2\sigma_{ncps, background} \quad (2.12)$$

where $2\sigma_{ncps, background}$ is two times the standard deviation of the normalized background counts during times when the instrument was zeroed with catalytically converted air (Figure 2.3). Limits of detection for the monitored compounds during ICARTT 2004 are shown in Table 2.4.

Table 2.4: Limits of detection for ICARTT 2004 and signal to noise ratio for calibrations run in 05/2005 for PTR-MS-ss and PTR-MS-hs

Compound	PTR-MS-ss LOD (pptv)	S/N PTR-MS-ss	PTR-MS-hs LOD (pptv)	S/N PTR-MS-hs
methanol	250	1.1	200	1.1
acetaldehyde	280	1.2	80	1.1
acetone	220	1.2	50	1.2
methyl ethyl ketone (MEK)	90	1.4	30	1.5
isoprene	70	1.6	40	1.6
methyl vinyl ketone + methacrolein (MVK+MACR)	70	1.4	20	1.6
monoterpenes	160	1.6	40	2.0
acetonitrile	70	1.4	10	1.4
benzene(1)	70	1.5	10	1.6
benzene(2)	80	1.5	20	1.5
toluene	60	3.5	20	3.3

Background signals were then converted to mixing ratios using the calibrations shown in Figures 2.A1-2.A11 to find the LOD (pptv).¹⁰⁴

Limits of detection for PTR-MS-ss were calculated for ICARTT 2004 using the background signal during from 7/15/04 until 7/16/04 when the signal was stable. For PTR-MS-hs, the background signal was taken during the period from 8/1/04 until 8/4/04,

a time of few power variations or outages at the deployment site, Appledore Island. The LODs shown in Table 2.5 represent values determined for ICARTT 2004.

There is, in general, at least a two fold improvement in the limit of detection for the high sensitivity instrument over the standard sensitivity instrument. The similar LOD for methanol is because of the large background (*i.e.* inefficient removal of methanol from the instrument and interferences).

Included in the table is the signal to noise ratio which was calculated using the calibrations from May 2005. Here, signal to noise may be considered to be

$$\frac{S}{N} = \frac{2\sigma_{ncps,background} - background_{ncps}}{background_{ncps}} \quad (2.13)$$

where $2\sigma_{ncps,background}$ is two times the standard deviation of the normalized background counts during the calibrations, and $background_{ncps}$ is the average of normalized background counts over the same time period during the calibrations. Large background signals for methanol and acetone significantly affect the S/N ratio from these calibrations. It should be noted that toluene had the lowest background counts during the calibrations, giving it the greatest signal to noise ratio for both PTR-MS-ss and PTR-MS-hs.

2.2.3 Field Measurement Sites

2.2.3.1 AIRMAP Continuous Monitoring at Thompson Farm.

Since the summer of 2003, a PTR-MS has been stationed at Thompson Farm (TF), a rural site in Durham, NH (43.11N, 70.95W, elevation 75ft). The site is surrounded by rolling hills and a mixed forest. PTR-MS-ss continuously monitored at

least 20 different VOCs while sub-sampling from a manifold drawing ambient air from the top of a 40 foot tower. Masses monitored and dwell times (integration time at each mass) for these compounds are constantly being updated and optimized. From 7/1-7/10/2004, 25 masses were measured, with a dwell time of 10 seconds for each mass. After 7/10/2004, dwell times were increased to 20 seconds/mass, doubling the cycle time to ~9 minutes. Molecules and corresponding masses quantified are shown in Table 2.5.

Table 2.5: Protonated masses measured during the ICARTT 2004 summer campaign

<u>compound</u>	<u>mass (protonated)</u>	<u>compound</u>	<u>mass (protonated)</u>
methanol	33	monoterpenes (fragment)	81
ethanol	47	monoterpenes	137
formaldehyde	31	methyl chloride (MeCl)*	51
acetaldehyde	45	styrene + peroxy isobutyryl nitrate (PiBN)*	105
acetone	59	acetonitrile	42
methyl ethyl ketone (MEK)	73	benzene	79
pentanal*	87	toluene	93
ethyl acetate*	89	C8 aromatics	107
hexanal	101	C9 aromatics	121
2,3 hexanal	99	C10 aromatics	135
peroxyacetyl nitrate + carbon disulfide (PAN + CS ₂)*	77	Dimethyl sulfide (DMS)	63
isoprene	69	acetic acid	61
methyl vinyl ketone + methacrolein (MVK+MAC)	71		

bold indicates masses quantified using calibration standards

Other masses commonly detected by PTR-MS have been summarized recently.⁸⁴ After every 15 cycles (from 7/1-7/10/2004) and 18 cycles (after 7/10/2004), outside air was run through a catalytic converter at 425 °C for four cycles to determine the system background signals. The set of background cycles was then averaged and subtracted from the signal for the corresponding VOC. The signal was then converted to mixing ratios

using calibration standards. The drift tube was kept at a constant 2.00(2) mbar and run at 600(5) volts.

2.2.3.2 Appledore Island.

During the summer of 2004 (June 1-August 15), the northeastern United States was host to ICARTT. As part of this field study, two PTR-MS instruments were deployed. One was responsible for measurements made at Thompson Farm, and a higher sensitivity instrument was deployed to Appledore Island (AI) (42.97N, 70.62W, sea level). PTR-MS-hs was located at the base of a watchtower on Appledore Island, and the inlet position extended approximately twelve feet above the top of the 70 ft tower. Inlet tubing was 3/8" Teflon[®] and extended ~80 feet from the PTR-MS-hs. Tubing was pumped by a 4.3 m³/hr (~72 LPM) diaphragm pump (Vacuubrand ME 4). Approximately 5 feet of 1/4" tubing was used to sample off the 3/8" tubing, and a downstream diaphragm pump (Vacuubrand MZ 2) provided a choked flow of about 1 L/minute. Flow through the 1/4" tubing was monitored by a 10 LPM MKS Mass-Flo[®] meter. As with the PTR-MS-ss, the PTR-MS-hs dwell times were 10 seconds from 7/1-7/10/2004 and 20 seconds after 7/10/2004 and the background counts were determined after every 15 and 18 cycles respectively.

2.3 Results and Discussion

2.3.1 Correlation between PTR-MS-ss and PTR-MS-hs

In order to compare instrument response between PTR-MS-ss and PTR-MS-hs, the two instruments were placed in a laboratory setting in Durham, NH, and sampled ambient air from outside of the laboratory window during May, 2005. Calibration factors (Table 2.3) were then used to convert the ion signals to mixing ratios, and the resultant mixing ratios were compared.

Correlations were done over time periods where the largest changes in ambient air VOC mixing ratios were observed, and those differences in mixing ratio are also shown in Table 2.6.

Table 2.6: Correlation between PTR-MS-ss and PTR-MS-hs from ambient air measurements and calibrations shown in Figures 2.5-2.15

<u>Compound</u>	<u>PTR-MS-hs/PTR-MS-ss</u>	<u>min MR</u> <u>(ppbv)</u>	<u>max MR</u> <u>(ppbv)</u>	<u>R²</u>
methanol	1.00(2)	2	20	0.94
acetaldehyde	0.85(1)	2	30	0.97
acetone	0.98(1)	1	20	0.99
methyl ethyl ketone (MEK)	1.10(2)	0.2	0.9	0.92
isoprene	1.34(4)	0.3	0.7	0.89
methyl vinyl ketone + methacrolein (MVK+MACR)	0.98(2)	0.1	0.4	0.77
monoterpenes	1.04(4)	0.8	1.6	0.86
acetonitrile	0.89(2)	0.3	0.6	0.83
benzene(1)	0.84(2)	0.1	0.3	0.84
benzene(2)	1.13(2)	0.3	0.6	0.92
toluene	0.97(4)	0.3	0.6	0.80

A 5 point moving average of the signals was used for the correlations, and a 10 second dwell time for each of the VOCs was used during the comparison. During the course of the comparison, PTR-MS-hs primary ion signal varied between 2.26×10^6 and

3.3×10^6 cps and PTR-MS-ss primary ion signal changed between 2.2×10^6 and 4.0×10^6 cps. An example (acetone) is shown in Figure 2.4.

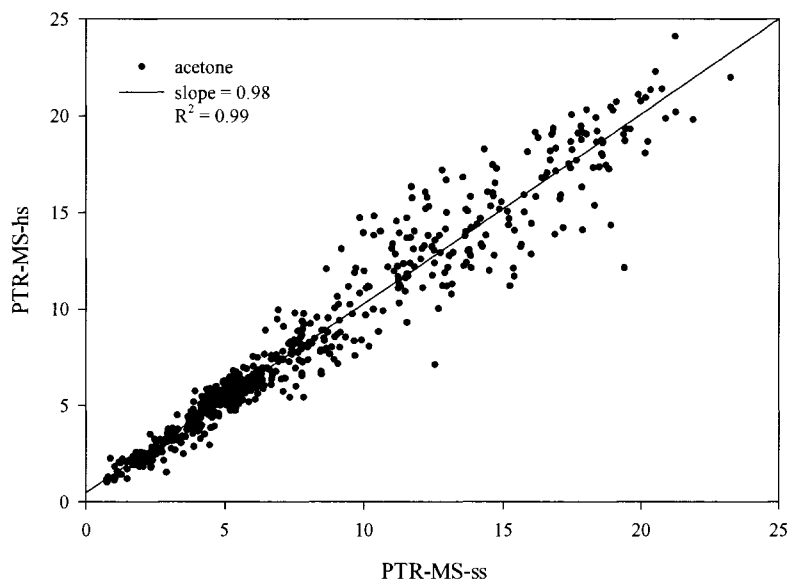


Figure 2.4: Comparison of acetone mixing ratios detected by PTR-MS-hs and PTR-MS-ss when sampling from the same ambient air inlet.

In general there was good agreement between the two instruments for mixing ratios of methanol, acetone, MEK, MVK+MACR, monoterpenes, and toluene. The low correlation coefficient for MVK+MACR was because of a large amount of scatter in the PTR-MS-ss data over the range analyzed. This was caused, in part, by instability in the primary ion source of PTR-MS-ss and the relatively small (200 pptv) range measured.

2.3.2 Correlation Between Calculation and Calibration Based Mixing Ratios

In cases where gas standards are not available, it is possible and relatively simple to calculate the mixing ratios based on (2.8) although greater accuracy is typically achieved by use of calibration standards (Section 2.2.2.1). However, it is useful to

compare these two methods for determining mixing ratios in order to properly evaluate the utility of the calculation method. Key to generating accurate mixing ratios using (2.8) are precise knowledge of the ion-molecule rate constant (Table 2.2), time for reaction in the drift tube, and transmission of molecules to the detector (2.8). Transmission of both the protonated VOC and hydronium ion are limited by the efficiency of ion transport to the quadrupole, transmission efficiency of the quadrupole, and detection efficiency of the electron multiplier.⁸⁴ Transmission values are provided by Ionicon for each instrument upon purchase. Creating a transmission curve is done by sampling the headspace of compounds over a mass range, and measuring the change in signal for the VOC and the hydronium ion. Another method is to increase the sample amount such that all of the hydronium ion is saturated, leading to less than 1×10^3 counts s^{-1} (cps) of hydronium ion and monitoring VOC signal. The ratio of the VOC signal to hydronium ion signal then defines the transmission for that particular mass. It is further important to account for fragmentation of particular VOCs, which is more relevant for larger molecular weight compounds. Table 2.7 gives the comparison for both PTR-MS-ss and PTR-MS-hs between using calculation and calibration methods for determining mixing ratios.

Table 2.7: Comparison between the calculation method for determining mixing ratios (2.8) using published proton transfer rate constants, and gas dilution methods to determine absolute mixing ratios using calibration standards

Compound	PTR-MS-ss calculation/calibration	PTR-MS-hs calculation/calibration
methanol	0.93(2)	0.78(1)
acetaldehyde	0.55(1)	0.55(1)
acetone	0.99(1)	0.58(1)*
MEK	0.71(1)	0.44(1)
isoprene	0.93(1)	0.32(1)
MVK+MACR ⁺	0.61(1)	0.27(1)
acetonitrile	1.16(1)	0.41(1)

Compound	PTR-MS-ss calculation/calibration	PTR-MS-hs calculation/calibration
benzene(1)	0.78(1)	0.53(1)
benzene(2)	0.70(1)	0.34(1)
toluene	0.90(1)	0.43(1)

* If the default ion-molecule rate constant, $2 \times 10^{-9} \text{ cm}^3 \text{ s}^{-1}$ (given by Ionicon) is used, the slope is 0.86(1)

+ based on the average ion-molecule rate constant of both compounds

Notably, PTR-MS-ss has much better agreement with the calculation method for determining mixing ratios. Transmission values used for this instrument were those given by Ionicon, and besides acetaldehyde and MVK+MACR, agreement with the calibration factors is acceptable as a first approximation. PTR-MS-hs shows poor agreement between the calculation method and calibrations. Again, Ionicon generated transmission values were used for this calculation. PTR-MS-ss and PTR-MS-hs were treated with considerably different care during deployments, as the location of deployment dictated their transport. PTR-MS-ss was transported carefully by vehicle to the monitoring station at TF. PTR-MS-hs was transported to AI, and the monitoring site required rough transport on ship, by hand, and by vehicle on rocky terrain. It is recommended by Ionicon that after each PTR-MS move, a new transmission curve should be generated. While the method for generation of a transmission curve is straightforward there are challenges in repeatability and quality. Errors between measured transmission values and those given by Ionicon have been reported to be up to 25%.⁷⁹

2.3.3 Comparison to Other Instruments

During ICARTT 2004, there were opportunities to check our PTR-MS measurements at AI with other measurements from other research groups. The ultimate mixing ratios determined by calibrations (Appendix Figures 2.A1-2.A11) were compared to other PTR-MS measurements and GC-MS measurements at the island. A few of these comparisons will be presented here. First, the NOAA research group of Joost de Gouw operated a PTR-MS on the NOAA ship, the Ronald Brown. Figure 2.5 shows comparisons of time series measurements and mixing ratio correlations between the PTR-MS-hs at AI and the PTR-MS of Joost de Gouw's research group. Data shown as black points correspond to measurements taken at AI, and red diamonds indicate measurements taken on the Ronald Brown. Measurements presented correspond to times when the Ronald Brown was in the vicinity of AI.

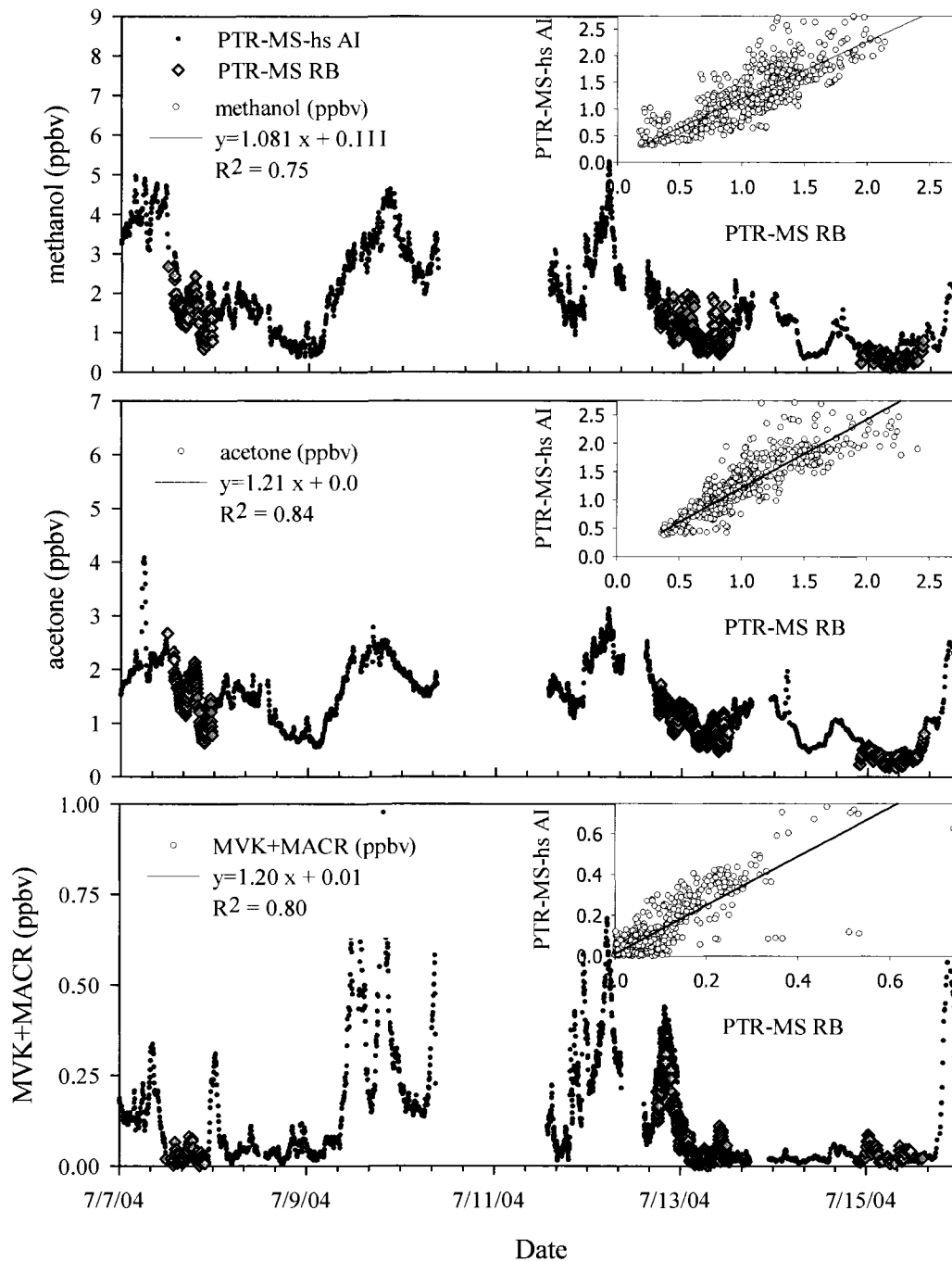


Figure 2.5: PTR-MS-hs time series and correlations of methanol, acetone, and MVK+MACR taken during ICARTT 2004 compared with PTR-MS measurements by Joost de Gouw's research group on the Ronald Brown. Linear equations refer to inset.

Overall, temporal variations between the measurements made using PTR-MS on the Ronald Brown and measurements made using PTR-MS-hs on AI are in good agreement. Plots of mixing ratio correlations between these three compounds indicates considerable scatter which may, in part, be because of local interferences and different operational parameters for these two instruments.

Somewhat more encouraging results are observed for benzene and toluene correlations on AI. Here, the Sive group collected canister samples that were later measured by GC-MS. Figures 2.6 and 2.7 show time series plots and correlations between PTR-MS-hs and GC-MS measurements for toluene and benzene.

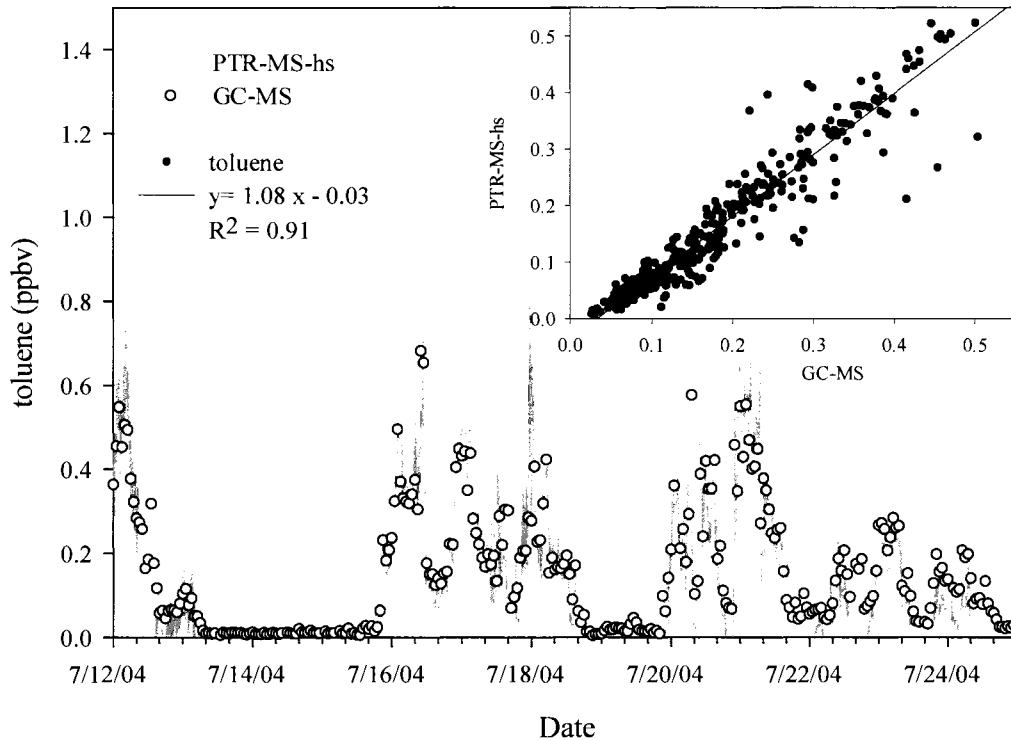


Figure 2.6: PTR-MS-hs and GC-MS intercomparison of toluene during ICARTT for period of 7/12-7/25/04. Linear equations refer to inset.

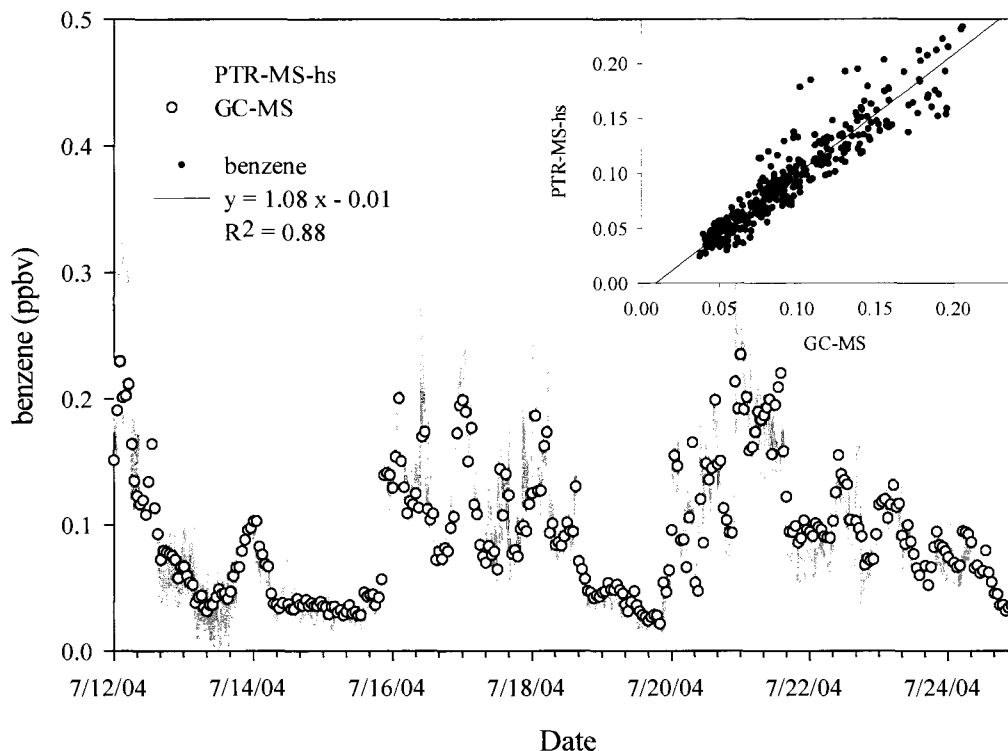


Figure 2.7: PTR-MS-hs and GC-MS intercomparison of benzene during ICARTT for period of 7/12-7/25/04. Linear equations refer to inset.

The period of 07/12-07/24/2004 is taken as a representative time series for the ICARTT 2004 campaign, and the agreement between GC-MS and PTR-MS-hs is excellent for toluene and benzene. PTR-MS-hs data during the period of 07/14-07/16 and 07/19-07/20/2004 was below the LOD of toluene (<20 pptv).

2.4 Summary and Conclusions

Two PTR-MS instruments (PTR-MS-hs and PTR-MS-ss) were deployed at two locations in New England (AI and TF respectively) during ICARTT 2004. Compounds were quantified using available gas standards for creation of calibration curves using gas

volume dilution methods. Sets of these calibrations over a one year period were compiled and show overall excellent agreement giving credence to long term stability of these instruments. PTR-MS-hs showed a limit of detection typically 3-5 times lower than PTR-MS-ss based on data collected during ICARTT 2004 and sensitivities determined from calibrations. Since this work, PTR-MS-ss has been upgraded to PTR-MS-hs by the addition of a third turbo molecular pump for the differential pumping region.

Calibrated mixing ratios for quantification of ambient VOC samples are compared to the calculation method. General agreement between these two methods is poor for PTR-MS-hs but acceptable to good for PTR-MS-ss. The agreement between the calculation and calibration methods for PTR-MS-ss is important in Chapter 4, where no calibration standards were available for some of molecules monitored. The differences in the calculated and calibrated methods for determining mixing ratios for PTR-MS-hs are likely because of changes in the transmission of molecules to the detector from field deployments. Other considerations in calculation of mixing ratios include accounting for proton transfer reactions from clusters to VOCs and air humidity, not accounted for in this study. Quantification of VOCs based on calibrations gives excellent agreement between the two instruments. PTR-MS-hs shows generally good agreement with PTR-MS measurements from the research group of Joost de Gouw, although there is significant scatter in the data sets used. PTR-MS-hs measurements of benzene and toluene show excellent agreement with GC-MS measurements made at AI.

Overall, PTR-MS is shown to be a reliable method for detection and quantification of VOCs, showing long term instrument response stability as determined

by calibration standards. Ability to determine mixing ratios with high time resolution and without the need for pre-treatment of samples make PTR-MS particularly flexible in atmospheric field studies.

2.5 Appendix

2.5.1 Calibration Standards

Table 2.A1: Calibration standard components and primary ion counts, cluster counts for a set of typical calibrations done in May 2005

Calibration Standard	primary ion PTR-MS-ss ($\times 10^6$ cps)	cluster ($\times 10^4$ cps)	primary ion PTR-MS-hs ($\times 10^6$ cps)	cluster ($\times 10^4$ cps)	components and mixing ratios (ppbv)
1	2.4(2)	8.0(8)	3.6(4)	3.5 (9)	methanol (512) acetone (508) MEK (519) acetaldehyde (500) benzene(512)
2	2.3(2)	10(10)	3.1(3)	5.9(7)	MVK (384) MACR(375) isoprene(499) monoterpenes (2078) (α -pinene, limonene, camphene, 3-carene)
3	2.3(2)	10.1(8)	2.9(3)	6(1)	acetonitrile(417) toluene(505) benzene(511)

Unweighted linear least squares was used to fit all calibration data with figures shown below (Figures 2.A1-2.A11).

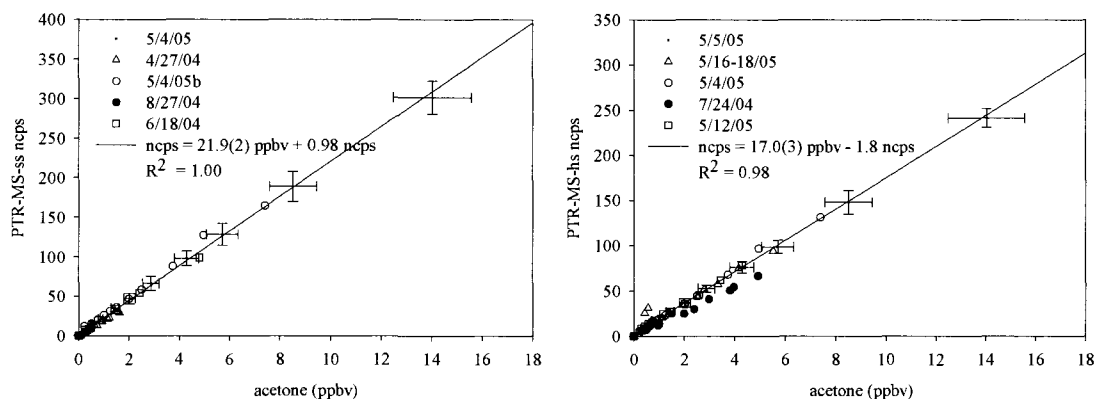


Figure 2.A1: Calibrations of the PTR-MS-ss (left) and PTR-MS-hs (right) of acetone based on calibrations done over a one year period.

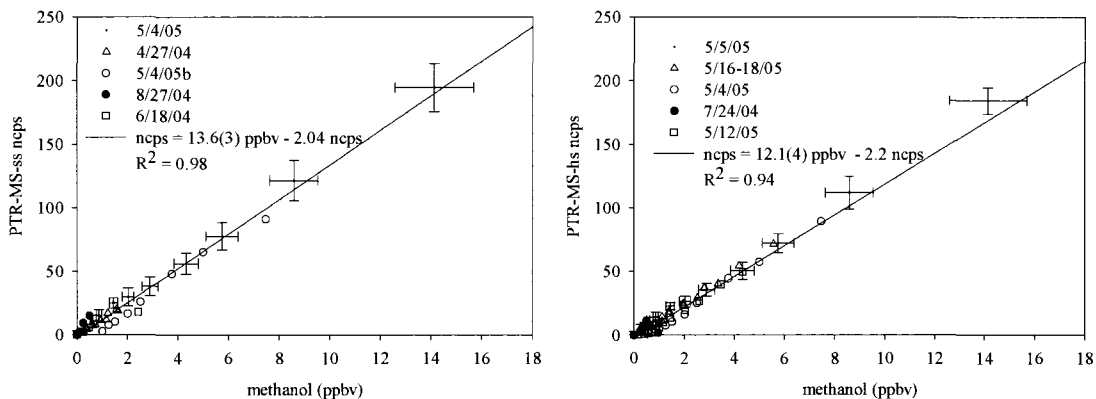


Figure 2.A2: Calibrations of the PTR-MS-ss (left) and PTR-MS-hs (right) of methanol based on calibrations done over a one year period.

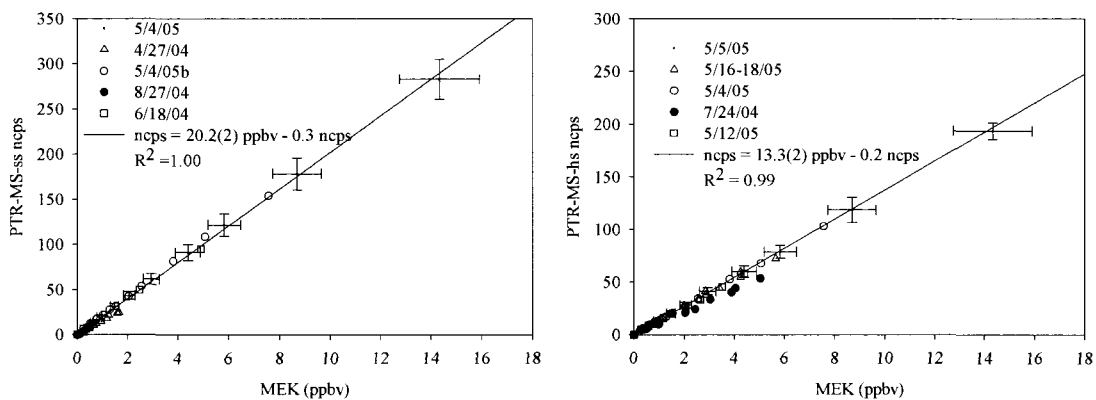


Figure 2.A3: Calibrations of the PTR-MS-ss (left) and PTR-MS-hs (right) of MEK based on calibrations done over a one year period.

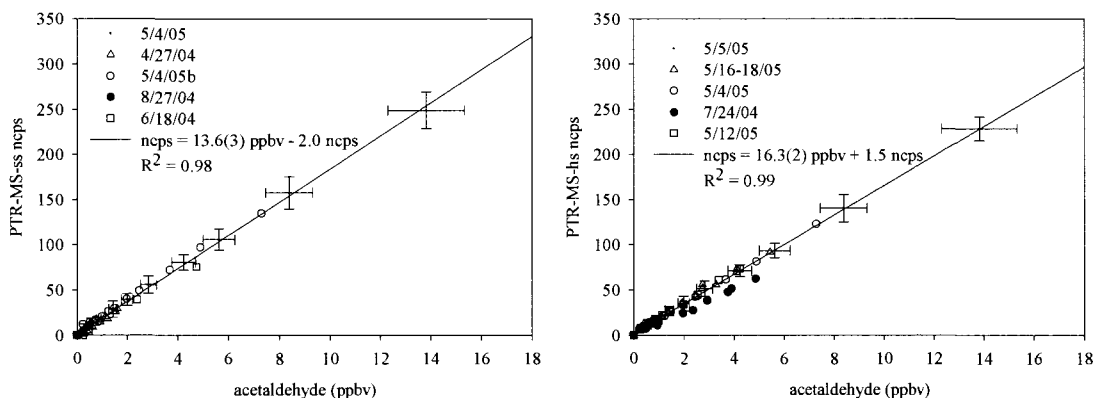


Figure 2.A4: Calibrations of the PTR-MS-ss (left) and PTR-MS-hs (right) of acetaldehyde based on calibrations done over a one year period.

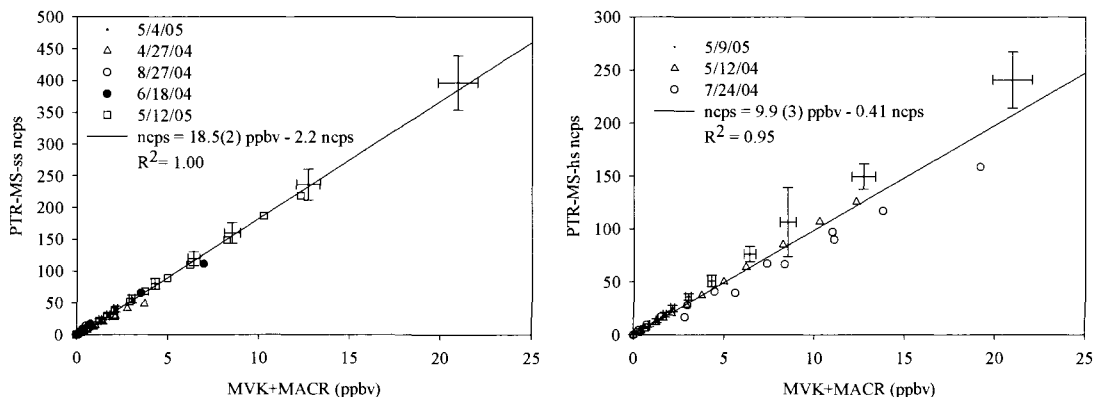


Figure 2.A5: Calibrations of the PTR-MS-ss (left) and PTR-MS-hs (right) of MVK+MACR based on calibrations done over a one year period.

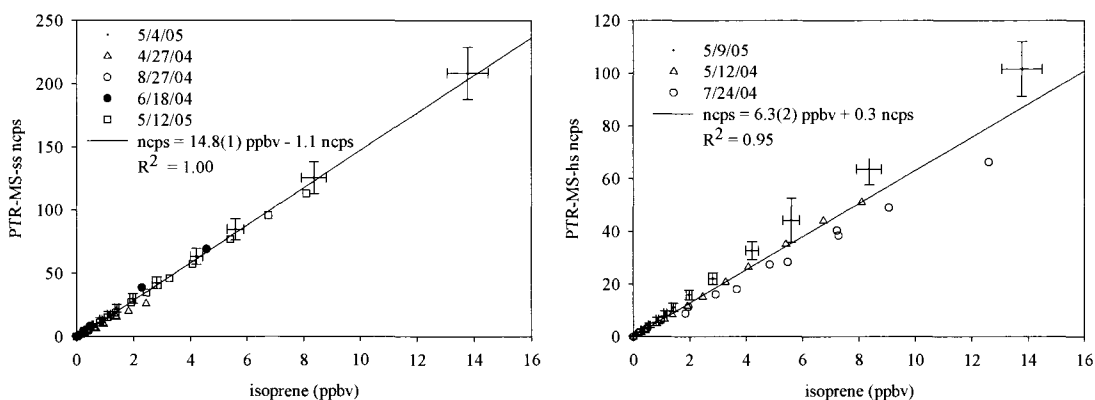


Figure 2.A6: Calibrations of the PTR-MS-ss (left) and PTR-MS-hs (right) of isoprene based on calibrations done over a one year period.

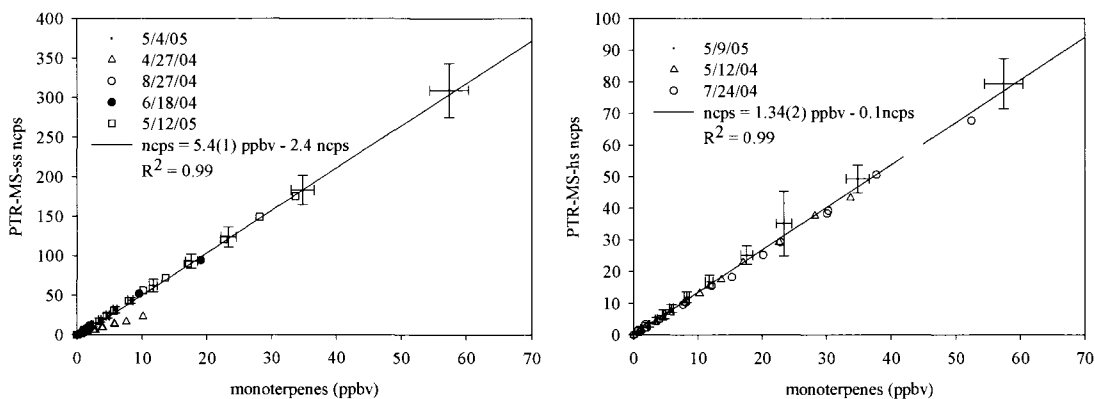


Figure 2.A7: Calibrations of the PTR-MS-ss (left) and PTR-MS-hs (right) of monoterpenes based on calibrations done over a one year period.

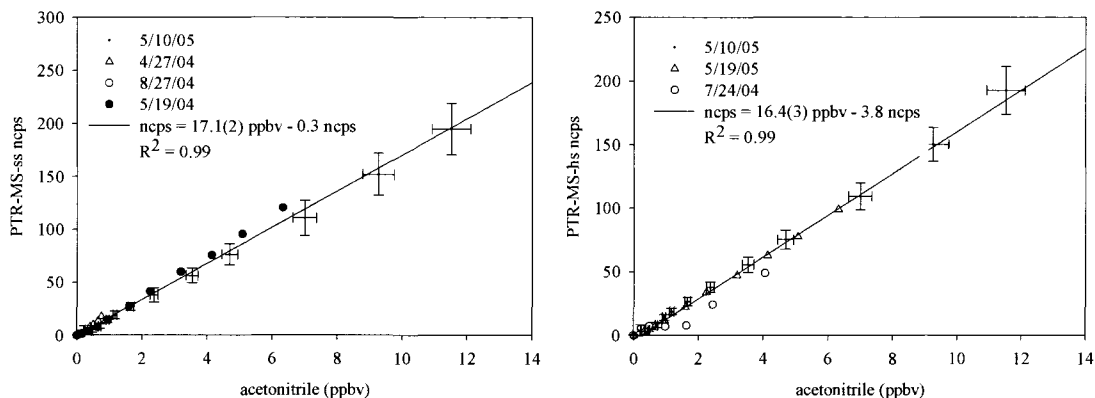


Figure 2.A8: Calibrations of the PTR-MS-ss (left) and PTR-MS-hs (right) of acetonitrile based on calibrations done over a one year period.

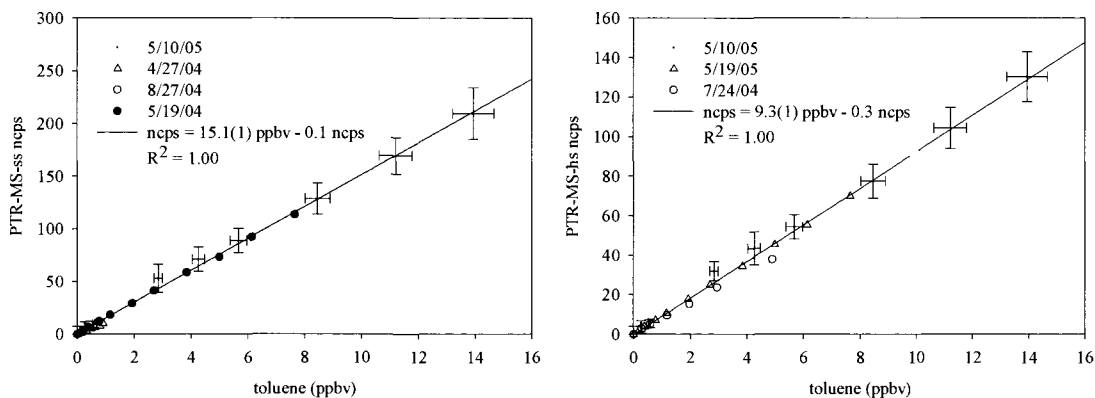


Figure 2.A9: Calibrations of the PTR-MS-ss (left) and PTR-MS-hs (right) of toluene based on calibrations done over a one year period.

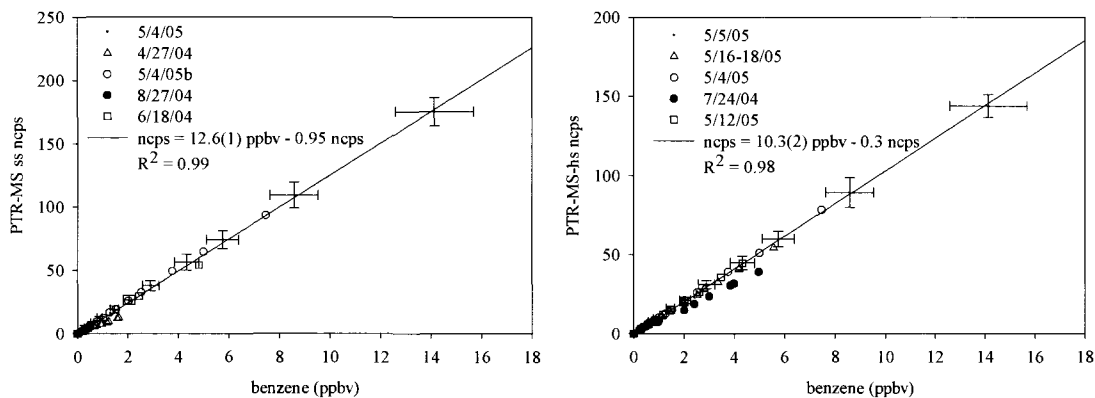


Figure 2.A10: Calibrations of the PTR-MS-ss (left) and PTR-MS-hs (right) of benzene(1) based on calibrations done over a one year period.

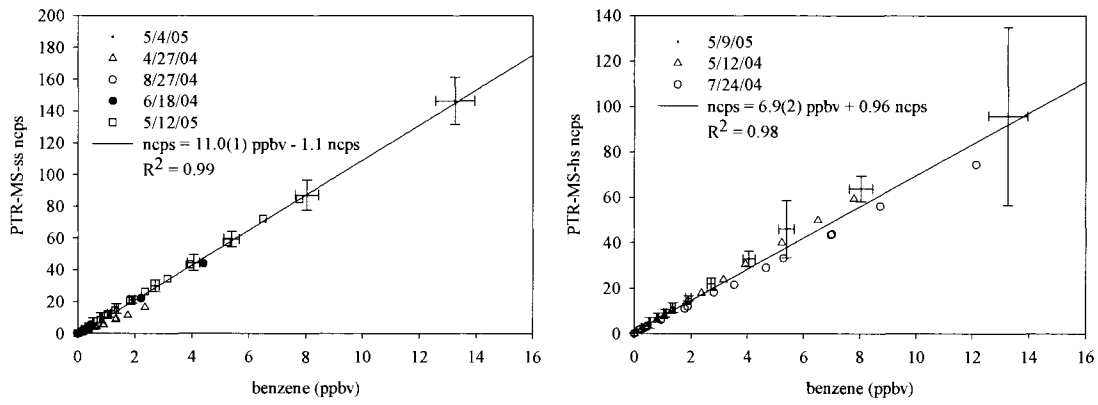


Figure 2.A11: Calibrations of the PTR-MS-ss (left) and PTR-MS-hs (right) of benzene(2) based on calibrations done over a one year period.

CHAPTER 3

MONITORING OF SELECT VOCs USING PTR-MS DURING ICARTT 2004: AVERAGE DIURNAL PROFILES, LOSS, AND DRY DEPOSITION

3.1 Introduction

Concentrations of trace gases in the atmosphere are dependent upon chemical reactivity, transport, emission, and wet and dry deposition. Wet deposition is the uptake of compounds to precipitation, whereas dry deposition is the transport of particles or gaseous compounds to the Earth's surface in the absence of precipitation.¹⁰⁵ Flux to the surface is determined by the product of the concentration of the compound of interest and the deposition velocity, v_d , which is a proportionality constant relating the flux (F) to the concentration (C) at a specific boundary layer height

$$v_d (\text{cm s}^{-1}) = \frac{-F (\text{g cm}^{-2} \text{ s}^{-1})}{C (\text{g cm}^{-3})} \quad (3.1)$$

Deposition to the surface is governed by a number of factors including atmospheric turbulence, the reactivity and solubility of gases, and size, density, and shape of particles. Further, surface characteristics determine deposition of compounds. Over vegetated areas deposition tends to be greater than over water, and deposition to vegetation is a significant sink and is related to diurnal cycles of the plant activities.¹⁰⁶⁻¹⁰⁸ Because deposition is governed by both meteorological and surface conditions, the values for

deposition velocities may vary greatly.¹⁰⁹ The process of deposition occurs in three steps: (a) the aerodynamic transport of compounds to the surface, (b) diffusion, and (c) uptake to the surface. When the transport to the surface occurs faster than the chemical lifetime of the compound, then deposition of that compound becomes an important removal process.¹¹⁰

Methods to determine the deposition of compounds fall broadly into two categories: direct and indirect methods. For the deposition of gases, the most direct method for determining uptake is the eddy covariance technique.¹¹¹ This technique requires instrumentation for measurement of vertical wind velocity and mixing ratios of VOCs.¹¹² Further, instruments must be collocated to make simultaneous and fast measurements for the correlation between the wind speed and concentrations of VOCs.¹¹² This technique is limited by instrument response time and a large number of correction terms in the flux calculation which include heat fluxes causing variations in air density.^{113,114} In order to overcome the technical challenges associated with the eddy covariance technique, variants of the eddy covariance technique have been developed. These include the eddy accumulation method,¹¹⁵ the relaxed eddy accumulation method,¹¹⁶ and the disjunct eddy covariance technique.⁶⁸ Because of the advance of fast response gas analyzers, disjunct eddy covariance has shown considerable promise in the measurement of trace gas fluxes.¹¹⁷⁻¹¹⁹ This method still requires high time resolution for sampling but is disjunct because the total time series has gaps due to measurement parameters (*i.e.* determining the flux of other compounds in a time series).⁶⁴ Because of

the high time resolution of PTR-MS, the disjunct eddy covariance technique has been used for measurement of trace gas fluxes in a number of studies.^{66,68,120-123}

Another direct technique for measuring the flux to the surface is the gradient method (modified Bowen ratio method).¹²⁴ In this method, sampling occurs at two different heights above a surface of interest (*e.g.* forest canopy, cropland). Differences in concentration are noted between the two sampling heights, and vertical flux is determined by calculation of the eddy diffusivity. This measurement assumes homogeneity of the surface and a measurable difference in concentrations between the two sampling heights. Both of these aspects are limitations of the gradient model as concentration differences typically do not exceed 5% of the mean concentration and most surface types vary significantly in makeup.¹²⁵ This technique further requires accurate measurements of gradients of other gases as the diffusivity (turbulent exchange coefficient) of the compound of interest is assumed to be the same as other monitored gases (*e.g.* H₂O, CO₂).^{109,126}

Site specific and global estimation of deposition may be determined by the use of dry deposition models. The simplest of these models is parameterized to compute deposition velocities based on the contribution of surface interactions, molecular diffusivity, and meteorological transport of compounds to the surface.¹²⁷ Analogous to Ohm's law, these contributions are given as resistances, and are further subdivided into contributing parallel and series resistances.^{127,128} Some of these models are dependent on experimentally determined deposition velocities for flux calculations.¹²⁹⁻¹³¹ Further improvements in the calculation of the resistance components have received a great deal

of study, and have ultimately been incorporated into sophisticated models.^{108,132-134} Currently, the most comprehensive of these models is the Modular Earth Submodel System with the EMDEP submodel.¹³³ Dry deposition also includes the uptake of gases and particles to water. Air-sea exchange flux is expressed in terms of a dimensionless Henry's law constant, the concentration of water, and a gas transport velocity.¹³⁵ Parameterization of the contributing components to trace gas water uptake have been proposed in a number of studies,¹³⁵⁻¹³⁸ and models have been developed to calculate deposition velocities to water.¹³⁴

In the absence of meteorological properties to calculate the deposition velocity, a rough estimate may be calculated by an indirect method of concentration monitoring.¹³⁹ Here, the concentrations of particular compounds are monitored over a specified period of time during which there is a stable boundary layer condition and minimal gas phase reactivity of the compound (*i.e.* minimal reaction with atmospheric oxidants). Assuming a constant nocturnal boundary layer height, the deposition velocity may be calculated by¹⁴⁰

$$v_d = \frac{d(\text{g cm}^{-3}) \times h(\text{cm})}{a(\text{g cm}^{-3}) \times t(\text{s})} \quad (3.2)$$

where d is the decrease in concentration of a compound over a period of time (t) having an average concentration (a) assuming a constant boundary layer height (h). The decrease in concentration over time may be determined by direct monitoring of mixing ratios of the compound of interest, and the accuracy of this is enhanced by instruments capable of

high time resolution measurements (*i.e.* in order to accurately determine peaks and troughs defining the deposition period). For compounds unreactive over the time period for deposition, the height used is typically the boundary layer height.^{110,125} This determination of deposition velocity (3.2) may then be used to calculate a flux (3.1) to determine the physical removal of VOCs from the atmosphere or implemented in modeling of VOC atmospheric loadings. In order to determine uptake to water surfaces, VOC concentration measurements are made in conjunction with wind speed to determine if increased wave production and turbulence correlate with variations in concentrations.¹⁴¹ These values can ultimately be used to determine whether water surfaces are sources or sinks for VOCs.

Dry deposition phenomena are particularly important for longer lived VOCs (*i.e.* those with lifetimes of days) as deposition may be the primary atmospheric removal process. In the absence of reactivity with NO_x, deposition of VOCs is most often observed during the night. Dry deposition as an atmospheric removal process is, in general, not well understood for most atmospheric trace gases. This is due to variability in surface types in different regions, turbulence, and atmospheric concentrations of the trace gases at different times.^{125,142,143} Specifically, the magnitude of these deposition processes is largely unknown. Trace gases typically have deposition velocities between 0.1 and 2 cm s⁻¹.¹²⁵ The deposition velocity estimate of acetone is generally taken as 0.1 cm s⁻¹ and is used in models for the atmospheric budget of this compound, but typically varies significantly from this value.^{144,145} In fact, while ocean sources of acetone have been inferred,¹⁴⁶ ocean uptake has also been reported,^{144,147,148} which has implications in

the atmospheric loading of this compound.^{145,149} Use of reliable estimates for deposition velocity is critical for accurate atmospheric modeling.^{109,125} Such models require accurate emission rates for calculation of VOC fluxes. Because of local variable such as light, temperature, compound makeup, and surface types, there is generally a very large variability from model outputs. This is true of new models, such as the Model of Emissions of Gases and Aerosols from Nature (MEGAN).¹⁵⁰ Because of this large variability in model predictions, it is useful to compare empirically determined emissions and depositions to those predicted by the global models.

3.1.2 Specific Aim

The diurnal profiles and average, maximum, and minimum mixing ratios for acetaldehyde, acetone, methanol, methyl ethyl ketone (MEK), methyl vinyl ketone and methacrolein (MVK + MACR) along with monoterpenes and isoprene are discussed for the ICARTT 2004 summer (June-August) campaign. Oxygenated compounds are included for deposition calculations because of long atmospheric nighttime lifetimes (Section 3.3) and their reliable detection via PTR-MS. Monoterpenes and isoprene are included as they are photochemical precursors to some of these oxygenated compounds.

This work aims to provide reasonable estimates for the loss and nighttime deposition velocities of these longer lived oxygenated volatile organic compounds during the summer months in New England. Deposition velocities at Thompson Farm (TF) are reported for these compounds during the night, as nighttime loss of the compounds via reaction with NO_3 is not significant and does not need to be considered in the estimation

of the deposition velocity.¹⁵¹⁻¹⁵³ Loss of VOCs to wind driven process is calculated at Appledore Island (AI). This work further emphasizes the variability in the mixing ratios of these compounds between these sites.

3.2 Experimental

Two PTR-MS instruments were stationed at two sites in New England: AI, and TF. The details of the sites and acquisition parameters for the instruments at each of these sites are described in Chapter 2. Of the compounds measured during ICARTT 2004, those quantified for this analysis were: methanol (m/z 37), acetone (m/z 59), acetaldehyde (m/z 45), MEK (m/z 73), MVK+MACR (m/z 71), monoterpenes (m/z 137), and isoprene (m/z 69). As MVK and MACR are isobaric compounds, they are unable to be resolved with PTR-MS and are reported as a sum. All of the compounds were quantified using calibration standards and methods described in Chapter 2. Limits of detection for these compounds are also given in Chapter 2.

Mixing ratios for each specific compound were hourly averaged and used for the analysis in the average diurnal trends (Section 3.3.2). Error is taken as the 95% confidence interval from these hourly averages. At TF, deposition velocities were calculated using the average decrease in mixing ratios during the night (10PM EDT until 6AM EDT) using the whole data set. Deposition velocities at TF were also calculated using this same method, but using sorted data to minimize marine influence (Section 3.3.3). The deposition velocities at TF were based on estimated boundary layer heights of 70, 100, and 125 m corresponding to the estimated nighttime nocturnal inversion layer.

At AI, uptake to the ocean was determined by sorting the averaged data to minimize continental influence (Section 3.3.4), and using wind speed data.

3.3 Results and Discussion

3.3.1 Average VOC Mixing Ratios at TF and AI

Average, maximum, minimum, and standard deviation of mixing ratios at TF and AI for a variety of gas phase compounds are shown in Table 3.1. These gases are emitted from biogenic sources, anthropogenic activities, and produced via photochemical oxidation of other compounds. Differences of VOC mixing ratios at these two sites have been previously reported, most notably with ozone.¹⁵³⁻¹⁵⁵ Elevated levels of ozone at AI, when compared to TF, have been observed and explained in detail.^{153,154,156} Briefly, the differences in ozone minima at TF and AI are because of titration by NO and deposition at TF, both of which are minor contributions to ozone loss at AI.¹⁵⁴ Additionally, despite their proximity, meteorological conditions are significantly different at the two sites, with a westerly winds at TF, and an additional southerly component at AI.¹⁵⁴

Table 3.1: Average, maximum, minimum, and standard deviation of all select VOCs measured during ICARTT 2004 at AI and TF.

	TF (ppbv)				AI (ppbv)			
	<u>ave.</u>	<u>max.</u>	<u>min.</u>	<u>st.dev.</u>	<u>ave.</u>	<u>max.</u>	<u>min.</u>	<u>std. dev.</u>
methanol	2.41	8.22	0.32	1.31	2.22	7.40	0.07	1.31
acetaldehyde	0.32	2.11	*	0.29	0.42	1.82	0.04	0.24
acetone	1.80	8.22	0.16	1.05	1.39	4.94	0.29	1.36
MEK	0.21	1.31	*	0.18	0.16	0.88	*	0.11
MVK+MACR	0.38	3.55	*	0.42	0.19	1.86	*	0.24
isoprene	0.51	6.96	*	0.48	0.14	1.17	*	0.12
monoterpenes	0.69	5.75	*	0.91	0.09	0.86	*	0.10

* = below limit of detection

3.3.1.1 Methanol.

Emission during plant growth and the oxidation of methane are the two most significant sources of methanol in the troposphere.^{7,157-160} In particular, plant growth has been estimated to contribute 100-122 Tg yr⁻¹ of methanol to the atmosphere.^{7,157} Besides plant growth and the oxidation of methane, atmospheric production of methanol may occur via the reaction of methyl peroxy radical (CH₃O₂) with itself and other peroxy radicals from the oxidation of VOCs.^{161,162} Riemer et al.¹⁶³ have reported methanol mixing ratios between 3.1 and 22 ppbv at a rural site in Tennessee, with a mean mixing ratio of 11 ppbv. Average mixing ratios of methanol at TF and AI are similar, at 2.41 and 2.22 ppbv, respectively. As the atmospheric lifetime of methanol is 17 days,¹⁶⁴ transport to AI should occur without further oxidation. Maximum mixing ratios at TF are approximately 1.8 ppbv larger than at AI. At TF, the minimum of 0.32 ppbv indicates local sources of methanol persistent throughout the night or incomplete atmospheric removal. Minimum values of methanol at AI were below the limit of detection for the PTR-MS.

3.3.1.2 Acetaldehyde.

Acetaldehyde is produced from leaf-wounded or oxidatively stressed pine and birch trees.¹⁶⁵ Further production of acetaldehyde comes from the photochemical oxidation of hydrocarbons¹⁶⁶ from incomplete combustion, typically noted in biomass burning episodes.¹⁶⁷ Another typical source of acetaldehyde is expected to be the OH radical oxidation of ethane and propane in the presence of NO.¹⁴⁹ The tropospheric acetaldehyde lifetime is estimated between 8 hours and 1 day.^{149,164,168} Singh et al.¹⁴⁹

have estimated an acetaldehyde total source of $\sim 220 \text{ Tg yr}^{-1}$ with a lifetime of ~ 1 day. There is also some evidence of an oceanic acetaldehyde source, although there is significant error in this estimate.¹⁴⁹ Acetaldehyde shows similar average, maximum, and minimum mixing ratios at both sites (Table 3.1). If acetaldehyde were emitted primarily from biogenic sources, it is unlikely that the mixing ratios would be similar at both TF and AI. Because of its relatively short lifetime (based on OH radical reaction), acetaldehyde mixing ratios should decrease during the transport to AI. The similarity in the average mixing ratios of acetaldehyde between these two sites is likely because of photochemical production of acetaldehyde from hydrocarbon precursors during transport to AI balanced by photochemical destruction of acetaldehyde.

3.3.1.3 Acetone.

Varied sources of acetone in the atmosphere contribute to the estimated global source of 95 Tg yr^{-1} .¹⁴⁵ These include anthropogenic emission, biomass burning, terrestrial vegetation, and plant decay.¹⁴⁵ Additionally, atmospheric oxidation of $\text{C}_3\text{-C}_5$ isoalkanes, methylbutenol, and monoterpenes also contribute to acetone in the troposphere. Oxidation of monoterpenes (120 Tg C yr^{-1}) by hydroxyl radical contributes $7 (4) \text{ Tg yr}^{-1}$ of acetone.¹⁴⁵ The photolysis of acetone is a significant source of hydroxyl radical in the upper troposphere and may contribute up to a third of the hydroxyl radical produced generated in this region.^{145,147} Acetone had an average mixing ratio ~ 400 pptv smaller at AI (1.4 ppbv) than at TF (1.8 ppbv). The maximum mixing ratio of acetone at TF (8.2 ppbv) is nearly double that observed at AI (4.9 ppbv). Larger mixing ratios of acetone at TF suggest a strong biogenic source of acetone at this location. Mixing ratios

of acetone at AI are smaller than at TF and imply uptake to the ocean during transport.^{148,169} The two major and nearly balanced contributors to acetone production in the troposphere are biogenic emission and secondary production from the oxidation of alkanes.¹⁴⁵ As acetone has a fairly long atmospheric lifetime of 61 days¹⁷⁰ and is produced by photochemical oxidation and biogenic emissions, it would be expected that mixing ratios of acetone at AI would larger than at TF.

3.3.1.4 MEK.

While no quantitative emissions have been determined for MEK, a first estimate global source of $\sim 11 \text{ Tg yr}^{-1}$ has been proposed, and anthropogenic sources of MEK are estimated at less than 1 Tg yr^{-1} .¹⁴⁹ This compound has also been shown to have biogenic sources.¹⁷¹ Median mixing ratios of MEK in the remote troposphere are estimated at 20 pptv.¹⁴⁹ One source of MEK in the troposphere is the oxidation of *n*-butane.^{85,172} Besides an oxidation product of butane, MEK has also been measured as a biogenic emission.^{173,174} MEK has a lifetime of between 7 and 13 days,¹⁷⁵ but very little is known about the origins and processing of MEK in the troposphere. MEK shows remarkably similar mixing ratios between the two locations: AI and TF. Mixing ratios of *n*-butane from the Sive group¹⁷⁶ GC/MS at TF give a maximum value of 599 pptv and an average of 116 pptv. The maximum mixing ratio of MEK is nearly three times greater than the maximum mixing ratio of *n*-butane, and the average value is two times greater. These mixing ratios of *n*-butane and the MEK mixing ratios detailed in Table 3.1 strongly suggest another source of MEK in the area. Similar average mixing ratios of MEK at both

TF (0.22 ppbv) and AI (0.16 ppbv) suggest either secondary production through photochemical reactions during transport or minimal deposition during transport.

3.3.1.5 Monoterpenes.

Monoterpenes ($C_{10}H_{16}$) make up a large class of molecules and are emitted into the atmosphere at rates around 123 Tg C yr^{-1} .² In the northeastern United States, the most abundant are α - and β -pinene.¹⁷⁷ Several studies have investigated the products of monoterpene reactions with hydroxyl radical both in the presence and absence of NO .¹⁷⁸ Major products measured from these reactions are pinonaldehyde, acetone, acetic acid, formic acid, and formaldehyde. However, product yields from these studies vary significantly^{77,179-185} and have been investigated¹⁸⁶ based on the proposed mechanisms elucidated by Peeters et al.¹⁸⁷ While the quantitative yields of the products are still unresolved, over 70% of the products are carbonyl containing compounds. Mixing ratios of monoterpenes and isoprene observed at TF are 5-6 times greater than those observed at AI. AI is a remote and rocky location with most biomass consisting of low level shrubs. Because of the short lifetimes of both isoprene and the monoterpenes, the time for continental to marine transport generally results in full oxidation of these compounds. At TF, average mixing ratios of monoterpenes are 0.69 ppbv, and this vegetated area is a source of these compounds. At AI, much smaller average mixing ratios of 90 pptv are observed. The significantly smaller mixing ratios at this site indicates that there is no (or a minor) source of monoterpenes at this site, and that monoterpenes are nearly fully oxidized during transport from the continent to the island. Loss of monoterpenes during

transport is further reflected in the maximum mixing ratio observed at TF (5.8 ppbv) when compared the maximum observed at AI (~900 pptv). These observations are consistent with the estimations of the lifetimes of α - and β -pinene during the day by reaction with OH radical (3.4 and 2.3 hours respectively) and at night by reaction with NO_3 (6 and 15 minutes respectively).¹⁰⁵

3.3.1.6 Isoprene.

Isoprene is one of the most important biogenic VOCs, as it contributes to approximately 44% of the VOC emissions to the atmosphere.¹⁸⁸ It is estimated that the total flux to the atmosphere is ~500 Tg C yr⁻¹.¹⁸⁸ Vegetation such as mosses, ferns, and trees are the primary sources of isoprene. Biogenic emissions of isoprene are strongly dependent on temperature and light.¹⁸⁹ While biogenic emissions dominate, anthropogenic sources of isoprene have been shown to be important in urban areas in winter.¹⁹⁰ Isoprene is reactive to atmospheric oxidants because of the presence of two carbon-carbon double bonds which are more sensitive to addition reactions of atmospheric oxidants compared to abstraction mechanisms for saturated compounds. Major loss mechanisms in the atmosphere include reaction with hydroxyl radical and NO_3 .^{2,191} Isoprene may also contribute more to tropospheric ozone production than anthropogenic VOCs in areas with high NO_x .^{192,193} Under high NO_x conditions, first generation products (~60%) of the hydroxyl radical reaction with isoprene are methyl vinyl ketone, methacrolein, formaldehyde and 3-methyl furan.¹⁹⁴⁻²⁰⁰ A more recent study has measured the first three products, but has not detected 3-methyl furan from the

oxidation of isoprene.²⁰¹ At TF, average isoprene mixing ratios were ~500 pptv, over four times larger than observed at AI (~140 pptv) indicating that vegetation at TF is a primary emission source of isoprene. However, there may be a small local source of isoprene at AI because of low level vegetation present on the island. Maximum mixing ratios at TF are ~7 ppbv and ~1 ppbv at AI. Lifetime of isoprene during the day is 1.7 hr from reaction with OH radical, and 0.8 hr by reaction with NO₃ at night.¹⁰⁵ While nighttime reaction of isoprene with NO₃ has generally been reported to be significant,²⁰² regional conditions at TF suggest that nighttime oxidation processes are minor.^{153,203} Recent work²⁰¹ has shown the primary pathways in the oxidation of isoprene by OH radical result in formation of MVK, MACR, and formaldehyde.

3.3.1.7 MVK+MACR.

From product studies of the OH radical oxidation of isoprene under high NO_x conditions, molar yields for MVK and MACR are approximately 30 and 20%, respectively.²⁰⁴ The average mixing ratio of MVK+MACR at TF is 0.38 ppbv which is double the mixing ratio at AI (0.19 ppbv). The maximum mixing ratios of MVK+MACR at AI and TF are 3.55 and 1.86 ppbv, respectively. Again, the larger mixing ratios of MVK+MACR at TF are because of the local source of isoprene. While the short atmospheric lifetime of isoprene essentially ensures complete oxidation to MVK+MACR by the time it reaches AI, the smaller MVK+MACR mixing ratios observed at AI are likely because of reaction with atmospheric oxidants during transport.

Differences in the mixing ratios for compounds measured at AI and TF are due primarily to site location and oxidation processes during transport to AI. This is most

apparent with monoterpenes which have very small average and maximum mixing ratios at AI compared to the source emission from TF. A similar trend is observed with isoprene where decreased mixing ratios are observed at AI when compared to TF. The oxidation products of isoprene, MVK+MACR, further show decreased mixing ratios at AI when compared to TF. This suggests some uptake of these compounds to the surface or further photochemical oxidation processes. Both methanol and acetone show similar average and maximum mixing ratios at both sites. As both of these are biogenically emitted and photochemically produced, somewhat larger values at AI from continental transport would be expected. This suggests that other processes are involved in removal of these two compounds from the atmosphere. Both MEK and acetaldehyde have similar mixing ratios at both sites, but acetaldehyde shows an increased average mixing ratio at AI, and is the only VOC in this analysis where this is observed. This is potentially from photochemical production during transport or evolution from the marine environment.

3.3.2 Average Diurnal Trends at TF and AI

A general understanding of the diurnal behavior of the compounds monitored is useful for comparing TF and AI. To do this, an hourly unweighted average of mixing ratios was calculated for each compound for the duration of ICARTT 2004. The average was calculated from all the data obtained by the PTR-MS at AI and TF with cycle times between 5 and 15 minutes (Chapter 2). The results are shown in Figures 3.3-3.5.

3.3.2.1 Biogenic VOCs at TF and AI.

The biogenic compounds isoprene, monoterpenes, and methanol are shown in Figure 3.1. TF shows strong diurnal trends for all of these compounds. Isoprene and methanol peak around mid-day. This similarity of the diurnal trends for both of these compounds is consistent with production of these compounds from a dominant biogenic source.²⁰⁵ Mixing ratios are at a minimum just before sunrise because of nighttime deposition, nighttime chemistry, and isoprene sources stop emitting during the evening. After the increase of methanol mixing ratios in the morning, mixing ratios remain fairly constant at around 3 ppbv during the day, decreasing at night to just greater than 1 ppbv before sunrise. Isoprene shows a peak mixing ratio of just less than 1 ppbv before sunset and a minimum of ~ 200 pptv before sunrise. Isoprene is emitted throughout the daylight hours but also reacts with OH radical. Figure 3.1 shows that isoprene increases in the morning to ~500 pptv, where it remains fairly constant because of emission balanced with OH radical reaction until the late afternoon. As OH radical concentration begins to decrease, an elevation of isoprene is observed peaking around 7PM EDT.

Conversely, monoterpenes show large mixing ratios of more than 1.5 ppbv at night, decreasing during the morning with a minimum ~300 pptv during mid-day. While monoterpenes are constantly emitted from trees, the profile observed from this data is due primarily to reaction with OH radical during the day and buildup of these compounds in the boundary layer at night.¹⁵³

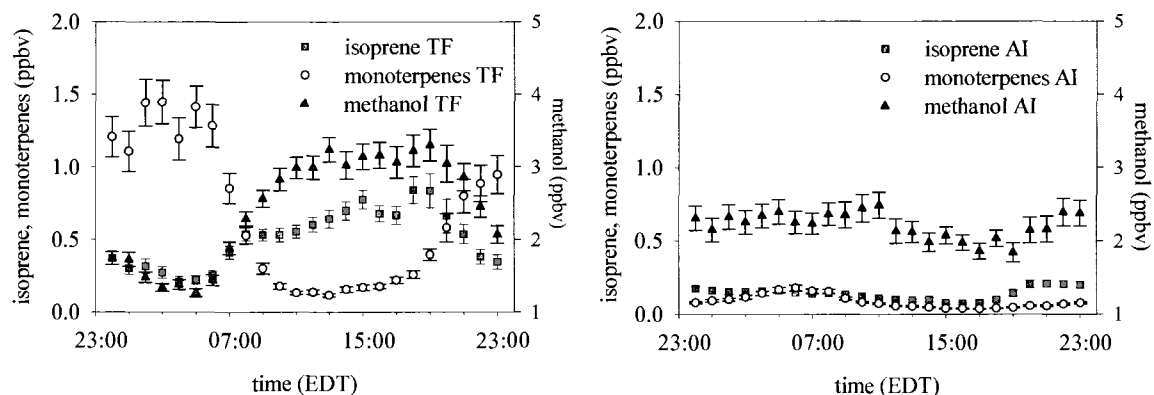


Figure 3.1: Average isoprene, monoterpene, and methanol mixing ratios at TF (left) and AI (right) for the duration of ICARTT 2004 (error bars indicate 95% confidence interval).

Diurnal trends for the compounds shown in Figure 3.1 are significantly different at AI than TF. Despite the proximity of AI to TF, the comparison between the continental and the marine location shows that considerable chemical consumption of these compounds occurs during transport.

At AI, methanol mixing ratios show a slight enhancement early in the day to around 2.5 ppbv and decrease throughout the day to maintain a fairly constant mixing ratio at night. Isoprene peaks just before sunset to ~300 pptv and decreases to ~100 pptv in the late afternoon. Monoterpenes at AI show little diurnal variation, again contrasting with observations of monoterpenes at TF. There is a shallow diurnal profile for the monoterpenes at AI, with a minimum in the late afternoon and a peak around 6AM EDT, while the peak mixing ratio of monoterpenes occurs in the very early morning hours (~2AM EDT) at TF.

Differences in the mixing ratios of these compounds are due almost exclusively to transport from the continent as there are few sources of these biogenic compounds on AI.

Decreases in methanol, isoprene, and monoterpenes are observed at AI throughout the day because of reaction of these compounds with OH radical. Mixing ratios increase late in the evening and remain constant throughout the night. At TF mixing ratios of these compounds are generally what is expected for vegetated areas. As monoterpenes are emitted constantly throughout the day and night, the decrease in monoterpene mixing ratio is because of reaction with hydroxyl radical. A strong source of isoprene allows for the increase in isoprene mixing ratios during the day, but notably mixing ratios increase at a greater rate after hydroxyl radical concentrations begin to wane (4PM EDT).

3.3.2.2 VOC Oxidation Products at TF and AI.

Typical atmospheric oxidation products of acetone, and MVK+MACR were compared and diurnal profiles are shown in Figure 3.2. Based on the average mixing ratios of these compounds, the increase during daytime hours at TF correlates with the emission of VOCs from vegetation. Essentially flat diurnal profiles at AI indicate well mixed and longer lived oxidized compounds detected at the island.

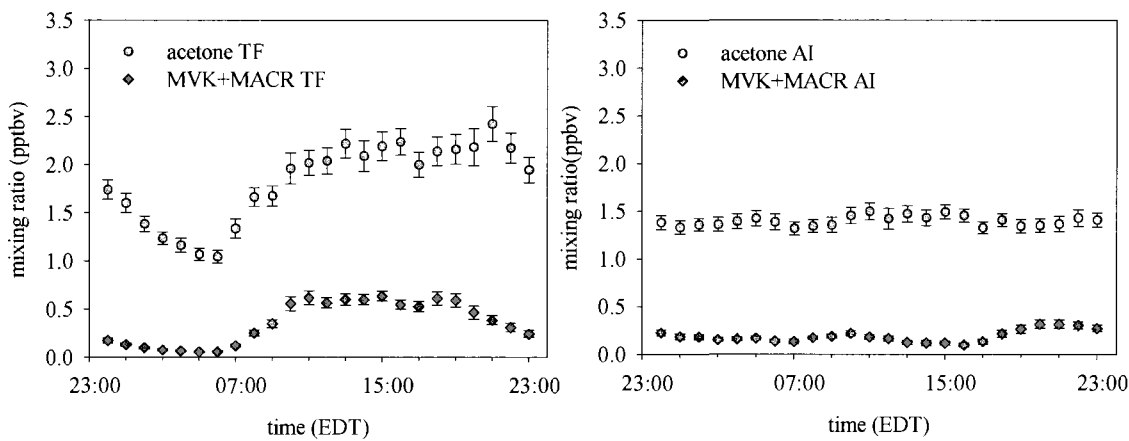


Figure 3.2: Average mixing ratios of acetone, and MVK+MACR at TF (left) and AI (right) during ICARTT 2004 (error bars indicate 95% confidence interval).

Differences in the diurnal trends between AI and TF are shown in Figure 3.2. Acetone and MVK+MACR peak during mid-day at TF. Acetone mixing ratios increase to more than 2 ppbv during this period, and MVK+MACR reaches a maximum of between 500 and 700 pptv. Minimum values of 1 ppbv for acetone <10 pptv for MVK+MACR are observed prior to sunrise at TF. MVK+MACR are the primary oxidation products from the isoprene. As acetone has varied sources and a long atmospheric lifetime, mixing ratios are expected to be somewhat larger at AI from photochemical production during transport.

At AI, minimal diurnal variation is observed for acetone and daily fluctuations of MVK+MACR are shallow and opposite of what is observed at TF. Here, mixing ratios of MVK+MACR reach a minimum value ~20 pptv during mid-day and a maximum around sunset that slowly decreases during nighttime. Mixing ratios of MVK+MACR increase with sunrise followed by a decrease during the day. Decrease in the mixing ratio of MVK+MACR at AI during the day suggests photochemical oxidation of these

compounds and nighttime decrease may indicate loss of these compounds because of deposition or reaction with NO_x from enhanced NO_x in the continental outflow.²⁰³

Increases in mixing ratios of acetaldehyde and MEK at TF begin at sunrise (Figure 3.3). Increases in the morning at TF lead to fairly constant mixing ratios of acetaldehyde during the day, with a decrease around 4PM EDT when hydroxyl radical concentrations decrease. The increase to ~400 pptv around 8PM EDT is then followed by a decrease overnight which may be due to deposition. MEK diurnal profiles are similar at TF, which also decrease in the late afternoon when hydroxyl radical concentrations are smaller. This indicates that the presence of MEK at TF is due not only to biogenic emissions but also photochemical production.

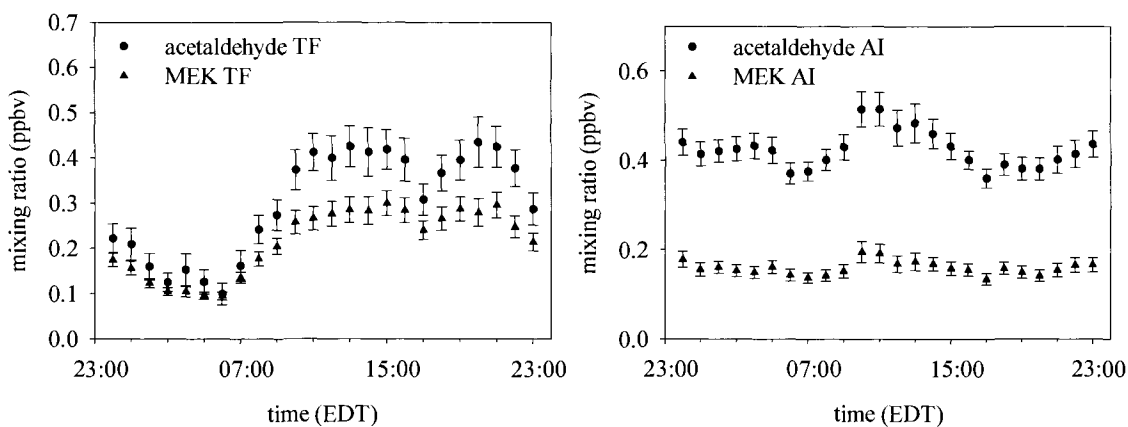


Figure 3.3: Average mixing ratios of acetaldehyde and MEK at TF (left) and AI (right) during ICARTT 2004 (error bars indicate 95% confidence interval).

At AI, no clear diurnal trend is observed although acetaldehyde and MEK at TF and AI have similar profiles (Figure 3.3). A decrease from the peak average acetaldehyde mixing ratio of 500 pptv to ~350 pptv from 9AM EDT until 4PM EDT is observed at AI. This decrease in acetaldehyde may be because of reactivity with atmospheric oxidants. It

can be seen that around sunrise (~6AM EDT) there is a marked drop in acetaldehyde and MEK at AI. An increase in the mixing ratio of acetaldehyde is observed at AI during from early evening (8PM EDT) until late evening (11PM EDT). In a similar case, MEK decreases from 200 pptv to 120 pptv during this same period at AI. Acetaldehyde mixing ratios at AI are all at least 100 pptv larger than those measured at TF. This suggests additional processing and additional sources of acetaldehyde (*e.g.* hydrocarbon oxidation) during transport to AI and inefficient deposition during the transport.

Acetone, MVK+MACR, acetaldehyde, and MEK at TF show similar trends of increase in mixing ratios during the day because of photochemical production (MVK+MACR) or a combination of both biogenic emission and photochemical production. All of these compounds show a decrease in mixing ratios around 4PM EDT when hydroxyl radical concentration begins to decrease, and a further increase in mixing ratios until ~10PM EDT. Following the peak mixing ratios, nighttime loss of VOCs occurs from dry deposition. A very different scenario is observed at AI, where the acetone profile is flat and nearly the average mixing ratio observed at TF, indicating loss of this VOC during transport to AI. MVK+MACR shows a decrease in mixing ratios at AI during mid-day because of photochemical oxidation. Both acetaldehyde and MEK show a decrease in mixing ratios throughout the day, likely because of photochemical consumption. This decrease is followed by a noticeable increase at night partially because of smaller reactivity with NO_x .

3.3.3 Deposition Velocities at TF

Based on (3.2), deposition velocities (cm s^{-1}) for compounds at TF were calculated using averaged data collected during ICARTT 2004 (Table 3.2) and the diurnal profiles of the compounds shown in Figures 3.3-3.5.

Table 3.2: TF deposition velocities calculated from hourly averaged diurnal profiles during ICARTT 2004 at boundary layer heights of 70, 100, and 125 m.

	Deposition Velocity, v_d (cm s^{-1})		
	70 m	100 m	125 m
methanol	0.19	0.27	0.34
acetaldehyde	0.26	0.38	0.47
acetone	0.18	0.26	0.33
MEK	0.21	0.30	0.38
MVK+MACR	0.46	0.66	0.82

Deposition velocity calculations allow for quantification of VOC loss to the surface by flux calculations (3.1). To ensure sampling of continental air masses for the determination of deposition velocity, mixing ratios of bromoform (CHBr_3) can be useful. Bromoform is an indicator of marine derived air masses; therefore sorting VOC data based on bromoform mixing ratios less than the median value (3.9 pptv) ensures that the sampled air masses are continental rather than marine.¹⁴⁸ Calculated deposition velocities at TF are based on boundary layer heights of 70, 100, and 125 m^{148,153} and are shown in Table 3.3.¹⁴⁸

Table 3.3: TF deposition velocities calculated from hourly averaged diurnal profiles where $\text{CHBr}_3 < \text{median}$, during ICARTT 2004 at boundary layer heights of 70, 100, and 125 m.

	Deposition Velocity, v_d (cm s^{-1})		
	70 m	100 m	125 m
methanol	0.23	0.33	0.42
acetaldehyde	0.20	0.28	0.35
acetone	0.13	0.19	0.24
MEK	0.24	0.34	0.43
MVK+MACR	0.47	0.68	0.84

When mixing ratio data is sorted as described above, deposition velocities remain essentially constant compared to unsorted data (data including marine derived air masses). Deposition velocities differing by $\sim 0.02 \text{ cm s}^{-1}$ (Table 3.3) indicate that the interference of marine derived air masses on data averaged during the campaign is minor.

It should be noted that MVK+MACR shows the highest deposition velocity (0.68 cm s^{-1}) which is at least twice the deposition velocity of the other compounds. Experimentally determined deposition velocities reported over a tropical rain forest for these two compounds were estimated between 0.02 and 0.45 cm s^{-1} .^{120,125}

Methanol and MEK have deposition velocities in the vicinity of 0.3 cm s^{-1} . The deposition velocity for MEK has been calculated in one study, with a value of 0.50 cm s^{-1} .¹⁵³ The deposition velocity of methanol at TF during ICARTT 2004 is similar to the deposition velocity calculated by Talbot et al.¹⁵³ of 0.54 cm s^{-1} . The average dry deposition velocity of methanol at TF of 0.27 cm s^{-1} is similar to the methanol deposition velocity determined by Karl et al.¹²⁰ of $0.27(14) \text{ cm s}^{-1}$ for a tropical rain forest. This value is more than that calculated (0.12 cm s^{-1}) by Jacob et al.²⁰⁶

The smallest deposition velocity at 100 m calculated from the averaged data is for acetone (0.19 cm s^{-1}). The acetone deposition velocity presented here is 0.10 cm s^{-1} smaller than the acetone + propanal deposition velocity calculated by Talbot et al.¹⁵³ MVK+MACR has a deposition velocity $\sim 0.4 \text{ cm s}^{-1}$ larger than previously reported values.¹⁵³ The large apparent deposition velocity of MVK+MACR may be because of enhanced surface uptake at TF or interference from other processes not considered. The deposition velocities are also compared to those reported by Karl et al.¹²⁰ and are shown

in Table 3.4. While the deposition of the compounds occurred over an Amazonian rain forest, the ultimate deposition velocity of these compounds is the same within error.

Table 3.4: Average deposition velocities at TF at a boundary layer height of 100 m compared to those reported by Karl et al.¹²⁰

<u>Compound</u>	<u>v_d, 100 m</u> <u>CHBr₃</u> <u>sorted</u>	<u>v_d, 100 m</u> <u>overall</u>	<u>v_d</u> [*]
methanol	0.33	0.27	0.27(0.14)
acetaldehyde	0.28	0.38	0.26(0.03)
acetone	0.19	0.26	0.14(0.01)
MEK	0.34	0.30	N/A
MVK+MACR	0.68	0.66	0.45(0.15)

*Karl et al.¹²⁰

Acetaldehyde shows a similar deposition velocity to what is reported by Karl et al.¹²⁰ but variations in the deposition velocity depending on location and average mixing ratios are noted by other studies.^{112,207} Acetaldehyde deposition has been reported to be between 0.02 and 0.3 cm s⁻¹.^{120,125,207}

In general, estimates for deposition velocities of methanol, acetone, acetaldehyde, MVK+MACR, and MEK compare well to other studies despite differences in surface composition and meteorological conditions. These estimates should be useful for regional atmospheric models and quantifying the atmospheric loading of these compounds when applied to summer conditions in New England.

3.3.4 VOC Loss at AI

Because of the high boundary layer above the marine environment at AI deposition of VOCs is calculated by correlations of wind speed (Figure 3.8) although there are other ways to estimate uptake to water.¹³⁵⁻¹³⁸ These data were sorted such that

isoprene mixing ratios were below the 10th percentile to minimize continental influence as isoprene is derived primarily from continental vegetation. As wind speed increases, there is some evidence for uptake to the ocean surface (Figure 3.4) for a few of the compounds.

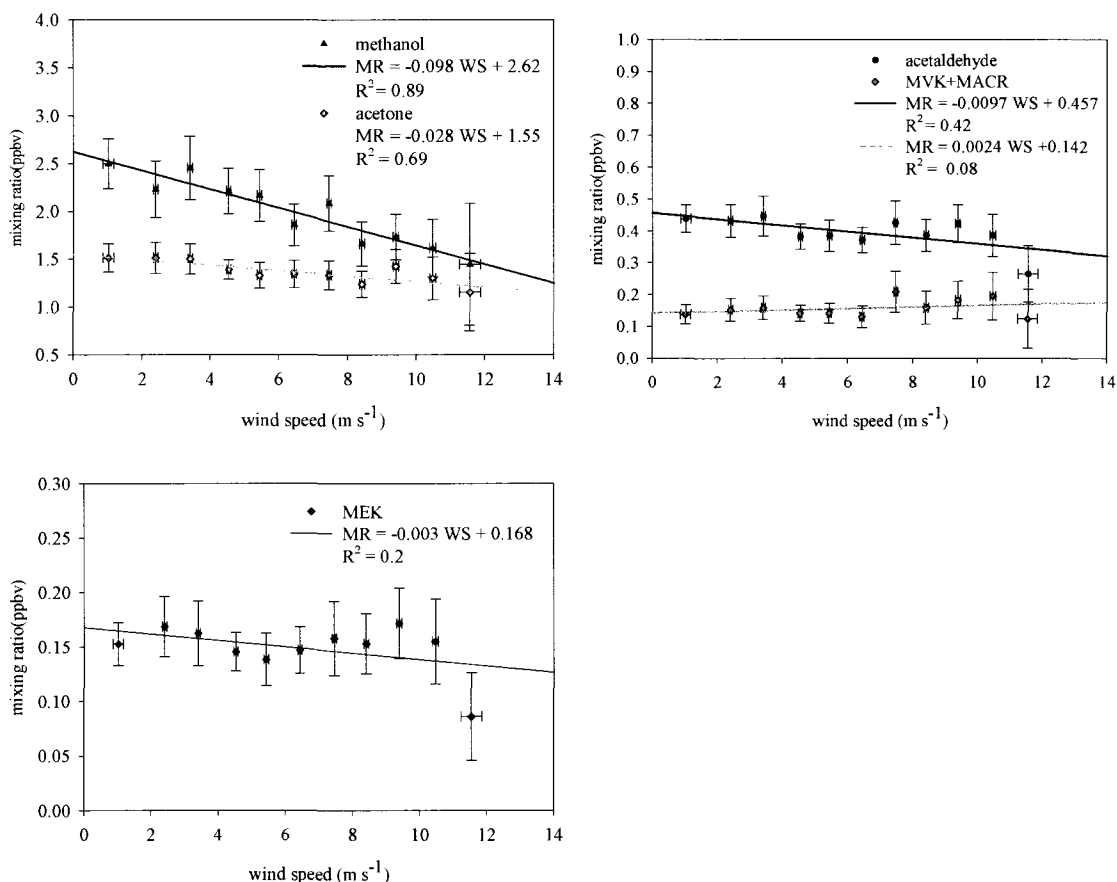


Figure 3.4: Correlation of methanol, acetone, acetaldehyde, MVK+MACR, and MEK with wind speed at AI during ICARTT 2004.

Slope of the mixing ratios with wind speed implies the effective loss of compounds through wind driven processes. The steepest slope of -0.10(1) ppbv s⁻¹ is observed with methanol, implying greater loss with increased wind speed. Acetone also has a significant loss because of wind processes (-0.03(1) ppbv s⁻¹). These wind driven

losses are due primarily to the greater solubility of methanol and acetone compared to the other compounds. Oceans have been reported to be both a source and a sink for acetone, leading to potential interference in this estimation of loss.^{145,148,169} It is unclear whether the ocean is a net sink or source of methanol.^{7,208} However, deposition velocities for methanol to ocean surfaces have been reported to be anywhere between 0.01-0.59 cm s⁻¹ with a dependence on wind speed.¹⁴¹

There are no clear trends of decreasing mixing ratios with increasing wind speed observed with acetaldehyde or MEK. The slope for acetaldehyde is -0.010(4) ppbv s m⁻¹, and MEK has a slope of -0.003(2) ppbv s m⁻¹. The large relative error in the MEK slope indicates that definitive loss through wind driven processes at AI is unlikely. The same is observed with MVK+MACR, where the slope is 0.002(3) ppbv s m⁻¹.

Overall, ocean uptake only seems significant for the two more soluble trace gases, methanol and acetone. This is in agreement with other studies.^{141,148} Each of these compounds show a decrease in mixing ratios as wind speed increases, indicating loss to the ocean environment because of wave processes and wind turbulence.

3.4 Summary and Conclusions

Methanol, acetone, acetaldehyde, MEK, MVK+MACR, isoprene, and monoterpenes were measured by PTR-MS at AI and TF during the ICARTT 2004 summer campaign. Averaged diurnal profiles during the course of July-August show significant differences between these two sites. TF is a rural site with primary emission sources of biogenic VOCs. AI is a remote marine site, and while there are still significant amounts of biogenic VOCs detected, the oxidation products from these VOCs show

larger mixing ratios. Deposition velocities of the compounds listed are generally in good agreement with other studies and may prove to be useful in determining the fate of these oxygenated VOCs in regional atmospheric models.

Biogenics such as isoprene and monoterpenes show strong source strength at TF. Emission of isoprene during the day is enough to offset oxidation by OH radical whereas monoterpenes show a sharp decrease in mixing ratios during the day at TF because of reaction with OH radical. A sharp increase in both of these compounds is observed when OH radical concentrations begin to decrease at ~4PM EDT. Methanol shows an increase during the day at TF from both photochemical production and biogenic sources. A similar trend is observed for acetone at TF, but here mixing ratios remain constant until the decrease in OH radical causes a decrease in the monitored acetone mixing ratio. From this it can be observed that acetone is not only biogenically derived, but has a strong photochemical source at TF. Similar trends for MVK+MACR, MEK, and acetaldehyde are observed at TF, but acetaldehyde seems to be more dependent on photochemical production from precursors. Deposition velocities of all of these compounds agree well with previously reported values, although MVK+MACR appears to deposit with greater affinity to vegetation at TF than the other compounds.

Mixing ratios of compounds at AI differ depending on their primary source. Isoprene and monoterpene mixing ratios at AI are much smaller than observed at TF because of photochemical destruction of these compounds during transport to AI. Both methanol and acetone mixing ratios remain elevated during transport to AI although oxidation of precursors should lead to somewhat elevated mixing ratios of these two

compounds during transport. This suggests that these compounds are lost via dry deposition to the ocean or to other unaccounted processes. In fact, both of these compounds show uptake to the water surface, in agreement with other studies.^{141,147,148} MVK+MACR at AI shows somewhat smaller mixing ratios compared to TF. The decrease of MVK+MACR during the daylight hours indicates that photooxidation of these compounds occurs at the island as there is no clear trend in the loss of these compounds to the ocean surface. Acetaldehyde and MEK show a significant increase in mixing ratios during the early morning hours at AI, followed by a decrease in the afternoon. This decrease does not seem to be related to deposition, but is likely photochemical destruction of these compounds. Interestingly, all of the compounds at AI show a decreased in mixing ratios during sunrise. There is some potential that these decreases in mixing ratios in the early morning at AI may correlate with the oxidation of VOCs by chlorine radical.⁴⁶

CHAPTER 4

OXIDATION OF α - AND β -PINENE BY CHLORINE ATOMS

4.1 Introduction

4.1.1 Environmental Chambers

In order to detail specific atmospheric reactions and transformations of VOCs, potential reactions (*e.g.* oxidation mechanisms or aerosol formation) must be evaluated in controlled conditions, isolating the reactive compounds from unconstrained variables present in the atmosphere. Once experimentally determined products and reaction mechanisms have been proposed, evidence for these reactions in ambient conditions may be undertaken by atmospheric field studies. The most common method for simplifying and controlling atmospheric conditions and composition is by use of environmental reaction chambers.^{1,12,41,76,183,209-223} In these enclosures, measured quantities gaseous compounds are added and mixed with clean air under well defined humidity and temperature. Addition of an illumination source for the chamber initiates photochemical reactions, and concentration profiles of reactants and products may then be monitored over time. Disappearance of reactants and product production (*i.e.* reaction kinetics) may then be related to ambient atmospheric conditions from field studies. Because of marine influenced air masses on continentally derived VOCs in the Northeast, there is a large potential for oxidation of monoterpenes by marine derived chlorine. Recently,

environmental chamber studies by Cai and Griffin²¹⁴ have shown secondary organic aerosol (SOA) formation from Cl radical oxidation of monoterpenes.

4.1.2 Chlorine Reactions with Monoterpenes

Monoterpenes (C₁₀H₁₆) are volatile organic compounds emitted by vegetation, with the emission generally dominated by forests.² The emission rates of monoterpenes are particularly large in the Northeastern United States.^{2,224-229} In this large class of molecules, α - and β -pinene predominate in the northern latitudes.^{2,224-229} Tropospheric chemistry in the Northeastern coastal region has been shown to be strongly influenced by these compounds.^{226,229} Further, it has been shown that the presence of both α - and β -pinene correlates with tropospheric particulate organic matter.^{211,230}

While it is known that ozone,^{183,211,231-241} NO₃,^{203,242,243} and hydroxyl radical^{180,182,185-187,222,244-260} are important oxidants for monoterpenes, chlorine radical may also oxidize these compounds as it has been shown to exist in significant concentrations during the early sunlight hours in the marine troposphere of the Northeastern US (Chapter 1).^{46,51}

Chlorine oxidation reactions may be important in the marine troposphere, and one study has investigated the SOA formation of chlorine atom oxidation of monoterpenes.²¹⁴ Three studies have addressed the kinetics associated with the chlorine oxidation of monoterpenes.²⁶¹⁻²⁶³ Of these, only two have addressed the kinetics of Cl atom reaction with α - and/or β -pinene.^{261,262} Hydrogen abstraction has been proposed to proceed via two different pathways: (i) a direct allylic H abstraction, or (ii) an addition-elimination

reaction, both forming allylic radical and HCl. In the case of β -pinene, Finlayson-Pitts et al.²⁶¹ estimate that the hydrogen abstraction pathway may account for up to 50% of the reaction.

In order to assess the potential reaction mechanisms of chlorine with monoterpenes, study of chlorine reactions with other biogenic alkenes is useful for understanding ultimate products and key reaction steps.

4.1.3 Chlorine Reactions with Other Alkenes

Chlorine reactions with noncyclic alkenes have undergone substantially more scientific inquiry than those involving monoterpenes.^{219,261,264-274} These studies are of particular interest because the ultimate products of chlorine oxidation may serve as unique markers of chlorine chemistry and may give some insight into chlorine reaction mechanisms. Of note is the chlorine oxidation of isoprene,^{264,265,268-270,273-275} a common tropospheric biogenic VOC with large reactivity to Cl because of its two double bonds. Chlorination of isoprene is of note as some of the ultimate products are also observed in the OH/NO oxidation of isoprene, implying that both OH/NO and Cl oxidation may be responsible for the oxidation products in areas where there is an influence of both continental and marine air.

In the chlorine initiated oxidation of isoprene in NO_x free air, major products represent both chlorine addition and hydrogen abstraction pathways.²⁷³ Kinetics and reaction mechanisms accounting for these pathways have been recently proposed by Orlando et al.²⁶⁴ Intermediates in the oxidation pathways after addition of oxidant are

alkyl peroxy radicals and alkoxy radicals.^{268,276} This study did not show expected oxidation products (from analogy to OH radical initiated oxidation) of methyl vinyl ketone (MVK) and methacrolein (MACR). Major products observed but not quantified were 1-chloro-3-methyl-3-buten-2-one (CMBO) and chloro-methyl-butenal (CMBA). In the absence of NO_x, Orlando et al.²⁶⁴ suggest that the major pathway for removal of oxygen from the peroxy radical to form the alkoxy radical is via reaction with other alkyl peroxy radicals. Products CMBO and CMBA have been used as markers of chlorine chemistry in urban environments.^{45,274,277}

In studies by Fantechi et al.²⁶⁸ major products of chlorine reaction with isoprene were reported as HCl, formaldehyde, formic acid, methyl glyoxal, CO, and CO₂. Intermediate radicals may originate from the elimination of CH₂Cl radical via secondary reactions with MVK or MACR to account for the observed formation of formyl chloride (HC(O)Cl).²⁶⁸ The pathway for methyl glyoxal formation proposed by Fantechi et al.²⁶⁸ was questioned by Orlando et al.²⁶⁴ citing that the more favorable elimination is of CH₃CO over elimination of CH₂Cl from CH₃(C=O)CH(O·)CH₂Cl.

It has been suggested that in the Cl oxidation of isoprene, the allylic abstraction pathway may account for up to 15% of the reaction. The abstraction pathway in the oxidation of isoprene was shown to account for less than 10% (a minor pathway), in disagreement with the estimation by Ragains et al.²⁷³ In a chamber study by Kaiser et al.²⁷⁸ a comprehensive analysis of the chlorine reaction with *cis*- and *trans*-2-butene was carried out. This study was done in N₂ with O₂ as a contaminant. Products formed from

the Cl oxidation were from Cl addition, elimination, and hydrogen abstraction mechanisms.

Products from the chlorine reaction with alkenes in the presence of molecular oxygen are comprised primarily of aldehydes and ketones. As these compounds are formed in an atmosphere of atomic chlorine, it is further useful to determine the reactivity of chlorine with a variety of aldehydes and ketones that may be formed in the reaction of monoterpenes with atomic chlorine.

4.1.4 Chlorine Reactions with Aldehydes/Ketones

Chlorine reactions with aldehydes have rate constants on the order of $10^{-10} \text{ cm}^3 \text{ molecule}^{-1} \text{ s}^{-1}$.^{264,266,279-281} For ketones, in the case of acetone, the reaction with Cl has a rate constant substantially smaller than what has been observed with saturated and unsaturated VOCs.²⁸²⁻²⁸⁵ The rate constant for the reaction of Cl with acetone is $3.0(4) \times 10^{-12} \text{ cm}^3 \text{ molecule}^{-1} \text{ s}^{-1}$.

There is significant variability in the reaction rate of chlorine with ketones, as shown by Notario et al.²⁸⁶ In this study, a series of ketones was reacted with chlorine atoms. Larger and branched ketones, such as 5-methyl-2-hexanone ($4.7 \times 10^{-10} \text{ cm}^3 \text{ molecule}^{-1} \text{ s}^{-1}$), have much larger rate constants than smaller ketones. Reaction of chlorine with chloroacetone was also investigated, with a rate coefficient of $3.5(4) \times 10^{-10} \text{ cm}^3 \text{ molecule}^{-1} \text{ s}^{-1}$.²⁸⁶

Fantechi et al.²⁶⁸ and Orlando et al.²⁶⁴ have proposed reactions of chlorine atoms with two common OH radical oxidation products of isoprene, MVK and MACR. Orlando et al.²⁶⁴ noted that chloroacetaldehyde was formed by chlorine addition to the terminal

carbon of MVK followed by elimination of CH₃CO. The product observed by Fantechi, et al.²⁶⁸ (methyl glyoxal) was not observed and was instead attributed to chloroacetone by Orlando et al.²⁶⁴ HCl forms through the reaction of chlorine atoms with CH₂O.^{287,288} Other products in the MVK reaction include CO, CO₂, formic acid, and formyl chloride. Formation of HCl in these systems indicates hydrogen abstraction pathways.

In the presence of molecular oxygen, typical intermediates in oxidation reactions are alkyl peroxy radicals. Addition of an atmospheric oxidant (*e.g.* Cl or OH radical) to an alkene will result in a radical that is available for O₂ addition which forms the corresponding alkyl peroxy radical. Formation of these alkyl peroxy radicals and their subsequent reactions are critical for elucidating product formation and reaction kinetics.

4.1.5 Chlorine Reactions with Alkyl Peroxy Radicals

Reactions of chlorine with alkyl peroxy radicals have been detailed in a few studies.²⁸⁹⁻²⁹³ Karlsson et al.²⁹⁴ proposed a number of different reaction pathways for the organoperoxy radical in the chlorine initiated oxidation of toluene. In the reaction



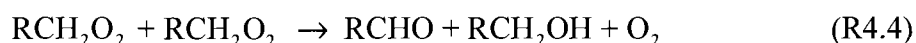
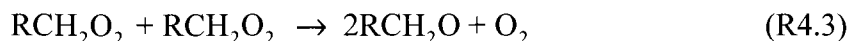
where R is a phenyl group, the rate constant is $1.5 \times 10^{-10} \text{ cm}^3 \text{ molecule}^{-1} \text{ s}^{-1}$. Reaction of chlorine atoms with the tolylperoxy radical may result in the formation of a Criegee intermediate (C.I.) through the reaction



or may proceed via the deoxygenation of the tolylperoxy radical to form ClO.²⁹⁴

Organoperoxy radicals have a different fate in the absence of other atmospheric

oxidants, namely, these peroxy radicals primarily self react. The rate constant for the self reaction of the tolylperoxy radical is $7(1)\times 10^{-12} \text{ cm}^3 \text{ molecule}^{-1} \text{ s}^{-1}$.²⁹⁵ There are three possible reactions for these tolylperoxy molecules,



with the reaction to form the peroxide (R4.5) accounting for 20% of the reaction, and an equal branching for formation of the aldehyde/alcohol (R4.4) and the benzyloxy radical (R4.3).

The radical formed (R4.3) may undergo a self reaction to form benzyl alcohol and benzaldehyde. Under atmospheric conditions (*i.e.* 20% O_2), the benzyloxy radical (RCH_2O) may react with O_2 to form benzaldehyde and hydroperoxy radical with a rate constant of $\sim 1 \times 10^{-14} \text{ cm}^3 \text{ molecule}^{-1} \text{ s}^{-1}$.^{291,295,296} In general, the overall fate of the organoperoxy radicals from the reactions (R4.3-4.5) is formation of aldehydes and alcohols.²⁹⁷

4.1.6 Specific Aims

The aims of this work are to detail the gas phase products detectable via PTR-MS from the chlorine atom oxidation of α - and β -pinene in an enclosed chamber at atmospheric pressure. Specifically, an environmental chamber (Section 4.2.1) was used to isolate the reactants and blacklights were used for the photodissociation of Cl_2 while gas phase products were monitored via PTR-MS-ss. These products are compared to

hydroxyl radical oxidation products detailed in the literature. Kinetics inherent to the OH radical oxidation and Cl radical oxidation are discussed. Reaction mechanisms are proposed based on the current understanding of chlorine oxidation mechanisms, observed products, and proposed mechanisms given for the hydroxyl radical oxidations. This experimental setup was used in the study for investigation of SOA formation from analogous reactions, and those results have been published elsewhere.²¹⁴

4.2 Experimental

4.2.1 Chamber²¹⁴

The research group (Xuyi Cai, Laura Cottrell) of Robert J. Griffin provided a 0.3 m elevated 260 cm × 260 cm × 130 cm (length, width, height) hemi-cylindrical FEP Teflon[®] chamber in a metal framework was filled with clean air, molecular chlorine, and selected monoterpenes (α -pinene, β -pinene). A cartoon of the basic experimental setup is shown in Figure 4.1. Temperature in the laboratory was maintained between 25-28 °C. Clean air was generated via a TEI (Franklin, MA) 111 zero air generator and subsequently run through an absorbing column to ensure removal of residual NO_x. Air was then run through a 500 °C catalytic converter and over activated charcoal. Water vapor was removed via a desiccant column and the injector flow was run through a dry ice packed cooler.

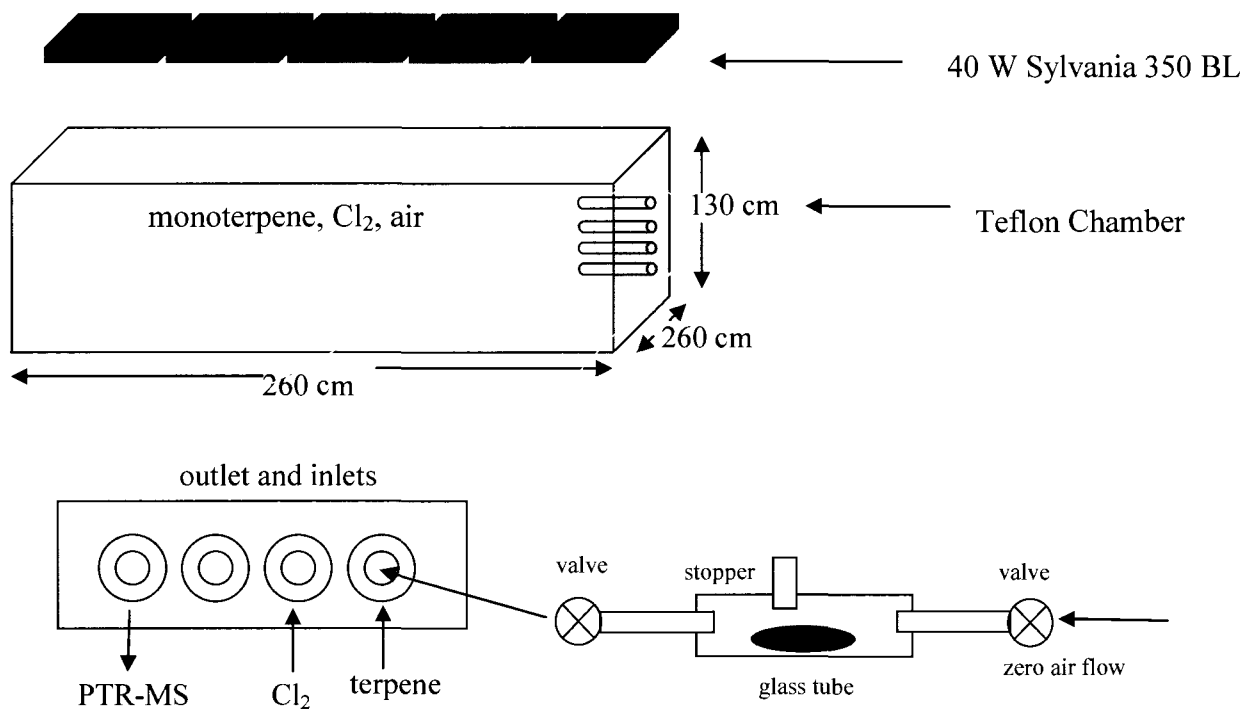


Figure 4.1: Schematic of the Teflon chamber showing components, dimensions, inlets, and outlets.

The VOC and an internal standard (hexafluorobenzene, 100 ppbv) were injected via a glass tube attached to the chamber, using the clean air for dispersion. The hexafluorobenzene standard was used to determine chamber leaks.

In each experiment, 90-420 ppbv of monoterpene was injected into the chamber. Molecular chlorine was injected from a certified cylinder containing 1000 ppm Cl₂ in nitrogen. For each chamber experiment, chlorine mixing ratios were ~100 ppbv.

Once reactants were allowed to mix in the chamber, Cl₂ was photolyzed to atomic chlorine (Cl) by twenty, 122-cm, 40-W Sylvania 350BL lights that generated 300-420 nm ultra-violet (UV) light. Two experiments each were performed for α -pinene and β -pinene. After each experiment, the chamber was irradiated with UV lights for 48 hours

and flushed with clean air for 36 hours. Gas phase products from the oxidation were measured using a PTR-MS-ss (Chapter 2).

4.2.2 PTR-MS-ss

4.2.2.1 Determining Mixing Ratios and Error.

During the course of the chamber experiments, the PTR-MS-ss was operated at a drift tube pressure of ~ 2 mbar and 600 V. The instrument was operated in scanning mode, acquiring data over the range 20-200 amu in 1 amu increments. PTR-MS-ss sub-sampled from a ~ 0.5 LPM flow from the chamber pumped by a Vacuubrand MZ-2 diaphragm pump. Cycle time for Case 1 (Section 4.3.1.1) was 37 seconds. To improve the limits of detection, cycle time for the other cases was increased to 91 seconds for the scan from 20-200 amu. Primary ion signals for Case 1, 2, 3a, and 3b were 2.5(2), 2.5(1), 2.6(1), and $3.0(1) \times 10^6$ cps respectively. Each mass between 20 and 200 amu was analyzed to determine changes in signal with time. Those masses showing a change in signal over time were noted. The mass was then used to ascertain likely products (based on chamber composition and suspected reaction pathways).

Signals for acetone, α -pinene, β -pinene, and acetaldehyde given in the Appendix (Table 4.A3) were converted to mixing ratios based on calibrations using (2.11) and Table 2.3. The compounds acetic acid, pinonaldehyde, and nopinone are known to fragment in PTR-MS.^{76,77,81} Signals of the parent ions and corresponding fragments (Table 4.A3) were converted to mixing ratios using (2.8), with the proton transfer reaction rate constant of 2×10^{-9} cm³ molecule⁻¹ s⁻¹, and transmission values given by

Ionicon. Calculated mixing ratios from each contributing fragment for each compound were then summed and are reported here as the mixing ratios for these compounds. These mixing ratios should be considered lower estimates for pinonaldehyde as other fragmentation products were not resolved and calibration standards were not available. For nopinone, masses 139 and 123 were used to determine the final mixing ratio; this should also be considered a lower estimate. The mixing ratio for acetic acid was taken as the sum of 43 amu and 61 amu. Because of shorter dwell times in one of the α -pinene experiments, the only resolved signals corresponding to pinonaldehyde were m/z 151 and m/z 109. A four point moving average showed the correlation between the fragmentation masses, which are listed in Table 4.A3. Common fragments of molecules are shown in Table 4.A3. Fragmentation is taken from references^{76,77} and from those observed in this study. The major contributor to the signal is shown in bold (Table 4.A3). It is important to note that this table includes masses observed in the OH/NO initiated oxidation of α - and β -pinene.

Mixing ratios are given in ppbv in Figures 4.2- 4.7 and Table 4.2, focusing on the decrease of monoterpene and evolution of products. References in the text to the yield of a particular molecule are molar yields, which are simply mixing ratios of products divided by starting mixing ratio of monoterpene.

Error in the signal is reported as the 95% confidence interval from the average of four cycles, yielding an error based on the average signal in 2.5 minutes (Case 1) and 6 minutes (Cases 2, 3a, 3b). Limits of detection (LODs) for PTR-MS-ss detection of gas phase compounds were determined by (2.12). The LODs for all the compounds

quantified during these experiments are shown in Table 4.1. Background signals were determined by passing chamber air through a catalytic converter catalytic converter (0.5% Pd on alumina at 450 °C) during the experiment (seen as missing data during the α -pinene experiments) or prior to stopping the experiments (in the case of β -pinene). This background signal was averaged and used for determining final mixing ratios and LODs shown in Table 4.1.

Table 4.1: LODs for compounds in the Cl atom oxidation of monoterpenes

<u>Case</u>	<u>Compound</u>	<u>LOD (ppbv)</u>
1	α -pinene	1.1
	acetone	0.4
	acetaldehyde	1.0
	acetic acid	1.6
	pinonaldehyde	1.2
2	α -pinene	1.1
	acetone	0.3
	acetaldehyde	0.3
	acetic acid	0.8
	pinonaldehyde	0.3
3a	β -pinene	0.7
	acetone	0.2
	nopinone	0.3
	m/z 151	0.2
3b	β -pinene	0.3
	acetone	0.4
	nopinone	0.3
	m/z 151	0.2

4.3 Results

4.3.1 Product Identification and Mixing Ratios for the Cl Initiated Oxidation of α - and β - Pinene

4.3.1.1 Case 1: 130 ppbv α -Pinene + 100 ppbv Cl_2

With initial mixing ratios of 130 ppbv of α -pinene and 100 ppbv of Cl_2 , the reaction results in complete oxidation of α -pinene after approximately 200 minutes (Figure 4.2). Major identified products from this oxidation are acetone, pinonaldehyde, and acetic acid. As mentioned previously, acetone is a persistent compound because of its significantly lower reactivity than pinonaldehyde. Pinonaldehyde is also formed, and is shown to be an intermediate product in this reaction.

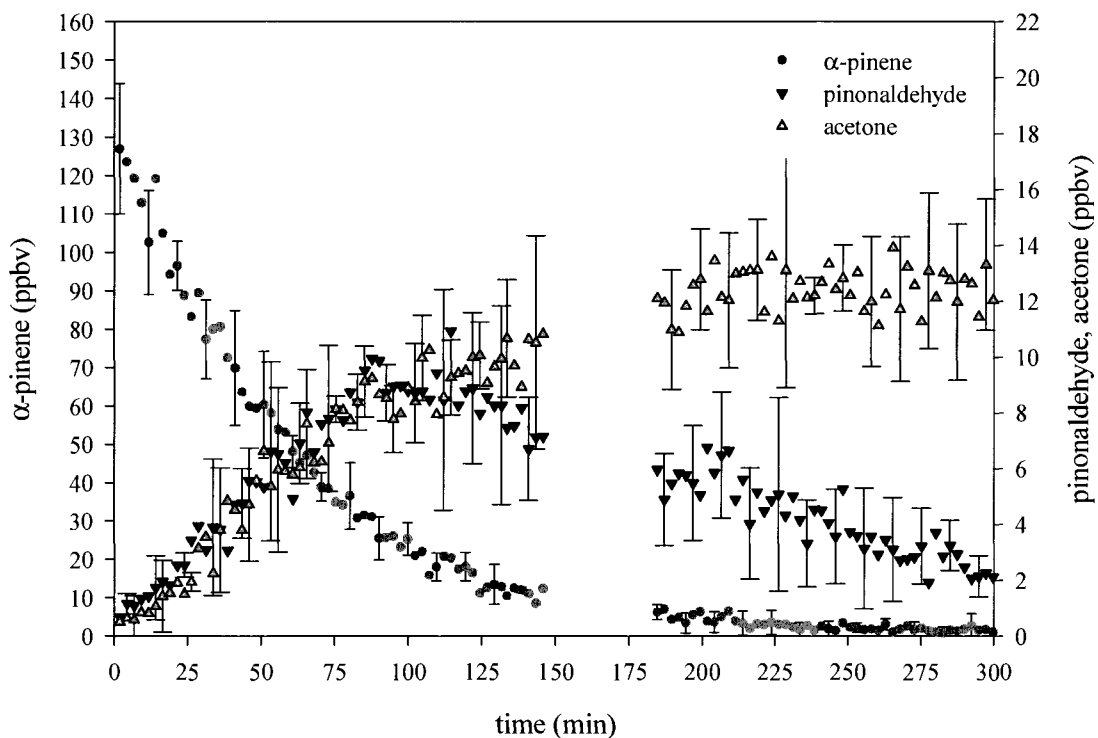


Figure 4.2: Gas phase molecules detected in the Cl oxidation of α -pinene (circles) including pinonaldehyde (down triangle) and acetone (up triangle).

Other signals observed during the course of this oxidation occur at 43 amu, 61 amu, and 45 amu (Figure 4.3). Both 43 amu and 61 amu are summed to correspond to the signal from acetic acid. The signal at 45 amu corresponds to acetaldehyde. Acetic acid is shown to make up a significant fraction of the ultimate products detected, with only a small contribution from acetaldehyde.

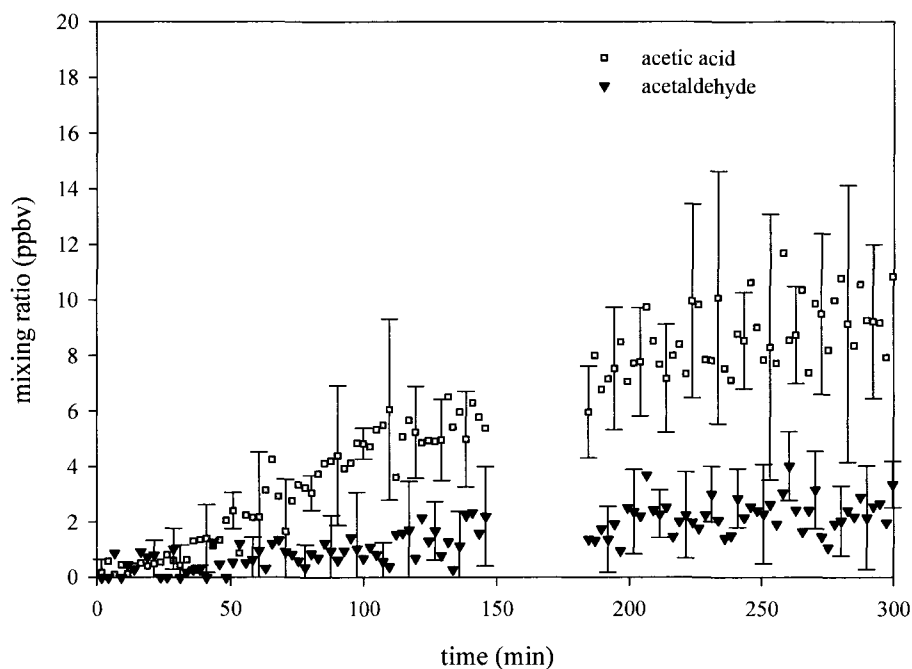


Figure 4.3: Gas phase products acetic acid (squares) and acetaldehyde (down triangle) observed in the Cl oxidation of α -pinene.

4.3.1.2 Case 2: 400 ppbv α -Pinene + 100 ppbv Cl_2

In the case of excess α -pinene, all chlorine is consumed during the course of the experiment. Mixing ratios of the reactant and two products are shown in Figure 4.4. For the purpose of clarity and because of the large excess of α -pinene, the left y-axis corresponds to α -pinene (ppbv) and the right y-axis shows the final mixing ratios for both pinonaldehyde and acetone. At the endpoint of the experiment, over 200 ppbv of α -pinene were still present in the chamber.

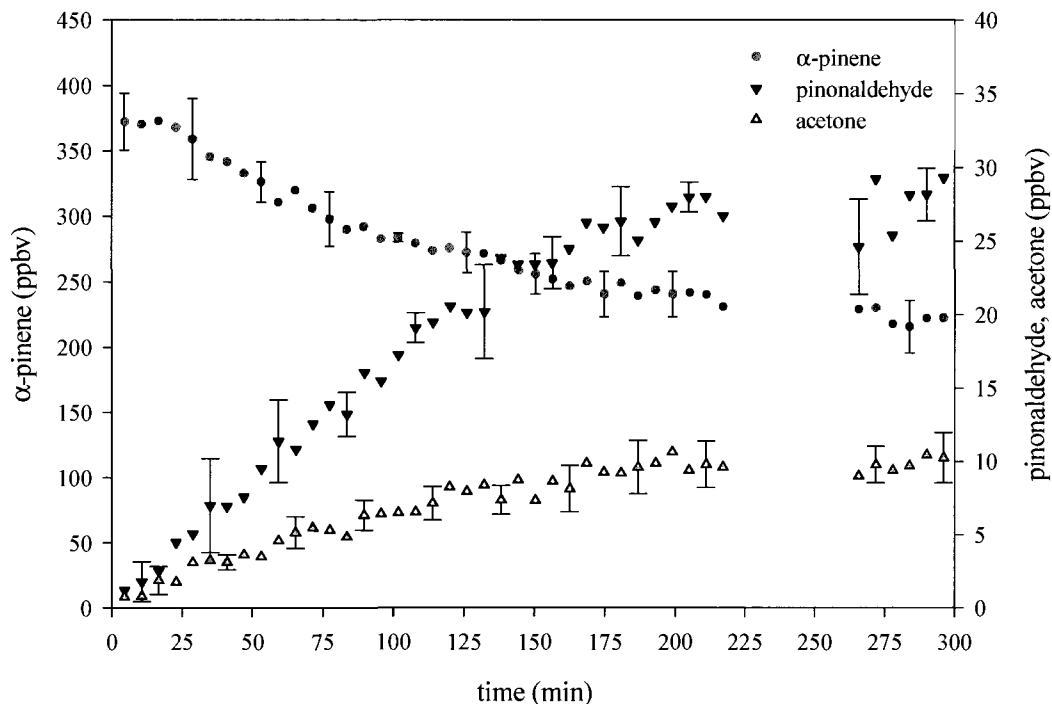


Figure 4.4: Gas phase molecules detected in the Cl oxidation of excess α -pinene (circles) including pinonaldehyde (down triangle) and acetone (up triangle).

As in Case 1, there is evidence for formation of acetic acid and acetaldehyde (Figure 4.5). Acetic acid mixing ratio has reached approximately 8 ppbv after 200 minutes of reaction, while less than 1 ppbv of acetaldehyde is observed.

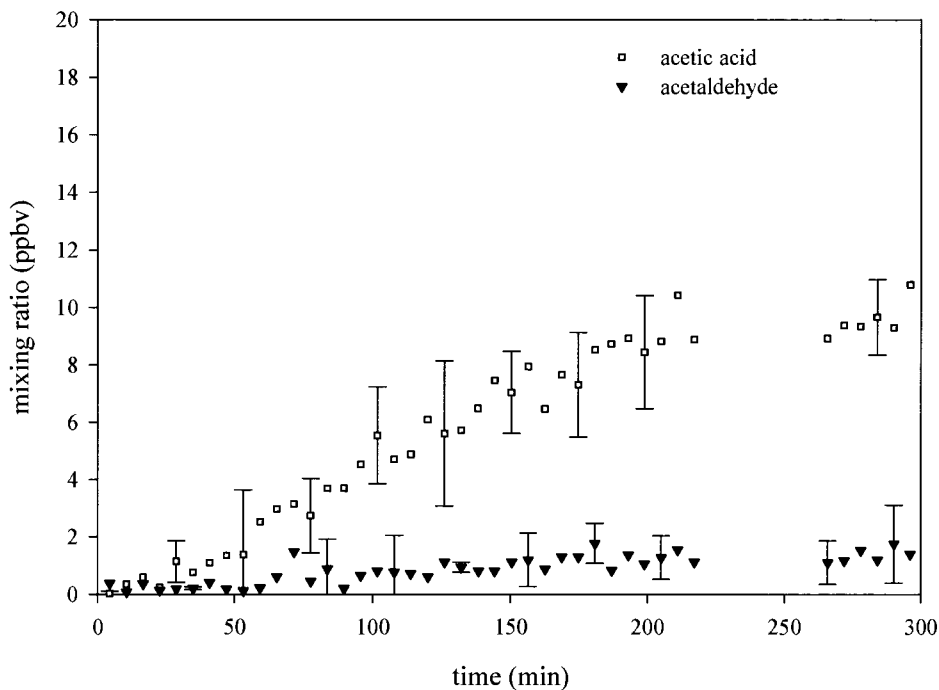


Figure 4.5: Gas phase products acetic acid (squares) and acetaldehyde (down triangle) observed in the Cl oxidation of excess α -pinene.

4.3.1.3 Case 3a: 93 ppbv β -Pinene + 100 ppbv Cl_2

In the case of β -pinene, major oxidation products from the OH/NO oxidation are nopinone and acetone.^{77,179,180,182-184,298} For the chlorine-initiated oxidation of β -pinene (Figure 4.6), the major product observed is acetone, accounting for over 10% of reaction products (on a molar basis).

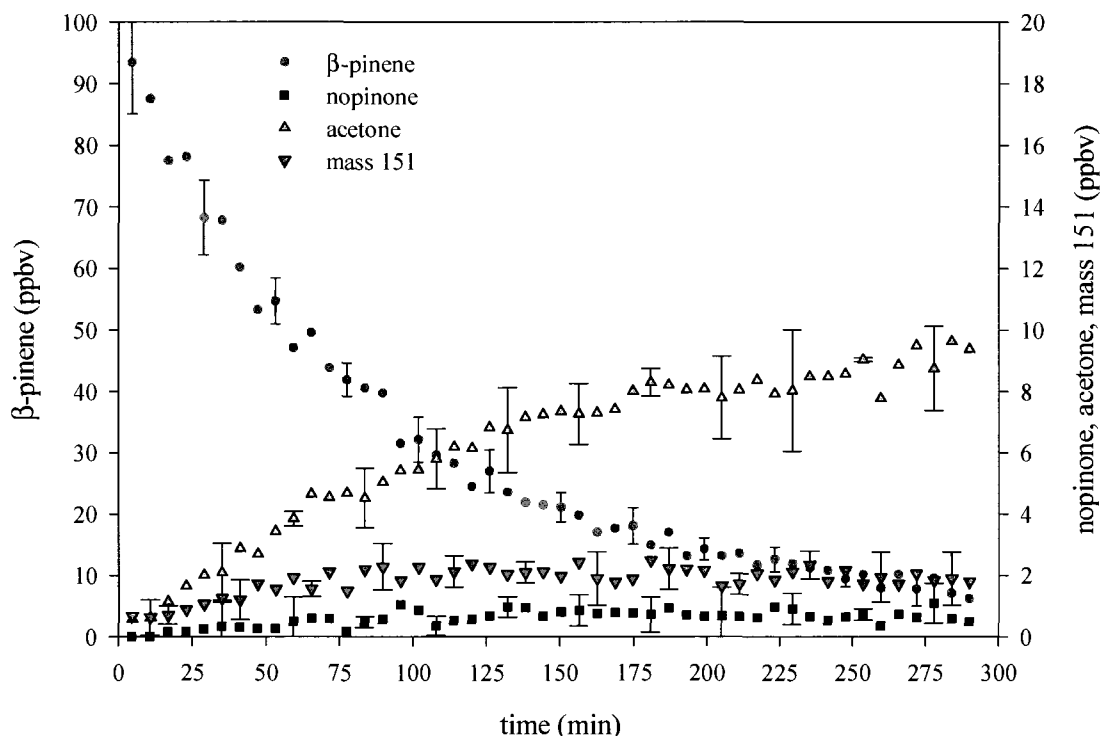


Figure 4.6: Gas phase molecules detected in the Cl oxidation of β -pinene (circles) including nopinone (squares), acetone (up triangle), and mass 151 (down triangle).

Figure 4.6 also indicates only a small amount of nopinone ($\sim 1\%$) formed during the reaction. In addition, and also noted by Lee et al.⁷⁶ (without yield), is the unidentified mass 151. This mass likely does not correspond to dehydrogenated pinonaldehyde, as the other fragmentation peaks corresponding to pinonaldehyde are not observed (or are below detection limits).

4.3.1.4 Case 3b: 80 ppbv β -Pinene + 100 ppbv Cl_2

This case mimics the conditions in Case 3a. Here, the experiment was stopped after 200 minutes. Again, the major product of acetone accounted for just over 10% of the molar yield of the reaction. A few ppbv of both nopinone and the unidentified mass

151 were observed during the course of the reaction as shown in Figure 4.7.

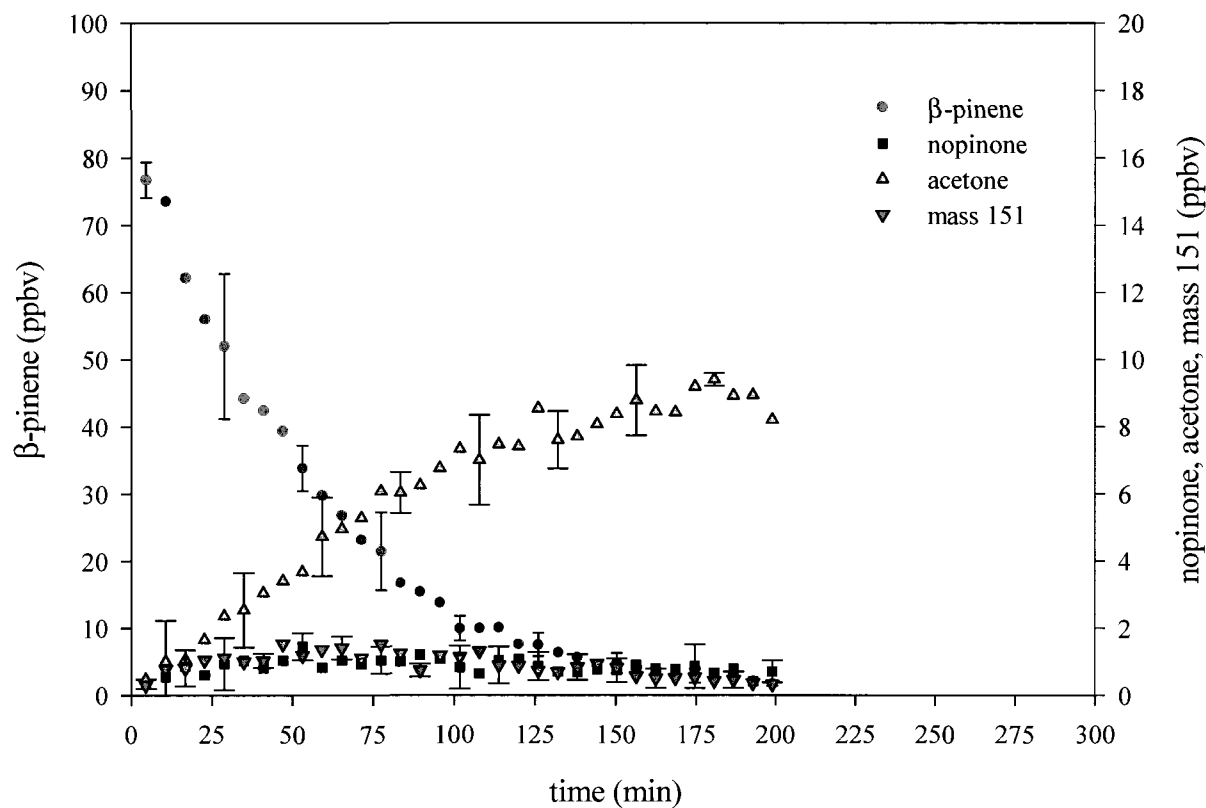


Figure 4.7: Gas-phase molecules detected in the Cl oxidation of β -pinene (circles) including nopinone (squares), acetone (up triangle), and mass 151 (down triangle).

While the initial mixing ratio of β -pinene is only 10 ppbv smaller than Case 3a, the reaction does proceed somewhat faster, with the reaction proceeding to completion after 200 minutes. This suggests an errantly large initial chlorine mixing ratio.

4.4 Discussion

4.4.1 Comparison to OH/NO Oxidation of α - and β -Pinene

Products quantified in the chlorine oxidation of α -pinene include pinonaldehyde, acetone, acetic acid, and acetaldehyde. Other masses detected but not quantified are shown in Table 4.A3. Products quantified in the chlorine oxidation of β -pinene include acetone, and unidentified mass 151, and a small amount (<1%) of nopinone. Molar yields (ppbv/ppbv) are shown below in Table 4.2.

Table 4.2: Molar yields of products from the Cl oxidation of α - and β -pinene

<u>Monoterpene</u>	<u>Starting MR (ppbv)</u>	<u>Product</u>	<u>% Yield</u>	<u>Notes</u>
α -pinene	100	acetone	10(2)	maximum at 100 minutes
		acetic acid	8(3)	
		acetaldehyde	1(1)	
		pinonaldehyde	8(2)	
α -pinene	400	acetone	3(1)	chlorine consumed completely excess α -pinene
		acetic acid	2(1)	
		acetaldehyde	<1	
		pinonaldehyde	7(1)	
β -pinene	80	acetone	10(2)	
		mass 151	2(1)	
		nopinone	< 1	

This signal at mass 151 corresponds to the dehydration product of pinonaldehyde (mass 169) in the oxidation of α -pinene, and has other associated fragments (Table 4.A3). These associated fragments that correlate to pinonaldehyde were not observed in the case

of β -pinene. Further, mass 151 has been observed in the OH/NO oxidation of β -pinene and has not been identified.⁷⁶

Oxidation of α - and β -pinene with OH/NO has been investigated and yields and products in common with the Cl oxidation are shown in Tables 4.3 and 4.4. Pinonaldehyde has been identified as the initial major OH radical oxidation product of α -pinene and has been measured via PTR-MS in three studies.^{76,77,103} Studies listed in Table 4.3 show a large variability in the molar yield of pinonaldehyde (6-87%). Peeters et al.¹⁸⁷ suggested higher yields of pinonaldehyde under low NO_x conditions although this does not seem completely consistent with experimental findings (Table 4.3). Differences in yields have been attributed to fast reaction of the initial pinonaldehyde forming adducts under high NO conditions, and decomposition of these adducts under low NO conditions.¹⁸⁶ It has also been suggested that different measurement techniques account for variability, where GC-FID and PTR-MS yield lower pinonaldehyde yields than FT-IR.²⁴⁴

A theoretical study performed by Fantechi et al.²⁹⁹ gave major products (%) of the OH radical oxidation of pinonaldehyde under high NO conditions as 4-hydroxypinonaldehyde (22.9), norpinonaldehyde (16.6), acetone (9.9), formaldehyde (12.9), organic nitrates (30.3), CO₂ (73.8), CO (16.6), formic acid (11.4), other carbonyls (16.6). Arey et al.²⁹⁸ gave molar yields for acetone and nopinone from the OH radical oxidation as 15(7) % and 30(5) % respectively.²⁹⁸ Table 4.3 lists major products and yields of the OH/NO oxidation of α -pinene.

Table 4.3: Measured major product molar yields (%) from the OH/NO oxidation of α -pinene

Reference	Detection Method	[NO]	Pinonaldehyde	Acetic acid	Acetaldehyde	Acetone
Arey et al. ²⁹⁸	GC/MS, GC-FID	~10 ppm	29(5)	-----	-----	-----
Aschmann et al. ¹⁸²	GC-FID API-MS	~6-9 ppm	-----	-----	-----	11(3) ^a
Peeters et al. ¹⁸⁷	Theoretical study	-----	35.7 ^b 59.5 ^c	8 ^b	-----	17.9 ^b 11.9 ^c
Hakola et al. ¹⁸⁰	GC/MS, GC-FTIR GC-FID	~10 ppm	28(5)	-----	-----	-----
Hatakeyama et al. ¹⁷⁹	FT-IR	1.8 ppm	78.5	-----	-----	-----
Larsen et al. ¹⁸⁴	FT-IR	~ 1 ppm	6(2)	-----	-----	11(3)
Lee et al. ⁷⁶	PTR-MS	1.1** HC:NO _x	47-83	1.4(2)	3.4(4)	6
Muller et al. ³⁰⁰	GC-MS HPLC-MS	~ 1 ppm	35.7	-----	-----	17.9
Noziere et al. ²⁵⁵	FT-IR	~200 ppb- 4 ppm	87(20)	-----	-----	9(6)
Orlando et al. ¹⁸³	FT-IR	~9-90 ppm	-----	-----	-----	5(2)
Vanhees et al. ²⁵⁸	HPLC	0	82(7)	-----	1.1(1)	6(2)
Wisthaler et al. ⁷⁷	PTR-MS	1-2 ppm	34(9)	-----	-----	11(2)
Reissell et al. ³⁰¹	GC-MS-FID	10 ppm	-----	-----	-----	11(3)
Capouet et al. ¹⁸⁶	box model	“high NO _x ” ^d	56(1) ^e 44(3) ^f	-----	-----	11.1(5) ^e 12.7(7) ^f
Capouet et al. ¹⁸⁶	box model	“NO _x free” ^d	26.4(4) ^e 20.4(6) ^f	-----	-----	0.37(5) ^e 0.47(5) ^f
Librando et al. ¹⁸⁵	FT-IR HPLC MS-MS	5-8 ppm*	-----	0	-----	12

^a Aschmann et al., 1998

^b predicted laboratory yield

^c predicted atmospheric yield

^d under UV light

^e primary yield

^f apparent yield

* CH₃ONO source for OH/NO radicals

** Ratio of α -pinene to NO_x (HC:NO_x)

API-MS-Atmospheric Pressure Ionization Mass Spectrometry

GC-FID- Gas Chromatography-Flame Ionization detection

PTR-MS- Proton Transfer reaction Mass Spectrometry

FT-IR-Fourier Transform Infrared Spectroscopy

HPLC-High Pressure Liquid Chromatography

Reported yields of acetone from the OH/NO oxidation of α -pinene are generally consistent between the studies. These yields are also similar to the observed yield of

acetone in Cl oxidation of α -pinene (~10 %). Only a few studies report the yield of acetaldehyde and acetic acid in the OH/NO oxidation of α -pinene (Table 4.3). Peeters et al.¹⁸⁷ predicted a yield of 8% of acetic acid in the OH/NO oxidation, similar to what is observed in the Cl oxidation (Table 4.2). Experimental results from Lee et al.⁷⁶ give a much lower yield of acetic acid (~1%). Lee et al.⁷⁶ also report a yield of ~3% for acetaldehyde, which is considerably higher than what is observed in the Cl oxidation.

In the OH/NO oxidation of β -pinene the major products are nopinone and acetone (Table 4.4). Here, the yield of nopinone is reported to be between 10-80% under high NO_x conditions. Lee et al.⁷⁶ reported a low value for nopinone of 10%, under excess NO_x. This is contrasted with the Cl oxidation, where nopinone yield is less than 1%. Besides nopinone, Lee et al.⁷⁶ also reported a yield of 1.4% for unidentified mass 151 in the OH/NO oxidation of β -pinene. This is similar to the estimation in the Cl oxidation of β -pinene, given in Table 4.2. Acetone yields in the Cl oxidation are similar to what is observed in the OH/NO oxidation of β -pinene (~10%).

Table 4.4: Measured major product molar yields (%) from the OH/NO oxidation of β -pinene

<u>Reference</u>	<u>Detection Method</u>	<u>[NO]</u>	<u>Nopinone</u>	<u>Acetone</u>
Hatakeyama et al. ¹⁷⁹	FT-IR	1.8 ppm	79(8)	-----
Orlando et al. ¹⁸³	FT-IR	~9-90 ppm	-----	2(2)
Hakola et al. ¹⁸⁰	GC/MS, GC-FTIR GC-FID	~10 ppm	27(4)	-----
Arey et al. ²⁹⁸	GC/MS, GC-FID	~10 ppm	30(4)	-----
Larsen et al. ¹⁸⁴	FT-IR	~1 ppm	25(5)	11(3)
Lee et al. ⁷⁶	PTR-MS	2.1** HC:NO _x	17	7.9
Wisthaler et al. ⁷⁷	PTR-MS	1-2 ppm	25(3)	13(2)
Aschmann et al. ¹⁸²	GC-FID API-MS	~6-9 ppm	-----	9(2)

** Ratio of β -pinene to NO_x (HC: NO_x)

Nitric oxide is included in studies (Tables 4.3 and 4.4) because in the atmosphere, the presence of nitric oxide allows for rapid deoxygenation of the alkyl peroxy radical to form NO_2 and the alkoxy radical.

The reaction proceeds in the troposphere because mixing ratios of NO are relatively high (generally tens to hundreds of pptv) compared to RO_2 . In the absence of NO, there are a number of other proposed pathways (R4.3-R4.5) described above. Other reaction products may be accessed by intramolecular rearrangements of α -pinene peroxy radicals, as detailed by the recent work by Vereecken et al.^{302,303}

In the oxidation of α -pinene, masses 93, 135, and 149 amu show a 2-3 fold increase in signal during the course of the experiments with α -pinene, and generally follow the trend of pinonaldehyde. Because these signals are not observed in the OH/NO oxidation of α -pinene, these masses may be tracers of chlorine chemistry. In particular, mass 93 may correspond to chloroacetone or propanoyl chloride.

In the oxidation of β -pinene by chlorine, protonated mass 95 was observed, but not in the OH/NO oxidation studies done by either Lee et al.⁷⁶ or Wisthaler et al.⁷⁷ This mass 95 may correspond to chloroacetic acid, or chloro-propanol isomers. Non-chlorinated compounds (either oxygenated or aliphatic) at this mass have structures that are unlikely given the reaction, or undetectable with PTR-MS.

4.4.2 Chlorine Reaction Rate Coefficients

As seen in Table 4.A1 (Appendix), chlorine adds to a simple alkene with a rate constant on the order of $10^{-10} \text{ cm}^3 \text{ molecule}^{-1} \text{ s}^{-1}$. In the case of ethene, this addition overwhelms the hydrogen abstraction pathway, which has a rate constant two orders of magnitude smaller ($\sim 10^{-12} \text{ cm}^3 \text{ molecule}^{-1} \text{ s}^{-1}$). For propene, the availability of hydrogen for abstraction increases, and hence the rate constant for the reaction increases to $\sim 10^{-11} \text{ cm}^3 \text{ molecule}^{-1} \text{ s}^{-1}$. Published chlorine reactions with larger alkenes give rate constants on the order of $\sim 10^{-10} \text{ cm}^3 \text{ molecule}^{-1} \text{ s}^{-1}$ but provide no specific insight into products formed. Ultimately, this strongly suggests that chlorine abstraction of hydrogen is a competitive pathway compared to the chlorine addition to the mono-unsaturated alkene. Because of large oxygen concentration and initial radical formation either by abstraction or addition, each monoterpene reacts to form an alkyl peroxy radical. One possible mechanism for deoxygenation of alkyl peroxy radical is the alkyl peroxy self reaction where chlorinated alkyl peroxy self reaction has a rate constant over two orders of magnitude larger than unchlorinated alkyl peroxy self reactions.³⁰⁴ Involvement of these self reactions in NO_x free conditions in the chlorine atom oxidation of monoterpenes will be discussed in Section 4.4.3.

4.4.3 Deoxygenation of Peroxy Radicals

In product studies of monoterpene reactions with hydroxyl radical, NO is frequently added in concentrations at least a few orders of magnitude larger than OH radical. In the OH radical oxidation, NO is responsible for the deoxygenation of the alkyl peroxy radical. The rate constant for reaction of NO with peroxy radical to form NO_2 is

$\sim 10^{-12} \text{ cm}^3 \text{ molecule}^{-1} \text{ s}^{-1}$,^{287,291,305-320} with the most recent study by Bacak et al.³²¹ assigning the rate constant as $7.46 \times 10^{-12} \text{ cm}^3 \text{ molecule}^{-1} \text{ s}^{-1}$ at 300K.

In this study, NO is absent in the mixture of Cl atoms and monoterpene, and even the ‘low’ NO_x cited in numerous publications is still many orders of magnitude larger than Cl atom concentration in this study. A potential chlorine radical abstraction of oxygen to form ClO from peroxy radical,



has a rate constant of $\sim 10^{-11} \text{ cm}^3 \text{ molecule}^{-1} \text{ s}^{-1}$.^{289,291-293} As concentration of chlorine atom is small ($\sim 10^{-5}$ ppbv), deoxygenation of the alkyl peroxy radical via reaction with Cl is unlikely. A possible scenario for the deoxygenation of the peroxy radical intermediates is the self reaction of these intermediates.

4.4.4 Proposed Chlorine Reaction Mechanisms

4.4.4.1 Alkyl Peroxy Hydrogen Abstraction Pathways.

Hydrogen abstraction from VOCs via chlorine radical is known to occur and compete with chlorine addition to the olefin. Whether by addition or hydrogen abstraction, an intermediate monoterpene radical is formed. Once the monoterpene radical is formed, it is oxygenated to form an alkyl peroxy radical. While this addition has a rate constant of $\sim 10^{-12} \text{ cm}^3 \text{ molecule}^{-1} \text{ s}^{-1}$, high concentration of oxygen in the chamber ($\sim 5 \times 10^{18} \text{ molecules cm}^{-3}$) ensures addition of oxygen within $\sim 10^{-7}$ seconds.²⁸⁷ Once this alkyl peroxy radical is formed it is likely that early in the reaction the mechanism will proceed via peroxy self reactions.^{264,272}

4.4.4.2 Criegee Intermediate Reaction Pathways.

Potential intermediates in the chlorine oxidation of monoterpenes are Criegee intermediate as chlorine may abstract a hydrogen molecule from the peroxy carbon. Numerous studies are dedicated to the Criegee intermediate both in solution and in the gas phase.^{216,322-328} Criegee intermediates in chlorine initiated oxidation of VOCs are discussed in two studies.^{294,329} It is generally accepted that the Criegee intermediate may follow one of four possible reaction pathways:³³⁰ (i) an oxygen atom may be dissociated from the Criegee resulting in carbonyl formation. However, a study³³¹ has suggested that this does not occur because little O(³P) has been observed from Criegee intermediates formed from ozonolysis; (ii) it will react with H₂O forming carbonyls, acids, and OH radical;³³⁰ (iii) the Criegee may undergo a 1,4 H shift to form a hydroperoxide, which may then further react to form other radicals and ketenes;²⁸⁸ and (iv) the Criegee intermediate can rearrange to form an ester or acid.²⁸⁸ The potential role of the Criegee intermediate in the chlorine oxidation of β -pinene is shown in Section 4.4.4.4.

4.4.4.3 Proposed Mechanisms Leading to Pinonaldehyde.

There are two potential pathways leading to pinonaldehyde formation in the Cl oxidation of α -pinene. One reaction pathway begins with addition of chlorine atom to α -pinene to form a secondary radical (Figure 4.8). Molecular oxygen adds to form the chlorinated alkyl peroxy radical, which undergoes a self reaction to form the alkoxy radical. This is followed by formation of the aldehyde and opening of the ring. Molecular

oxidation of ethyl chloride in the absence of NO, the reaction pathway resulting from chlorine atom elimination was estimated to be no greater than 10%.²⁷⁶

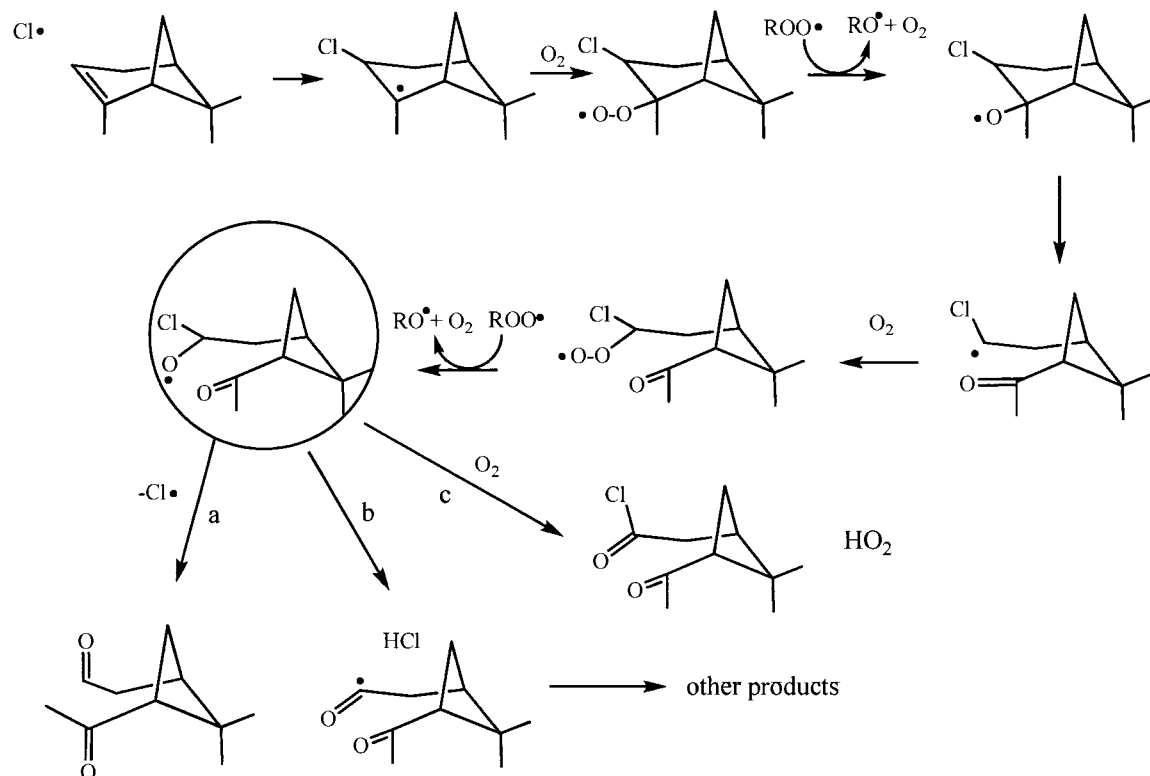


Figure 4.9: Proposed mechanism for the addition of chlorine to α -pinene forming an initial tertiary radical to form products via three different pathways; (a) elimination of Cl radical, (b) elimination of HCl, and (c) hydrogen abstraction by molecular oxygen.

It was shown that in the presence of NO, deoxygenation of the alkyl peroxy radical leads to a chemically activated alkoxy radical because of high exothermicity of the reaction.³³² The excited alkoxy radical showed enhanced channels for both HCl elimination and carbon-chlorine bond scission.³³² As alkyl peroxy self reactions are slightly endothermic,³³³ enhancement of either the HCl elimination channel or carbon-chlorine bond scission is not expected, but are still the major (>90%) pathways for the decomposition of the chlorinated alkoxy radical.

4.4.4.4 Mechanisms Leading to Acetone and Acetic Acid.

As in the formation of pinonaldehyde, there seem to be two significant pathways for acetone formation in the chlorine atom initiated oxidation of α -pinene. Figure 4.10 is the suggested mechanism for these two pathways.

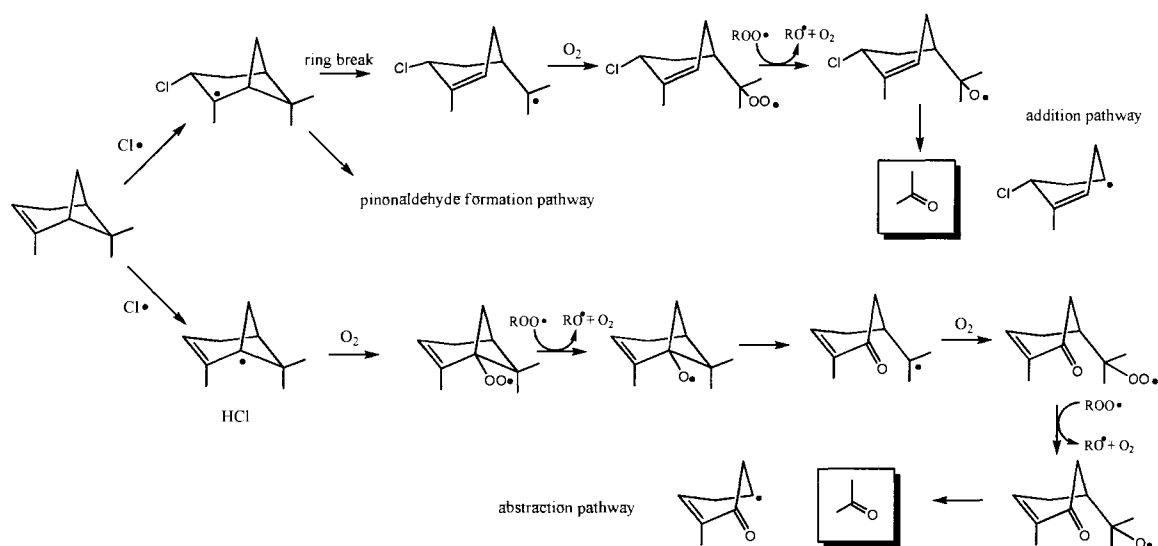


Figure 4.10: Proposed acetone formation pathways via Cl addition and H-abstraction in the Cl initiated oxidation of α -pinene.

It should be noted that the initial step in one pathway leading to acetone formation is also the initial step shown in Figure 4.9, namely, formation of the tertiary radical. What differs between these two pathways is the ring opening that occurs on the order of 10^{-4} seconds after radical formation in the pathway leading to acetone formation.³³⁴

A pathway to acetic acid may also be rationalized and is shown in Figure 4.11. The mechanism for formation of acetic acid from α -pinene is not possible for β -pinene and no acetic acid was observed in the β -pinene oxidation. In the presence of water vapor

(as in the PTR-MS drift tube) the elimination product acetyloxy radical will abstract hydrogen to form acetic acid.

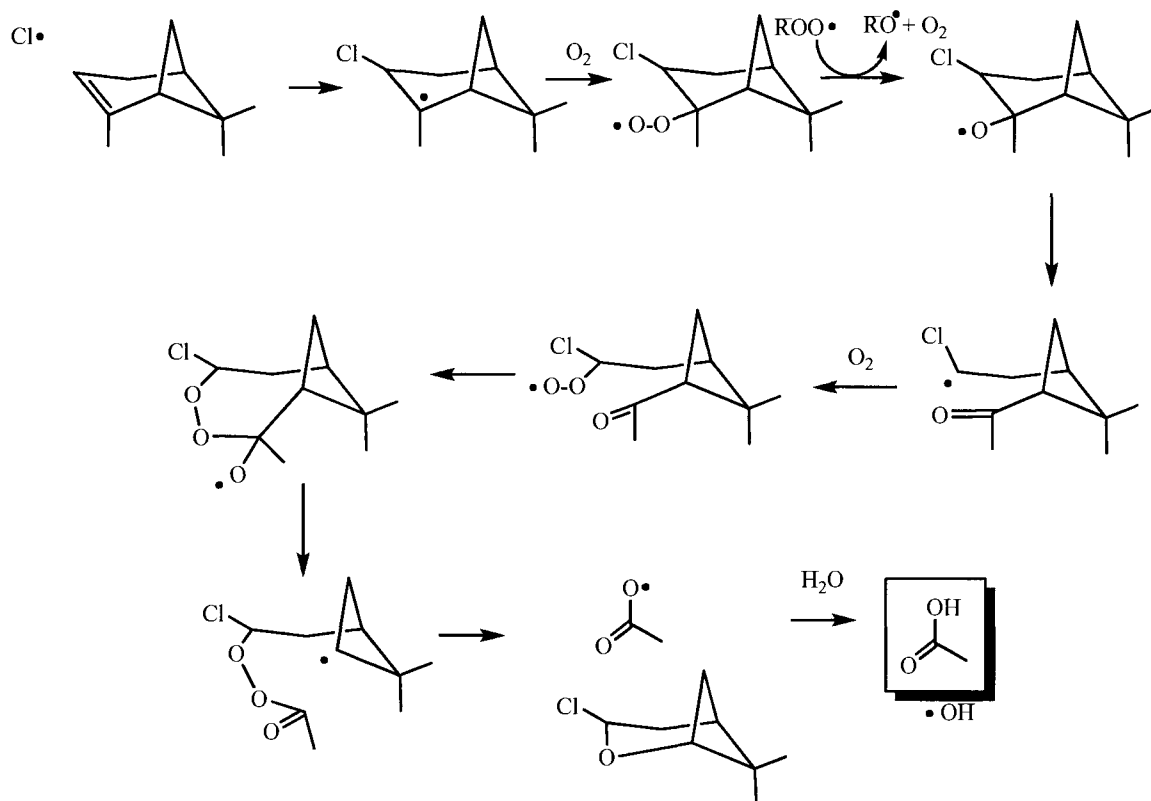


Figure 4.11: Proposed acetic acid formation in the Cl initiated oxidation of α -pinene.

The speculative step in formation of acetic acid is addition of the alkyl peroxy radical to the carbonyl. In a study by Iwahama et al.,³³⁵ a similar mechanism was proposed based on the observed product of a cyclic peroxide. Ketohydroperoxides have also been shown to undergo cyclization by the peroxide addition to the carbonyl followed by fragmentation to an acid.³³⁶ In the oxidation of ethyne, Maranzana et al.³³⁷ report that peroxy addition to the carbonyl is an unfavorable process. In ethyne, this requires formation of a four membered ring. This four membered ring forms with a barrier of ~ 14

kcal mol⁻¹, and the proposed ring formation in Figure 4.11 should have a barrier between 5-14 kcal mol⁻¹.³³⁸ Validity of this proposed mechanism requires further investigation.

4.4.4.5 Mechanisms Leading to Nopinone.

While experimental evidence shows almost no nopinone formed in the chlorine initiated oxidation of β -pinene, Figure 4.12 illustrates three pathways that should lead to nopinone formation. The top reaction in Figure 4.12 proceeds via loss of CH₂Cl radical after peroxy radical is formed. This yields the stable Criegee intermediate, which, in the presence of water may slowly convert to nopinone. As conditions in the chamber were dry, this pathway to nopinone will not occur in the reaction chamber.

The second possible mechanism for formation of nopinone is through addition of chlorine to form a tertiary radical, addition of O₂, subsequent peroxy self reactions to deoxygenate the chlorinated alkyl peroxy radical, and elimination of CH₂Cl. As the alkoxy radical is chlorinated in the β -position, reactions involving loss of HCl and dehydrogenation via reaction with O₂ as observed in the case of pinonaldehyde formation are not likely pathways.

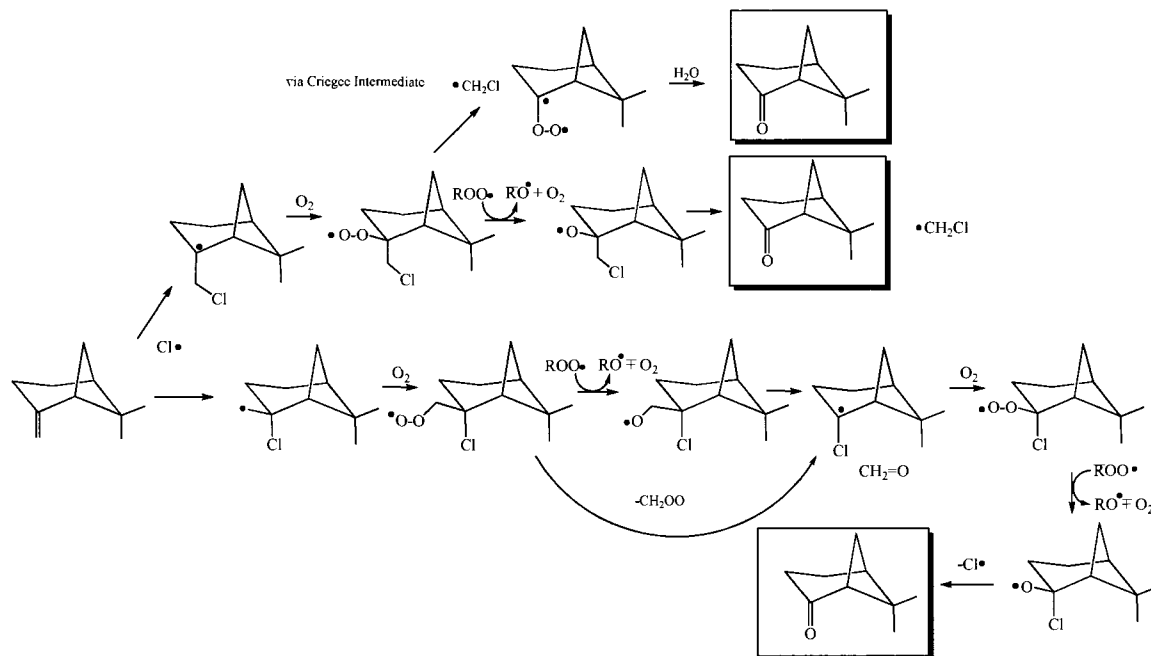


Figure 4.12: Proposed reaction pathways for the formation of nopinone from the Cl initiated oxidation of β -pinene.

Another mechanistic pathway in the Cl initiated oxidation of β -pinene is loss of either CH_2Cl or CH_2O in the course of nopinone formation (Figure 4.12). There is also evidence from Jenkin et al.³³⁹ that there is a loss of a Criegee intermediate (CH_2OO) prior to deoxygenation of the alkyl peroxy radical by another alkyl peroxy radical. The final step in this pathway involves elimination of chlorine radical to form nopinone. As there is no α -hydrogen present on the chlorinated carbon, other pathways (elimination of HCl and hydrogen abstraction via O_2) will not occur.

As seen in Section 4.3.1.3 and 4.3.1.4, essentially no nopinone is observed in the β -pinene oxidation. While reactions may be proposed for the formation, it is clear that if little or no nopinone is formed in this system, reactions that are analogous to those of OH/NO oxidation are, in fact, not occurring. Because hydrogen abstraction is fast in the

chlorine system ($\sim 10^{-5}$ seconds at 100 ppbv β -pinene), it is likely that the initial β -chlorinated alkyl peroxy β -pinene tertiary radical is available for hydrogen abstraction reactions leading to other products. Another possibility is that elimination of CH_2Cl radical is a thermodynamically unfavorable process compared to other potential elimination reactions (*e.g.* ClO elimination). Further investigation incorporating kinetic and thermodynamic considerations are necessary to establish the validity of the proposed reactions.

4.4.4.6 Mechanisms Leading to Acetone (β -Pinene).

As seen in Case 3a and 3b, acetone is formed in significant amounts (around 10%) in the chlorine oxidation of β -pinene. Potential pathways for formation of acetone from the oxidation are shown in Figure 4.13. Here, two pathways potentially lead to acetone.

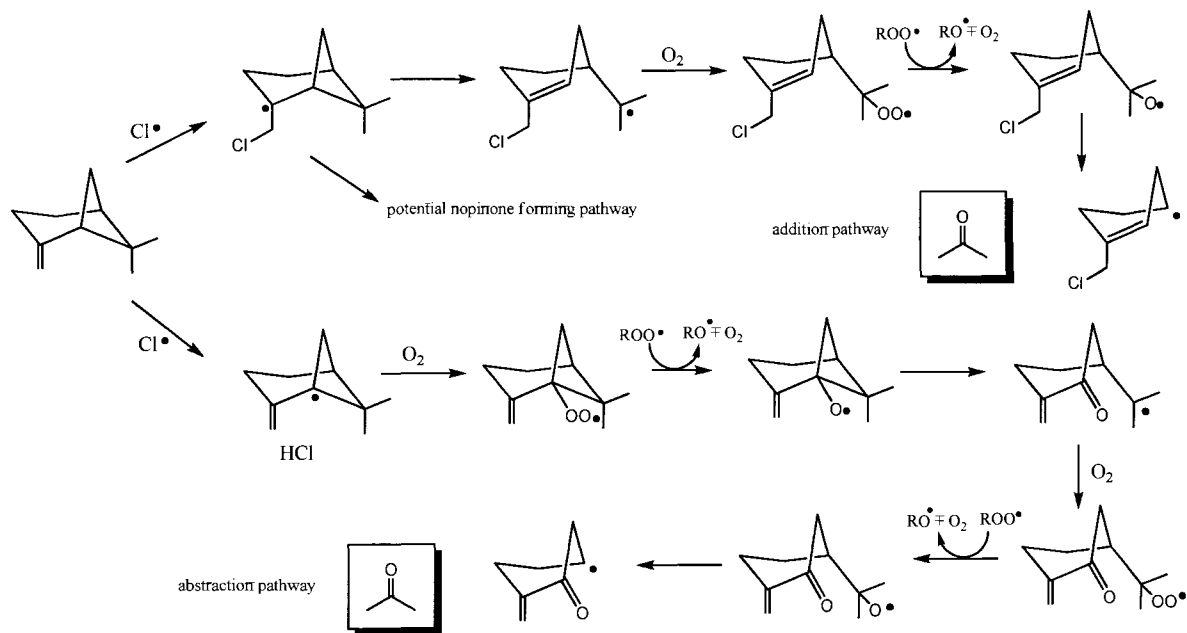


Figure 4.13: Proposed reaction pathways for the formation of acetone from the Cl initiated oxidation of β -pinene.

Here it should be noted again that the nopinone forming pathway is not observed in the experimental data. The other two pathways involve a ring breaking step of the β -pinene, analogous to what is observed in the prompt acetone formation from α -pinene.

4.5 Summary and Conclusions

Employing experimental conditions analogous to the work done by Cai and Griffin²¹⁴ on SOA formation, gas phase products from the chlorine initiated oxidation of α - and β -pinene were quantified and reaction mechanisms were postulated based on known mechanisms for OH/NO oxidations and known kinetic parameters.

Pinonaldehyde and acetone are formed in the chlorine initiated oxidation of α -pinene, and are also observed in the OH/NO oxidation of α -pinene. The yield of pinonaldehyde for chlorine oxidation is somewhat lower than what is observed in the OH/NO oxidation (Tables 4.2 and 4.3). Pinonaldehyde formation may proceed through formation of the chlorinated secondary radical rather than through the tertiary radical. Unique to chlorine oxidation is the decomposition of the α -chlorinated alkoxy radical (derived from the initial chlorinated tertiary radical), which is more likely to form products other than pinonaldehyde via either the elimination of HCl or hydrogen abstraction to form the halogenated pinonaldehyde. Acetone may be formed through a ring breaking mechanism, and the yield in the chlorine oxidation is similar to what is observed in the OH/NO oxidation. Acetone is also the major product (~10%) observed in the chlorine oxidation of β -pinene, and there is some evidence for nopinone formation. Acetone yield is similar to what is observed in the OH/NO oxidation of β -pinene, but nopinone yield is much lower (Table 4.4). Also observed in the case of β -pinene is a signal at 151 amu, which has been observed in the OH/NO oxidation with a similar yield of ~2%.

An interesting difference between the oxidation of α - and β -pinene is formation of acetic acid and acetaldehyde. Acetaldehyde has a very low yield in the oxidation of α -pinene and is not observed at all in the β -pinene case. Acetic acid is a major product (up to ~8%) in the oxidation of α -pinene but is not observed at all in the oxidation of β -pinene.

Chlorine reactions with monoterpenes and intermediates proceed faster than what is observed in the OH/NO oxidation. Most importantly, hydrogen abstraction pathways are more accessible (*i.e.* have larger reaction rates) in the chlorine oxidation than OH oxidation. Because of an absence of NO in these experiments, deoxygenation of alkyl peroxy radicals does not occur via formation of NO₂, but potentially via the somewhat slower alkyl peroxy self reactions. Other potential pathways for deoxygenation of these alkyl peroxy radicals are unlikely given the conditions in the chamber. However, the mechanisms proposed require further study to assess their validity.

4.6 Appendix

Table 4.A1: Summary of potential early reactions and associated rate constants in the Cl initiated oxidation of α - and β -pinene. When no compound specific rate data are available, general reaction rate constants are given and indicated in the reaction column.

<u>Reaction</u>	<u>Rate constant</u> ($\text{cm}^3 \text{ molecule}^{-1} \text{ s}^{-1}$)	<u>Description</u>	<u>Reference</u>
$\text{C}_{2-8}\text{H}_{6-18} + \text{Cl} \rightarrow \text{C}_{2-8}\text{H}_{5-17} + \text{HCl}$	$0.5\text{-}4 \times 10^{-10}$	Hydrogen abstraction from simple alkanes	340
$\text{C}_2\text{H}_4 + \text{Cl} \rightarrow \text{C}_2\text{H}_3 + \text{HCl}$	5.17×10^{-13}	Hydrogen abstraction from ethylene	341
$\text{CH}_3\text{CH}=\text{CH}_2 + \text{Cl} \rightarrow \text{CH}_2\text{CH}=\text{CH}_2 + \text{HCl}$	3.62×10^{-11}	Hydrogen abstraction from propylene	342
$\text{C}_2\text{H}_4 + \text{Cl} \rightarrow \text{C}_2\text{H}_4\text{Cl}$	2.93×10^{-10}	Addition of Cl to ethylene	287,343
$\text{CH}_3\text{CH}=\text{CH}_2 + \text{Cl} \rightarrow \text{CH}_2\text{CHCH}_2\text{Cl}$	3.11×10^{-10}		
$\text{CH}_3\text{CH}=\text{CH}_2 + \text{Cl} \rightarrow \text{CH}_2\text{CHCH}_2\text{Cl}$	2.7×10^{-10}	Addition of Cl to propylene	344
$\text{CH}_3\text{CHO} + \text{Cl} \rightarrow \text{HCl} + \text{CH}_3\text{CO}$	7.5×10^{-11}	Hydrogen abstraction from simple aldehyde	345
$\text{Cl} + \alpha\text{-pinene} \rightarrow \text{products}$	4.7×10^{-10}	Chlorine reaction with α -pinene	261
$\text{Cl} + \beta\text{-pinene} \rightarrow \text{products}$	5.3×10^{-10}	Chlorine reaction with β -pinene	261

Table 4.A2: Summary of potential intermediate reactions of oxygen and oxygenated compounds with associated rate constants in the Cl initiated oxidation of α - and β -pinene. When no compound specific rate data are available, general reaction rate constants are given and indicated in the reaction column.

<u>Reaction</u>	<u>Rate constant</u> ($\text{cm}^3 \text{ molecule}^{-1} \text{ s}^{-1}$)	<u>Description</u>	<u>Reference</u>
$\text{C}_2\text{H}_4\text{Cl} + \text{O}_2 \rightarrow \text{CH}_3\text{CHClO}_2$	1.04×10^{-11}	Addition of O_2 to chlorinated alkane radical	346
$\text{C}_{10}\text{H}_{15} + \text{O}_2 \rightarrow \text{C}_{10}\text{H}_{15}\text{O}_2$	2.16×10^{-12}	Addition of O_2 to alkane radical	347*
$\text{CH}_2\text{ClCH}_2\text{O}_2 + \text{CH}_2\text{ClCH}_2\text{O}_2 \rightarrow \text{O}_2 + 2\text{CH}_2\text{ClCH}_2\text{O}$	5.99×10^{-12}	Chlorinated alkyl peroxy self reaction	304

<u>Reaction</u>	<u>Rate constant</u> ($\text{cm}^3 \text{ molecule}^{-1} \text{ s}^{-1}$)	<u>Description</u>	<u>Reference</u>
$\text{CH}_2\text{ClCH}_2\text{O}_2 + \text{CH}_2\text{ClCH}_2\text{O}_2 \rightarrow \text{O}_2 + 2\text{CH}_3\text{CHClO}$	4.9×10^{-12}	Chlorinated alkyl peroxy self reaction	304
$\text{C}_2\text{H}_5\text{O}_2 + \text{C}_2\text{H}_5\text{O}_2 \rightarrow \text{CH}_3\text{CH}_2\text{O} + \text{CH}_3\text{CH}_2\text{O} + \text{O}_2$	4.4×10^{-14}	Alkyl peroxy self reaction	348
$\text{CH}_2\text{ClCH}_2\text{OO} + \text{NO} \rightarrow \text{products}$	1.02×10^{-11} 9.7×10^{-12}	Deoxygenation by NO to form chlorinated alkoxy radical	320,349
$\text{C}_2\text{H}_5\text{O}_2 + \text{NO} \rightarrow \text{C}_2\text{H}_5\text{O} + \text{NO}_2$	8.9×10^{-12}	Deoxygenation by NO to form alkoxy radical	350
$\text{CH}_3\text{O}_2 + \text{CH}_3\text{O}_2 \rightarrow (\text{CH}_3\text{O})_2 + \text{O}_2$	$< 3.01 \times 10^{-14}$	Peroxy self reaction to form dimer	306
$\text{CH}_3\text{O}_2 + \text{CH}_3\text{O}_2 \rightarrow 2\text{CH}_3\text{O} + \text{O}_2$	1.29×10^{-13}	Formation of alkoxy radical and oxygen from peroxy self reaction	305
$\text{CH}_3\text{O}_2 + \text{Cl} \rightarrow \text{HCl} + \text{CH}_2\text{OO}$	$0.73\text{-}2.01 \times 10^{-10}$	Formation of Criegee (H abstraction from peroxy radical)	289,291,293
$\text{CH}_3\text{O}_2 + \text{Cl} \rightarrow \text{ClO} + \text{CH}_3\text{O}$	$2.01\text{-}7.69 \times 10^{-11}$	Deoxygenation of peroxy radical by Cl	289,291,293
* for the terpene γ -terpinene			

Table 4.A3: Masses, fragments, and isotopes common in the oxidation of α - and β -pinene. Parent ions shown in bold.

<u>Compound</u>	<u>Detected masses</u>	<u>Structures</u>	<u>Description</u>	<u>Reference</u>
α -pinene	81, 82, 137, 138	C_6H_9^+ , $\text{C}_{10}\text{H}_{16}^+$	Fragmentation ion, ^{13}C isotope, and parent ion	Wisthaler ⁷⁷ , Lee ⁷⁶
	67, 81, 82, 95, 137, 138	C_5H_6^+ , C_6H_9^+ , $\text{C}_{10}\text{H}_{16}^+$	Two fragmentation ions, ^{13}C isotope, and parent ion	Tani ⁹⁹
β -pinene	81, 82, 137, 138	C_6H_9^+ , $\text{C}_{10}\text{H}_{16}^+$	Fragmentation ion, ^{13}C isotope, and parent ion	Wisthaler, Lee
	67, 81, 82, 95, 137, 138	C_5H_6^+ , C_6H_9^+ , $\text{C}_{10}\text{H}_{16}^+$	Two fragmentation ions, ^{13}C isotope, and parent ion	Tani

<u>Compound</u>	<u>Detected masses</u>	<u>Structures</u>	<u>Description</u>	<u>Reference</u>
acetone	60, 59	C ₃ H ₆ O ⁺	Parent ion	Wisthaler
acetaldehyde	45	C ₂ H ₄ O ⁺	Parent ion	Lee
formic acid	47	CH ₂ O ₂ ⁺	Parent ion	Lee
formaldehyde	31	CH ₂ O ⁺	Parent ion	Lee
acetic acid	61	C ₂ H ₄ O ₂ ⁺	Parent ion	Lee
acetic acid	61 , 43	C ₂ H ₄ O ₂ ⁺	Parent ion, acylium ion	This study
pinonaldehyde	71, 72, 99, 107, 108, 109, 123, 151 , 152, 169, 170	C ₁₀ H ₁₆ O ₂ ⁺	Fragmentation ions, 151 is dehydration product of molecular ion 169	Lee
	43, 71, 72, 81, 99, 107, 108, 109, 123, 151 , 152, 169, 170	C ₁₀ H ₁₆ O ₂ ⁺	Fragmentation ions, 151 is dehydration product of molecular ion 169	Wisthaler
	71, 99, 107, 109, 123, 151 , 152, 169	C ₁₀ H ₁₆ O ₂ ⁺	Fragmentation ions, 151 is dehydration product of molecular ion 169	This study
nopinone	140, 139 , 122, 121, 93, 83	C ₉ H ₁₄ O ⁺	Parent ion in bold, fragments	Wisthaler
	83, 93, 97, 103, 121, 122, 139 , 140, 141	C ₉ H ₁₄ O ⁺	Parent ion in bold, fragments	Lee
	121, 139	C ₉ H ₁₄ O ⁺	Nopinone and fragments	This study

Table 4.A4: Mixing ratio and rate constant conversions, where 1 ppbv = 2.46×10¹⁰ molecules cm⁻³

Chlorine atom reaction with	Rate constant (cm ³ molecule ⁻¹ s ⁻¹)	Conversion factor 1.48 × 10 ¹²	Rate constant (ppb ⁻¹ min ⁻¹)
α-pinene	4.7 × 10 ⁻¹⁰		783
β-pinene	5.3 × 10 ⁻¹⁰		694
Pinonaldehyde	1 × 10 ⁻¹⁰		148

To approximate the photodissociation of Cl₂ (because of the absence of spectrophotometers in the chamber), the output spectrum from the lamps was obtained.³⁵¹ This output spectrum for the UV source lamps and the absorption cross section for Cl₂ are shown in Figure 4.A1.³⁵¹

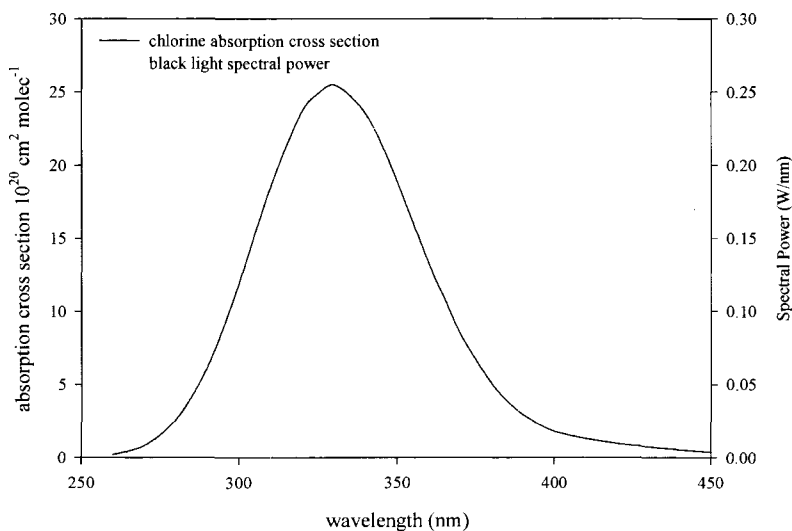


Figure 4.A1: (a) The output spectrum for UV source and (b) the absorption cross section (σ) of Cl₂ over the range of 260 - 420 nm.

As there were 20 UV lamps above the chamber, the spectral power was multiplied by 20 to determine the total power. The photon flux (photons cm⁻² s⁻¹) was calculated by determining the energy at each 10 nm wavelength from 310 to 420 nm by the relationship

$$E = \frac{hc}{\lambda} \quad (4.A1)$$

where h is Planck's constant, c is the speed of light, and λ is the wavelength. The spectral power (J s⁻¹) at 10 nm intervals was then divided by the corresponding energy and the area of the chamber to determine I , the photon flux (photons cm⁻² s⁻¹). For the reaction



the photodissociation of Cl_2 atoms in the chamber over time is

$$\frac{d[\text{Cl}_2]}{dt} = -k_1[\text{Cl}_2] \quad (4.A3)$$

where k_1 is the first-order photolysis rate constant (s^{-1}). This first-order photolysis rate constant depends on the absorption cross section of the molecule (σ), the quantum yield (ϕ), and the photon flux (I), all of which are wavelength dependent, and may be expressed as¹⁰⁵

$$k_1 = \int_{\lambda} \sigma(\lambda)\phi(\lambda)I(\lambda)d\lambda \quad (4.A4)$$

The photolysis rate constant was calculated at each 10 nm interval, assuming a quantum yield, ϕ , of 1.³⁵² The resultant photolysis rates yielded a k_1 value of $8.9 \times 10^{-5} \text{ s}^{-1}$.

Upon integration, (4.A3) becomes

$$[\text{Cl}_2]_t = [\text{Cl}_2]_0 \times e^{-k_1 t} \quad (4.A5)$$

which determines the consumption of molecular chlorine in the reaction chamber.

References

1. Shaw, S. L.; Mitloehner, F. M.; Jackson, W.; DePeters, E. J.; Fadel, J. G.; Robinson, P. H.; Holzinger, R.; Goldstein, A. H. *Environ. Sci. Technol.* **2007**, *41*, 1310-1316.
2. Guenther, A.; Hewitt, C. N.; Erickson, R.; Fall, R.; Geron, C.; Graedel, T.; Harley, P.; Klinger, L.; Lerdau, M.; McKay, W.; Pierce, T.; Scholes, B.; Steinbrecher, R.; Tallamraju, R.; Taylor, J.; Zimmerman, P. *J. Geophys. Res., [Atmos.]* **1995**, *100*, 8873-8892.
3. Ciccioli, P.; Brancaleoni, E.; Frattoni, M.; Cecinato, A.; Pinciarelli, L. *Anal. Lett.* **2001**, *34*, 937-955.
4. Lemieux, P. M.; Lutes, C. C.; Santoianni, D. A. *Prog. Energy Combust. Sci.* **2004**, *30*, 1-32.
5. Sanchez, M.; Karnae, S.; John, K. *Int. J. Environ. Res. Public Health* **2008**, *5*, 130-138.
6. Wu, B.-Z.; Feng, T.-Z.; Sree, U.; Chiu, K.-H.; Lo, J.-G. *Anal. Chim. Acta* **2006**, *576*, 100-111.
7. Singh, H.; Chen, Y.; Tabazadeh, A.; Fukui, Y.; Bey, I.; Yantosca, R.; Jacob, D.; Arnold, F.; Wohlfrom, K.; Atlas, E.; Flocke, F.; Blake, D.; Blake, N.; Heikes, B.; Snow, J.; Talbot, R.; Gregory, G.; Sachse, G.; Vay, S.; Kondo, Y. *J. Geophys. Res., [Atmos.]* **2000**, *105*, 3795-3805.
8. Olivier, J. G. J.; Bouwman, A. F.; Van Der Maas, C. W. M.; Berdowski, J. J. M. *Environ. Monit. Assess.* **1994**, *31*, 93-106.
9. Dominguez-Taylor, P.; Ruiz-Suarez, L. G.; Rosas-Perez, I.; Hernandez-Solis, J. M.; Steinbrecher, R. *Atmos. Environ.* **2007**, *41*, 2780-2790.

10. Helmig, D.; Ortega, J.; Duhl, T.; Tanner, D.; Guenther, A.; Harley, P.; Wiedinmyer, C.; Milford, J.; Sakulyanontvittaya, T. *Environ. Sci. Technol.* **2007**, *41*, 1545-1553.
11. Li, D. W.; Shi, Y.; He, X. Y.; Chen, W.; Chen, X. *Bot. Stud.* **2008**, *49*, 67-72.
12. Raeisaenen, T.; Ryyppoe, A.; Kellomaeki, S. *Atmos. Environ.* **2008**, *42*, 4160-4171.
13. Caplain, I.; Cazier, F.; Nouali, H.; Mercier, A.; Dechaux, J.-C.; Nollet, V.; Joumard, R.; Andre, J.-M.; Vidon, R. *Atmos. Environ.* **2006**, *40*, 5954-5966.
14. McGaughey, G. R.; Desai, N. R.; Allen, D. T.; Seila, R. L.; Lonneman, W. A.; Fraser, M. P.; Harley, R. A.; Pollack, A. K.; Ivy, J. M.; Price, J. H. *Atmos. Environ.* **2004**, *38*, 3363-3372.
15. Rubin, J. I.; Kean, A. J.; Harley, R. A.; Millet, D. B.; Goldstein, A. H. *J. Geophys. Res., [Atmos.]* **2006**, *111*, D03305/1-D03305/7.
16. *IPCC, 2007: Climate Change 2007: The Physical Science Basis. Contribution of Working Group I to the Fourth Assessment Report of the Intergovernmental Panel on Climate Change*; Solomon, S.; Qin, D.; Manning, M.; Chen, Z.; Marquis, M.; Averyt, K. B.; Tignor, M.; Miller, H. L., Eds.; Cambridge University Press, Cambridge, United Kingdom and New York, NY, USA, 2007.
17. IARC *Monograph 7*, 1987
18. Atkinson, R.; Arey, J. *Chem. Rev. (Washington, DC, U. S.)* **2003**, *103*, 4605-4638.
19. Barrie, L. A.; Bottenheim, J. W.; Schnell, R. C.; Crutzen Paul, J.; Rasmussen, R. A. *Nature (London, U.K.)* **1988**, *334*, 138-141.
20. Kreher, K.; Johnston, P. V.; Wood, S. W.; Nardi, B.; Platt, U. *Geophys. Res. Lett.* **1997**, *24*, 3021-3024.
21. Khalil, M. A. K.; Moore, R. M.; Harper, D. B.; Lobert, J. M.; Erickson, D. J.; Koropalov, V.; Sturges, W. T.; Keene, W. C. *J. Geophys. Res., [Atmos.]* **1999**, *104*, 8333-8346.
22. Cox, R. A.; Derwent, R. G.; Eggleton, A. E. J.; Lovelock, J. E. *Atmos. Environ.* **1976**, *10*, 305-308.
23. Ballschmiter, K. *Chemosphere* **2003**, *52*, 313-324.

24. Platt, U. *Water, Air, Soil Pollut.* **2000**, *123*, 229-244.
25. Platt, U.; Hoenninger, G. *Chemosphere* **2003**, *52*, 325-338.
26. Chameides, W. L.; Davis, D. D. *J. Geophys. Res.* **1980**, *85*, 7383-7398.
27. Chatfield, R. B.; Crutzen, P. J. *J. Geophys. Res.* **1990**, *95*, 22319-22341.
28. Hoffmann, T.; O'Dowd, C. D.; Seinfeld, J. H. *Geophys. Res. Lett.* **2001**, *28*, 1949-1952.
29. LeBras, G.; Platt, U. *Geophys. Res. Lett.* **1995**, *22*, 599-602.
30. Matveev, V.; Hebestreit, K.; Stutz, J.; Platt, U.; Blake, D.; Luria, M.; Peleg, M.; Rosen, D.; Tov-Alper, D. S. *Geophys. Res. Lett.* **2001**, *106*, 599-602.
31. Nagao, I.; Matsumoto, K.; Tanaka, H. *Geophys. Res. Lett.* **1999**, *26*, 3377-3380.
32. Shon, Z.-H.; Kim, N. *Atmos. Environ.* **2002**, *36*, 4289-4298.
33. Singh, H. B.; Kasting, J. F. *J. Atmos. Chem.* **1988**, *7*, 261-285.
34. Stutz, J.; Hebestreit, K.; Alike, B.; Platt, U. *J. Atmos. Chem.* **1999**, *34*, 65-85.
35. Zafiriou, O. C. *J. Geophys. Res.* **1974**, *79*, 2730-2732.
36. Read, K. A.; Mahajan, A. S.; Carpenter, L. J.; Evans, M. J.; Faria, B. V. E.; Heard, D. E.; Hopkins, J. R.; Lee, J. D.; Moller, S. J.; Lewis, A. C.; Mendes, L.; McQuaid, J. B.; Oetjen, H.; Saiz-Lopez, A.; Pilling, M. J.; Plane, J. M. C. *Nature (London, U.K.)* **2008**, *453*, 1232-1235.
37. Davis, D.; Crawford, J.; Lui, S.; McKeen, S.; Bandy, A.; Thornton, D.; Rowland, F.; Blake, D. *J. Geophys. Res.* **1996**, *101*, 2135-2147.
38. Platt, U.; Janssen, C. *Faraday Discuss.* **1996**, *100*, 175-198.
39. Solomon, S.; Garcia, R. R.; Ravishankara, A. R. *J. Geophys. Res., [Atmos.]* **1994**, *99*, 20,491-9.
40. Tuckermann, M.; Ackermann, R.; Goelz, C.; Lorenzen-Schmidt, H.; Senne, T.; Stutz, J.; Trost, B.; Unold, W.; Platt, U. *Tellus, Ser. B* **1997**, *49B*, 533-555.
41. Tanaka, P. L.; Oldfield, S.; Neece, J. D.; Mullins, C. B.; Allen, D. T. *Environ. Sci. Technol.* **2000**, *34*, 4470-4473.

42. Tanaka, P. L.; Riemer, D. D.; Chang, S.; Yarwood, G.; McDonald-Buller, E. C.; Apel, E. C.; Orlando, J. J.; Silva, P. J.; Jimenez, J. L.; Canagaratna, M. R.; Neece, J. D.; Mullins, C. B.; Allen, D. T. *Atmos. Environ.* **2003**, *37*, 1393-1400.
43. Chang, S.; McDonald-Buller, E.; Kimura, Y.; Yarwood, G.; Neece, J.; Russell, M.; Tanaka, P.; Allen, D. *Atmos. Environ.* **2002**, *36*, 4991-5003.
44. Knipping, E. M.; Dabdub, D. *Environ. Sci. Technol.* **2003**, *37*, 275-284.
45. Chang, S.; Allen, D. T. *Environ. Sci. Technol.* **2006**, *40*, 251-262.
46. Pszenny, A. A. P.; Fischer, E. V.; Russo, R. S.; Sive, B. C.; Varner, R. K. *J. Geophys. Res., [Atmos.]* **2007**, *112*, D10S13/1-D10S13/10.
47. Pszenny, A. A. P.; Keene, W. C.; Jacob, D. J.; Fan, S.; Maben, J. R.; Zetwo, M. P.; Springer-Young, M.; Galloway, J. N. *Geophys. Res. Lett.* **1993**, *20*, 699-702.
48. National Institutes of Standards and Technology; Chemical Kinetics Database, <http://kinetics.nist.gov/kinetics/>.
49. Wingenter, O. W.; Kubo, M. K.; Blake, N. J.; Smith, T. W., Jr.; Blake, D. R.; Rowland, F. S. *J. Geophys. Res., [Atmos.]* **1996**, *101*, 4331-4340.
50. Singh, H. B.; Gregory, G. L.; Anderson, B.; Browell, E.; Sachse, G. W.; Davis, D. D.; Crawford, J.; Bradshaw, J. D.; Talbot, R.; et al. *J. Geophys. Res., [Atmos.]* **1996**, *101*, 1907-1917.
51. Pechtl, S.; von Glasow, R. *Geophys. Res. Lett.* **2007**, *34*, L11813/1-L11813/5.
52. Keene, W. C.; Khalil, M. A. K.; Erickson, D. J., III; McCulloch, A.; Graedel, T. E.; Lobert, J. M.; Aucott, M. L.; Gong, S. L.; Harper, D. B.; Kleiman, G.; Midgley, P.; Moore, R. M.; Seuzaret, C.; Sturges, W. T.; Benkovitz, C. M.; Koropalov, V.; Barrie, L. A.; Li, Y. F. *J. Geophys. Res., [Atmos.]* **1999**, *104*, 8429-8440.
53. Finlayson-Pitts, B. J. *Chem. Rev.* **2003**, *103*, 4801-4822.
54. Schweitzer, F.; George, C. *J. Atmos. Chem.* **1999**, *34*, 101-117.
55. Chameides, W. L.; Stelson, A. W. *J. Geophys. Res.* **1992**, *97*, 20565-20580.
56. Erickson, D. J., III; Seuzaret, C.; Keene, W. C.; Gong, S. L. *J. Geophys. Res., [Atmos.]* **1999**, *104*, 8347-8372.

57. Finlayson-Pitts, B. J.; Ezell, M. J.; Pitts, J. N., Jr. *Nature (London, U.K.)* **1989**, *337*, 241-244.
58. Vogt, R.; Crutzen, P. J.; Sander, R. *Nature (London, U.K.)* **1996**, *383*, 327-330.
59. Keene, W. C.; Stutz, J.; Pszenny, A. A. P.; Maben, J. R.; Fischer, E. V.; Smith, A. M.; von Glasow, R.; Pechtl, S.; Sive, B. C.; Varner, R. K. *J. Geophys. Res., [Atmos.]* **2007**, *112*, D10S12/1-D10S12/15.
60. Sive, B., C.; Zhou, Y.; Troop, D.; Wang, Y.; Little William, C.; Wingenter Oliver, W.; Russo Rachel, S.; Varner Ruth, K.; Talbot, R. *Anal. Chem.* **2005**, *77*, 6989-98.
61. Lindinger, W.; Hansel, A.; Jordan, A. *Int. J. Mass Spectrom. Ion Processes* **1998**, *173*, 191-241.
62. Hansel, A.; Jordan, A.; Holzinger, R.; Prazeller, P.; Vogel, W.; Lindinger, W. *Int. J. Mass Spectrom. Ion Processes* **1995**, *149/150*, 609-619.
63. Lindinger, W.; Jordan, A. *Chem. Soc. Rev.* **1998**, *27*, 347-354.
64. Ammann, C.; Brunner, A.; Spirig, C.; Neftel, A. *Atmos. Chem. Phys.* **2007**, *6*, 4643-4651.
65. Karl, T.; Harren, F.; Warneke, C.; de Gouw, J.; Grayless, C.; Fall, R. *J. Geophys. Res., [Atmos.]* **2005**, *110*, D15302/1-D15302/11.
66. Spirig, C.; Neftel, A.; Ammann, C.; Dommen, J.; Grabmer, W.; Thielmann, A.; Schaub, A.; Beauchamp, J.; Wisthaler, A.; Hansel, A. *Atmos. Chem. Phys.* **2005**, *5*, 465-481.
67. Steeghs, M.; Bais, H. P.; De Gouw, J.; Goldan, P.; Kuster, W.; Northway, M.; Fall, R.; Vivanco, J. M. *Plant Physiol.* **2004**, *135*, 47-58.
68. Rinne, H. J. I.; Guenther, A. B.; Warneke, C.; DeGouw, J. A.; Luxembourg, S. L. *Geophys. Res. Lett.* **2001**, *28*, 3139-3142.
69. de Gouw, J. A.; Warneke, C.; Scheeren, H. A.; van der Veen, C.; Bolder, M.; Scheele, M. P.; Williams, J.; Wong, S.; Lange, L.; Fischer, H.; Lelieveld, J. *J. Geophys. Res., [Atmos.]* **2001**, *106*, 28453-28467.

70. Crutzen, P. J.; Williams, J.; Poschl, U.; Hoor, P.; Fischer, H.; Warneke, C.; Holzinger, R.; Hansel, A.; Lindinger, W.; Scheeren, B.; Lelieveld, J. *Atmos. Environ.* **2000**, *34*, 1161-1165.
71. Sprung, D.; Jost, C.; Reiner, T.; Hansel, A.; Wisthaler, A. *J. Geophys. Res., [Atmos.]* **2001**, *106*, 28511-28528.
72. de Gouw, J. A.; Warneke, C.; Parrish, D. D.; Holloway, J. S.; Trainer, M.; Fehsenfeld, F. C. *J. Geophys. Res., [Atmos.]* **2003**, *108*, ACH2/1-ACH2/8.
73. Jiang, M.; Marr, L. C.; Dunlea, E. J.; Herndon, S. C.; Jayne, J. T.; Kolb, C. E.; Knighton, W. B.; Rogers, T. M.; Zavala, M.; Molina, L. T.; Molina, M. J. *Atmos. Chem. Phys.* **2005**, *5*, 3377-3387.
74. Kolb, C. E.; Herndon, S. C.; McManus, J. B.; Shorter, J. H.; Zahniser, M. S.; Nelson, D. D.; Jayne, J. T.; Canagaratna, M. R.; Worsnop, D. R. *Environ. Sci. Technol.* **2004**, *38*, 5694-5703.
75. Lee, A.; Goldstein, A. H.; Keywood, M. D.; Gao, S.; Varutbangkul, V.; Bahreini, R.; Ng, N. L.; Flagan, R. C.; Seinfeld, J. H. *J. Geophys. Res., [Atmos.]* **2006**, *111*, D07302/1-D07302/18.
76. Lee, A.; Goldstein, A. H.; Kroll, J. H.; Ng, N. L.; Varutbangkul, V.; Flagan, R. C.; Seinfeld, J. H. *J. Geophys. Res., [Atmos.]* **2006**, *111*, D17305/1-D17305/25.
77. Wisthaler, A.; Jensen, N. R.; Winterhalter, R.; Lindinger, W.; Hjorth, J. *Atmos. Environ.* **2001**, *35*, 6181-6191.
78. Warneke, C.; de Gouw, J. A.; Kuster, W. C.; Goldan, P. D.; Fall, R. *Environ. Sci. Technol.* **2003**, *37*, 2494-2501.
79. Steinbacher, M.; Dommen, J.; Ammann, C.; Spirig, C.; Neftel, A.; Prevot, A. S. H. *Int. J. Mass Spectrom.* **2004**, *239*, 117-128.
80. Tani, A.; Hayward, S.; Hansel, A.; Hewitt, C. N. *Int. J. Mass Spectrom.* **2004**, *239*, 161-169.
81. de Gouw, J. A.; Goldan, P. D.; Warneke, C.; Kuster, W. C.; Roberts, J. M.; Marchewka, M.; Bertman, S. B.; Pszenny, A. A. P.; Keene, W. C. *J. Geophys. Res., [Atmos.]* **2003**, *108*, ACH 10/1-ACH 10/18.
82. Hayward, S.; Hewitt, C. N.; Sartin, J. H.; Owen, S. M. *Environ. Sci. Technol.* **2002**, *36*, 1554-1560.

83. Kuster, W. C.; Jobson, B. T.; Karl, T.; Riemer, D.; Apel, E.; Goldan, P. D.; Fehsenfeld, F. C. *Environ. Sci. Technol.* **2004**, *38*, 221-228.
84. de Gouw, J.; Warneke, C. *Mass Spectrom. Rev.* **2007**, *26*, 223-257.
85. de Gouw, J.; Warneke, C.; Karl, T.; Eerdekens, G.; van der Veen, C.; Fall, R. *Int. J. Mass Spectrom.* **2003**, *223-224*, 365-382.
86. Lindinger, C. *Ionicon PTR-MS Manual*, Ionicon Analytik, 2003
87. Hansel, A. In *Europhysics News* 2004; Vol. 35.
88. Arnold, S. T.; Viggiano, A. A.; Morris, R. A. *J. Phys. Chem. A* **1998**, *102*, 8881-8887.
89. Ionicon, www.ptrms.com.
90. Hunter, E. P. L.; Lias, S., G. *J. Phys. Chem. Ref. Data* **1998**, *27*, 413-656.
91. Lindinger, W. In *Gaseous Ion Chemistry and Mass Spectrometry*; Futrell, J. H., Ed.; John Wiley and Sons: New York, 1986.
92. Zhao, J. Z., *Renyi Atmos. Environ.* **2004**, *38*, 2177-2185.
93. Hansel, A.; Jordan, A.; Warneke, C.; Holzinger, R.; Wisthaler, A.; Lindinger, W. *Plasma Sources Science & Technology* **1999**, *8*, 332-336.
94. Keck, L.; Oeh, U.; Hoeschen, C. *Int. J. Mass Spectrom.* **2007**, *264*, 92-95.
95. Warneke, C.; Holzinger, R.; Hansel, A.; Jordan, A.; Lindinger, W.; Poschl, U.; Williams, J.; Hoor, P.; Fischer, H.; Crutzen, P. J.; Scheeren, H. A.; Lelieveld, J. *J. Atmos. Chem.* **2001**, *38*, 167-185.
96. Dotan, I.; Albritton, D. L.; Lindinger, W.; Pahl, M. *J. Chem. Phys.* **1976**, *65*, 5028-5030.
97. Warneke, C.; van der Veen, C.; Luxembourg, S.; de Gouw, J. A.; Kok, A. *Int. J. Mass Spectrom.* **2001**, *207*, 167-182.
98. Lee, A.; Shade, G. W.; Holzinger, R.; Goldstein, A. H. *Atmos. Chem. Phys.* **2005**, *5*, 505-513.
99. Tani, A.; Hayward, S.; Hewitt, C. N. *Int. J. Mass Spectrom.* **2003**, *561-578*.

100. Christian, T. J.; Kleiss, B.; Yokelson, R. J.; Holzinger, R.; Crutzen, P. J.; Hao, W. M.; Shirai, T.; Blake, D. R. *J. Geophys. Res., [Atmos.]* **2004**, *109*, D02311/1-D02311/12.
101. Karl, T.; Fall, R.; Crutzen, P. J.; Jordan, A.; Lindinger, W. *Geophys. Res. Lett.* **2001**, *28*, 507-510.
102. Karl, T.; Guenther, A.; Lindinger, C.; Jordan, A.; Fall, R.; Lindinger, W. *J. Geophys. Res., [Atmos.]* **2001**, *106*, 24157-24167.
103. Holzinger, R.; Lee, A.; Paw U, K. T.; Goldstein, A. H. *Atmos. Chem. Phys.* **2005**, *5*, 67-75.
104. Taipale, R.; Ruuskanen, T. M.; Rinne, J.; Kajos, M. K.; Hakola, H.; Pohja, T.; Kulmala, M. *Atmos. Chem. Phys.* **2008**, *8*, 6681-6698.
105. Seinfeld, J. H.; Pandis, S. N. *Atmospheric Chemistry and Physics*; Wiley: New York, 1998.
106. Fuentes, J. D.; Gillespie, T. J. *Atmos. Environ., Part A* **1992**, *26A*, 1165-73.
107. Lenschow, D. H.; Pearson, R., Jr.; Stankov, B. B. *JGR, J. Geophys. Res., [Sect.] C* **1982**, *87*, 8833-7.
108. Ganzeveld, L.; Lelieveld, J. *J. Geophys. Res.* **1995**, *100*, 20999-21012.
109. Lovett, G. M. *Ecol. Apps.* **1994**, *4*, 630-650.
110. Stickler, A.; Fischer, H.; Bozem, H.; Gurk, C.; Schiller, C.; Martinez-Harder, M.; Kubistin, D.; Harder, H.; Williams, J.; Eerdekens, G.; Yassaa, N.; Ganzeveld, L.; Sander, R.; Lelieveld, J. *Atmos. Chem. Phys.* **2007**, *7*, 3933-3956.
111. Rinne, J.; Douffet, T.; Prigent, Y.; Durand, P. *Environ. Pollut. (Amsterdam, Neth.)* **2008**, *152*, 630-635.
112. Custer, T.; Schade, G. *Tellus, Ser. B* **2007**, *59B*, 673-684.
113. Moncrieff, J.; Valentini, R.; Greco, S.; Seufert, G.; Ciccioli, P. *J. Exp. Bot.* **1997**, *48*, 1133-1142.
114. Loescher, H. W.; Law, B. E.; Mahrt, L.; Hollinger, D. Y.; Campbell, J.; Wofsy, S. C. *J. Geophys. Res., [Atmos.]* **2006**, *111*, D21S90/1-D21S90/19.
115. Desjardins, R. L. *Boundary-Layer Meteorology* **1977**, *11*, 147-154.

116. Businger, J. A.; Oncley, S. P. *J. Atmos. Ocean. Tech.* **1990**, *7*, 349-352.
117. Lenschow, D. H.; Mann, J.; Kristensen, L. *J. Atmos. Ocean. Tech.* **1994**, *11*, 661-673.
118. Kaimal, J. C.; Gaynor, J. E. *J. Climate Appl. Meteor.* **1983**, *22*, 863-880.
119. Dabberdt, W. F.; Lenschow, D. H.; Horst, T. W.; Zimmerman, P. R.; Oncley, S. P.; Delany, A. C. *Science (Washington, DC, U. S.)* **1993**, *260*, 1472-1481.
120. Karl, T.; Potosnak, M.; Guenther, A.; Clark, D.; Walker, J.; Herrick, J. D.; Geron, C. *J. Geophys. Res., [Atmos.]* **2004**, *109*, D18306/1-D18306/19.
121. Warneke, C.; Luxembourg, S. L.; de Gouw, J. A.; Rinne, H. J. I.; Guenther, A. B.; Fall, R. *J. Geophys. Res., [Atmos.]* **2002**, *107*, ACH 6/1-ACH 6/11.
122. Karl, T. G.; Spirig, C.; Rinne, J.; Stroud, C.; Prevost, P.; Greenberg, J.; Fall, R.; Guenther, A. *Atmos. Chem. Phys.* **2002**, *2*, 279-291.
123. Karl, T.; Guenther, A.; Spirig, C.; Hansel, A.; Fall, R. *Geophys. Res. Lett.* **2003**, *30*, 2186.
124. Goldstein, A. H.; Daube, B. C.; Munger, J. W.; Wofsy, S. C. *J. Atmos. Chem.* **1995**, *21*, 43-59.
125. Wesely, M. L.; Hicks, B. B. *Atmos. Environ.* **2000**, *34*, 2261-2282.
126. Rinne, J.; Tuovinen, J. P.; Laurila, T.; Hakola, H.; Aurela, M.; Hyyen, H. *Agr. Forest Meteor.* **2000**, *103*, 25-37.
127. Hicks, B. B.; Baldocchi, D. D.; Meyers, T. P.; Hosker, R. P.; Matt, D. R. *Water, Air, Soil Pollut.* **1987**, *36*, 311-330.
128. Wesely, M. L. *Atmos. Environ.* **1989**, *23*, 1293-1304.
129. Dentener, F. J.; Crutzen, P. J. *J. Geophys. Res.* **1993**, *98*, 7149-7163.
130. Levy, H., II; Moxin, W. J. *Tellus, Ser. B* **1989**, *41*, 256-271.
131. Kasibhatla, P. S.; Levy, H., II; Moxin, W. J. *J. Geophys. Res., [Atmos.]* **1993**, *98*, 7165-80.

132. Joeckel, P.; Tost, H.; Pozzer, A.; Bruehl, C.; Buchholz, J.; Ganzeveld, L.; Hoor, P.; Kerkweg, A.; Lawrence, M. G.; Sander, R.; Steil, B.; Stiller, G.; Tanarhte, M.; Taraborrelli, D.; van Aardenne, J.; Lelieveld, J. *Atmos. Chem. Phys.* **2007**, *6*, 5067-5104.
133. Kerkweg, A.; Buchholz, J.; Ganzeveld, L.; Pozzer, A.; Tost, H.; Joeckel, P. *Atmos. Chem. Phys.* **2007**, *6*, 4617-4632.
134. Pozzer, A.; Joeckel, P.; Sander, R.; Williams, J.; Ganzeveld, L.; Lelieveld, J. *Atmos. Chem. Phys.* **2007**, *6*, 5435-5444.
135. *The Role of Air-Sea Exchange in Geochemical Cycling*; Liss, P. S.; Merlivat, L., Eds. Reidel, Dordrecht, 1986.
136. Nightingale, P. D.; Malin, G.; Law, C. S.; Watson, A. J.; Liss, P. S.; Liddicoat, M. I.; Boutin, J.; Upstill-Goddard, R. C. *Global Biogeochem. Cycles* **2000**, *14*, 373-387.
137. Wanninkhof, R. *J. Geophys. Res.* **1992**, *97*, 7373-7382.
138. Yvon-Lewis, S. A.; Butler, J. H. *J. Geophys. Res., [Atmos.]* **2002**, *107*, ACH1/1-ACH1/9.
139. Hicks, B. B. *Water, Air, Soil Pollut.* **1986**, *30*, 75-90.
140. Sanhueza, E.; Holzinger, R.; Kleiss, B.; Donoso, L.; Crutzen, P. J. *Atmos. Chem. Phys.* **2004**, *4*, 275-280.
141. Carpenter, L. J.; Lewis, A. C.; Hopkins, J. R.; Read, K. A.; Longley, I. D.; Gallagher, M. W. *Global Biogeochem. Cycles* **2004**, *18*, GB4027/1-GB4027/8.
142. Wesely, M. L. *Handb. Weather, Clim. Water* **2003**, *1*, 347-355.
143. Zhang, L.; Brook, J. R.; Vet, R. *Atmos. Chem. Phys.* **2003**, *3*, 2067-2082.
144. Singh, H. B.; Tabazadeh, A.; Evans, M. J.; Field, B. D.; Jacob, D. J.; Sachse, G.; Crawford, J. H.; Shetter, R.; Brune, W. H. *Geophys. Res. Lett.* **2003**, *30*, ASC 13/1-ASC 13/5.
145. Jacob, D. J.; Field, B. D.; Jin, E. M.; Bey, I.; Li, Q.; Logan, J. A.; Yantosca, R. M.; Singh, H. B. *J. Geophys. Res., [Atmos.]* **2002**, *107*, ACH 5/1-ACH 5/19.
146. Singh, H. B.; Chen, Y.; Staudt, A.; Jacob, D. J.; Blake, D. R.; Heikes, B.; Snow, J. *Nature* **2001**, 1078-1081.

147. Marandino, C. A.; De Bruyn, W. J.; Miller, S. D.; Prather, M. J.; Saltzman, E. S. *Geophys. Res. Lett.* **2005**, *32*, L15806/1-L15806/4.
148. Mao, H.; Talbot, R.; Nielsen, C.; Sive, B. *Geophys. Res. Lett.* **2006**, *33*, L02803/1-L02803/4.
149. Singh, H. B.; Salas, L. J.; Chatfield, R. B.; Czech, E.; Fried, A.; Walega, J.; Evans, M. J.; Field, B. D.; Jacob, D. J.; Blake, D.; Heikes, B.; Talbot, R.; Sachse, G.; Crawford, J. H.; Avery, M. A.; Sandholm, S.; Fuelberg, H. *J. Geophys. Res., [Atmos.]* **2004**, *109*, D15S07/1-D15S07/20.
150. Guenther, A.; Karl, T.; Harley, P.; Wiedinmyer, C.; Palmer, P. I.; Geron, C. *Atmos. Chem. Phys.* **2006**, *6*, 3181-3210.
151. Atkinson, R. *Atmos. Environ.* **2000**, *34*, 2063-2101.
152. Brown, S. S.; Dibb, J. E.; Stark, H.; Aldener, M.; Vozella, M.; Whitlow, S.; Williams, E. J.; Lerner, B. M.; Jakoubek, R.; Middlebrook, A. M.; DeGouw, J. A.; Warneke, C.; Goldan, P. D.; Kuster, W. C.; Angevine, W. M.; Sueper, D. T.; Quinn, P. K.; Bates, T. S.; Meagher, J. F.; Fehsenfeld, F. C.; Ravishankara, A. R. *Geophys. Res. Lett.* **2004**, *31*, L07108/1-L07108/5.
153. Talbot, R.; Mao, H.; Sive, B. *J. Geophys. Res., [Atmos.]* **2005**, *110*, D09307/1-D09307/16.
154. Darby, L. S.; McKeen, S. A.; Senff, C. J.; White, A. B.; Banta, R. M.; Post, M. J.; Brewer, W. A.; Marchbanks, R.; Alvarez, R. J., II; Peckham, S. E.; Mao, H.; Talbot, R. *J. Geophys. Res., [Atmos.]* **2007**, *112*, D16S91/1-D16S91/17.
155. Mao, H.; Talbot, R. *J. Geophys. Res., [Atmos.]* **2004**, *109*, D20305.
156. Mao, H.; Talbot, R. *J. Geophys. Res., [Atmos.]* **2004**, *109*, D21304/1-D21304/19.
157. Galbally, I. E.; Kirstine, W. *J. Atmos. Chem.* **2002**, *43*, 195-229.
158. Fall, R. In *Reactive Hydrocarbons in the Atmosphere*; Hewitt, C. N., Ed.; Academic Press: San Diego, 1999, p 41-96.
159. MacDonald, R. C.; Fall, R. *Atmos. Environ., Part A* **1993**, *27A*, 1709-1713.
160. Warneke, C.; Karl, T.; Judmaier, H.; Hansel, A.; Jordan, A.; Lindinger, W.; Crutzen, P. J. *Global Biogeochem. Cycles* **1999**, *13*, 9-17.

161. Madronich, S.; Calvert, J. G. *J. Geophys. Res., [Atmos.]* **1990**, *95*, 5697-5716.
162. Tyndall, G. S.; Orlando, J. J.; Wallington, T. J.; Hurley, M. D. *J. Phys. Chem. A* **2001**, *105*, 5380-5384.
163. Riemer, D.; Pos, W.; Milne, P.; Farmer, C.; Zika, R.; Apel, E.; Olszyna, K.; Kliendienst, T.; Lonneman, W.; Bertman, S.; Shepson, P.; Starn, T. *J. Geophys. Res., [Atmos.]* **1998**, *103*, 28111-28128.
164. National Research Council *Rethinking the Ozone Problem in Urban and Regional Air Pollution*; National Academy Press: Washington, D.C., 1991.
165. Kimmerer, T. W.; Kozlowski, T. T. *Plant Physiol.* **1982**, *69*, 840-847.
166. Carlier, P.; Hannachi, H.; Mouvier, G. *Atmos. Environ.* **1986**, *20*, 2079-2099.
167. Holzinger, R.; Warneke, C.; Hansel, A.; Jordan, A.; Lindinger, W.; Scharffe, D. H.; Schade, G.; Crutzen, P. J. *Geophys. Res. Lett.* **1999**, *26*, 1161-1164.
168. Kleiss, B.; Dissertation, Johannes Gutenberg-Universitaet in Mainz, 2004.
169. Warneke, C.; de Gouw, J. A. *Atmos. Environ.* **2001**, *35*, 5923-5933.
170. Atkinson, R. *J. Phys. Chem. Ref. Data, Monograph 2* **1994**, *2*, 1-216.
171. De Gouw, J. A.; Howard, C. J.; Custer, T. G.; Fall, R. *Geophys. Res. Lett.* **1999**, *26*, 811-814.
172. Jenkin, M. E.; Saunders, S. M.; Pilling, M. J. *Atmos. Environ.* **1997**, *31*, 81-104.
173. Koenig, G.; Brunda, M.; Puxbaum, H.; Hewitt, C. N.; Duckham, S. C.; Rudolph, J. *Atmos. Environ.* **1995**, *29*, 861-874.
174. Fehsenfeld, F. C.; Calvert, J. G.; Fall, R.; Goldan, P. D.; Guenther, A.; Hewitt, C. N.; Lamb, B.; Lui, S.; Trainer, M.; Westberg, H.; Zimmerman, P. *Global Biogeochem. Cycles* **1992**, *6*, 389-430.
175. Romero, M. T. B.; Blitz, M. A.; Heard, D. E.; Pilling, M. J.; Price, B.; Seakins, P. W.; Wang, L. *Faraday Discuss.* **2005**, *130*, 73-88.
176. Sive, B. C. *personal communication*; 2007.
177. Rinne, J.; Hakola, H.; Laurila, T.; Rannik, U. *Atmos. Environ.* **2000**, *34*, 1099-1107.

178. Calogirou, A.; Larsen, B. R.; Kotzias, D. *Atmos. Environ.* **1999**, *33*, 1423-1439.
179. Hatakeyama, S.; Izumi, K.; Fukuyama, T.; Akimoto, H.; Washida, N. *J. Geophys. Res., [Atmos.]* **1991**, *94*, 947-958.
180. Hakola, H.; Arey, J.; Aschmann, S. M.; Atkinson, R. *J. Atmos. Chem.* **1994**, *18*, 75-102.
181. Noziere, B.; Spittler, M.; Ruppert, L.; Barnes, I.; Becker, K. H. *PSI-Proceedings* **1997**, *97-02*, 90-92.
182. Aschmann, S. M.; Reissell, A.; Atkinson, R.; Arey, J. *J. Geophys. Res., [Atmos.]* **1998**, *103*, 25553-25561.
183. Orlando, J. J.; Noziere, B.; Tyndall, G. S.; Orzechowska, G. E.; Paulson, S. E.; Rudich, Y. *J. Geophys. Res., [Atmos.]* **2000**, *105*, 11561-11572.
184. Larsen, B. R.; Di Bella, D.; Glasius, M.; Winterhalter, R.; Jensen, N. R.; Hjorth, J. *J. Atmos. Chem.* **2001**, *38*, 231-276.
185. Librando, V.; Tringali, G. *J. Environ. Manage.* **2005**, *75*, 275-282.
186. Capouet, M.; Peeters, J.; Noziere, B.; Mueller, J. F. *Atmos. Chem. Phys.* **2004**, *4*, 2285-2311.
187. Peeters, J.; Vereecken, L.; Fantechi, G. *Phys. Chem. Chem. Phys.* **2001**, *3*, 5489-5504.
188. Sharkey, T. D.; Yeh, S. *Annu. Rev. Plant Physiol. Plant Mol. Biol.* **2001**, *52*, 407-436.
189. Guenther, A.; Zimmerman, P. R.; Harley, P. C. *J. Geophys. Res., [Atmos.]* **1993**, *D7*, 12609-12617.
190. Reimann, S.; Calanca, P.; Hofer, P. *Atmos. Environ.* **2000**, *34*, 109-115.
191. Poisson, N.; Kanakidou, M.; Crutzen, P. J. *J. Atmos. Chem.* **2000**, *36*, 157-230.
192. Roberts, J. M.; Williams, J.; Baumann, K.; Buhr, M. P.; Goldan, P. D.; Holloway, J.; Hubler, G.; Kuster, W. C.; McKeen, S. A.; Ryerson, T. B.; Trainer, M.; Williams, E. J.; Fehsenfeld, F. C.; Bertman, S. B.; Nouaime, G.; Seaver, C.; Grodzinsky, G.; Rodgers, M.; Young, V. L. *J. Geophys. Res., [Atmos.]* **1998**, *103*, 22473-22490.

193. Williams, J.; Roberts, J. M.; Fehsenfeld, F. C.; Bertman, S. B.; Buhr, M. P.; Goldan, P. D.; Hubler, G.; Kuster, W. C.; Ryerson, T. B.; et al. *Geophys. Res. Lett.* **1997**, *24*, 1099-1102.
194. Gu, C. L.; Rynard, C. M.; Hendry, D. G.; Mill, T. *Environ. Sci. Technol.* **1985**, *19*, 151-155.
195. Tauzon, E. C.; Atkinson, R. *Int. J. Chem. Kinet.* **1990**, *22*, 1221-1236.
196. Atkinson, R.; Aschmann, S. M.; Tuazon, E. C.; Arey, J.; Zielinska, B. *Int. J. Chem. Kinet.* **1989**, *21*, 593-604.
197. Grosjean, D. *Quimica Nova* **1995**, *18*, 184-201.
198. Killus, J. P.; Whitten, G. Z. *Environ. Sci. Technol.* **1984**, *18*, 142-148.
199. Miyoshi, A.; Hatakeyama, S.; Washida, N. *J. Geophys. Res., [Atmos.]* **1994**, *99*, 18779-18787.
200. Paulson, S. E.; Flagan, R. C.; Seinfeld, J. H. *Int. J. Chem. Kinet.* **1992**, *24*, 79-101.
201. Sprengnether, M.; Demerjian, K. L.; Donahue, N. M.; Anderson, J. G. *J. Geophys. Res., [Atmos.]* **2002**, *107*, ACH8/1-ACH8/13.
202. Roberts, J. M.; Marchewka, M.; Bertman, S. B.; Goldan, P.; Kuster, W.; de Gouw, J.; Warneke, C.; Williams, E.; Lerner, B.; Murphy, P.; Apel, E.; Fehsenfeld, F. C. *J. Geophys. Res., [Atmos.]* **2006**, *111*, D23S12/1-D23S12/9.
203. Ambrose, J. L.; Mao, H.; Mayne, H. R.; Stutz, J.; Talbot, R.; Sive, B. C. *J. Geophys. Res., [Atmos.]* **2007**, *112*, D21302/1-D21302/19.
204. Ruppert, L.; Becker, K. H. *Atmos. Environ.* **2000**, *34*, 1529-1542.
205. Holzinger, R.; Jordan, A.; Hansel, A.; Lindinger, W. *Atmos. Environ.* **2001**, *35*, 2525-2532.
206. Jacob, D. J.; Field, B. D.; Li, Q.; Blake, D. R.; de Gouw, J.; Warneke, C.; Hansel, A.; Wisthaler, A.; Singh, H. B.; Guenther, A. *J. Geophys. Res., [Atmos.]* **2005**, *110*, D08303/1-D08303/17.
207. Rottenberger, S.; Kuhn, U.; Wolf, A.; Schebeske, G.; Oliva, S. T.; Tavares, T. M.; Kesselmeier, J. *Atmos. Environ.* **2005**, *39*, 2275-2279.

208. Heikes, B. G.; Chang, W.; Pilson, M. E. Q.; Swift, E.; Singh, H. B.; Guenther, A.; Jacob, D. J.; Field, B. D.; Fall, R.; Riemer, D.; Brand, L. *Global Biogeochem. Cycles* **2002**, *16*, 80/1-80/13.
209. Fenske, J. D.; Hasson, A. S.; Ho, A. W.; Paulson, S. E. *J. Phys. Chem. A* **2000**, *104*, 9921-9932.
210. Iinuma, Y.; Boge, O.; Gnauk, T.; Herrmann, H. *Atmos. Environ.* **2004**, *38*, 761-773.
211. Jang, M.; Kamens, R. M. *Atmos. Environ.* **1998**, *33*, 459-474.
212. Jang, M.; Kamens, R. M. *Environ. Sci. Technol.* **1998**, *32*, 1237-1243.
213. Pinto, D. M.; Tiiva, P.; Miettinen, P.; Joutsensaari, J.; Kokkola, H.; Nerg, A.-M.; Laaksonen, A.; Holopainen, J. K. *Atmos. Environ.* **2007**, *41*, 4877-4887.
214. Cai, X.; Griffin, R. J. *J. Geophys. Res., [Atmos.]* **2006**, *111*, D14206/1-D14206/14.
215. Docherty, K. S.; Wu, W.; Lim, Y. B.; Ziemann, P. J. *Environ. Sci. Technol.* **2005**, *39*, 4049-4059.
216. Docherty, K. S.; Ziemann, P. J. *Aerosol Sci. Technol.* **2003**, *37*, 877-891.
217. Ferronato, C.; Orlando, J. J.; Tyndall, G. S. *J. Geophys. Res., [Atmos.]* **1998**, *103*, 25579 - 25586.
218. Orlando, J. J.; Piety, C. A.; Nicovich, J. M.; McKee, M. L.; Wine, P. H. *J. Phys. Chem. A* **2005**, *109*, 6659-6675.
219. Orlando, J. J.; Tyndall, G. S.; Bilde, M.; Ferronato, C.; Wallington, T. J.; Vereecken, L.; Peeters, J. *J. Phys. Chem. A* **1998**, *102*, 8116-8123.
220. Orlando, J. J.; Tyndall, G. S.; Paulson, S. E. *Geophys. Res. Lett.* **1999**, *26*, 2191-2194.
221. Pinho, P. G.; Pio, C. A.; Carter, W. P. L.; Jenkin, M. E. *J. Atmos. Chem.* **2007**, *57*, 171-202.
222. Winer, A. M.; Lloyd, A. C.; Darnall, K. R.; Pitts, J. N., Jr. *J. Phys. Chem.* **1976**, *80*, 1635-9.

223. Ziemann, P. J. *J. Phys. Chem. A* **2003**, *107*, 2048-2060.
224. Geron, C.; Rasmussen, R.; Arnts, R. R.; Guenther, A. *Atmos. Environ.* **2000**, *34*, 1761 - 1781.
225. Chen, M.; Talbot, R.; Mao, H.; Sive, B.; Chen, J.; Griffin, R. J. *J. Geophys. Res., [Atmos.]* **2007**, *112*, D10S05.
226. Goldan, P. D.; Kuster, W. C.; Williams, E.; Murphy, P. C.; Fehsenfeld, F. C.; Meagher, J. *J. Geophys. Res., [Atmos.]* **2004**, *109*, D21309/1-D21309/14.
227. Guenther, A.; Geron, C.; Pierce, T.; Lamb, B.; Harley, P.; Fall, R. *Atmos. Environ.* **2000**, *34*, 2205-2230.
228. Lamb, B.; Westberg, H.; Allwine, G.; Quarles, T. *J. Geophys. Res., [Atmos.]* **1985**, *90*, 2380-90.
229. Warneke, C.; De Gouw, J. A.; Goldan, P. D.; Kuster, W. C.; Williams, E. J.; Lerner, B. M.; Jakoubek, R.; Brown, S. S.; Stark, H.; Aldener, M.; Ravishankara, A. R.; Roberts, J. M.; Marchewka, M.; Bertman, S.; Sueper, D. T.; McKeen, S. A.; Meagher, J. F.; Fehsenfeld, F. C. *J. Geophys. Res., [Atmos.]* **2004**, *109*, D10309/1-D10309/14.
230. Odum, J. R.; Hoffmann, T.; Bowman, F.; Collins, D.; Flagan, R. C.; Seinfeld, J. H. *Environ. Sci. Technol.* **1996**, *30*, 2580-2585.
231. Bonn, B.; Moortgat, G. K. *Atmos. Chem. Phys.* **2002**, *2*, 183-196.
232. Burkholder, J. B.; Baynard, T.; Ravishankara, A. R.; Lovejoy, E. R. *J. Geophys. Res., [Atmos.]* **2007**, *112*, D10216/1-D10216/16.
233. Chen, J.; Griffin, R. J. *Atmos. Environ.* **2005**, *39*, 7731-7744.
234. Glasius, M.; Lahaniati, M.; Calogirou, A.; Di Bella, D.; Jensen, N. R.; Hjorth, J.; Kotzias, D.; Larsen, B. R. *Environ. Sci. Technol.* **2000**, *34*, 1001-1010.
235. Grosjean, D.; Williams, E. L., II; Grosjean, E.; Andino, J. M.; Seinfeld, J. H. *Environ. Sci. Technol.* **1993**, *27*, 2754-8.
236. Iinuma, Y.; Boege, O.; Mueller, K.; Gnauk, T.; Herrmann, H. *Transp. Chem. Transform. Troposphere, Proc. EUROTRAC Symp., 7th* **2002**, 442-445.
237. Jaoui, M.; Kamens, R. M. *J. Atmos. Chem.* **2003**, *44*, 259-297.

238. Jonsson, A. M.; Hallquist, M.; Saathoff, H. *J. Aerosol Sci.* **2007**, *38*, 843-852.
239. Nizkorodov, S. A.; Bateman, A. P.; Mang, S. A.; Pan, X.; Underwood, J. S.; Walser, M. L.; Xing, J.; Dessiaterik, Y.; Laskin, J.; Laskin, A. *Prepr. Ext. Abstr. ACS Natl. Meet., Am. Chem. Soc., Div. Environ. Chem.* **2007**, *47*, 314-316.
240. Schrader, W.; Geiger, J.; Hoffmann, T.; Klockow, D.; Korte, E. H. *J. Chromatogr., A* **1999**, *864*, 299-314.
241. Yu, J.; Cocker, D. R., III; Griffin, R. J.; Flagan, R. C.; Seinfeld, J. H. *J. Atmos. Chem.* **1999**, *34*, 207-258.
242. Waengberg, I.; Barnes, I.; Becker, K. H. *Environ. Sci. Technol.* **1997**, *31*, 2130-2135.
243. Spittler, M.; Barnes, I.; Bejan, I.; Brockmann, K. J.; Benter, T.; Wirtz, K. *Atmos. Environ.* **2006**, *40*, S116-S127.
244. Aschmann, S. M.; Atkinson, R.; Arey, J. *J. Geophys. Res., [Atmos.]* **2002**, *107*, ACH 6/1-ACH 6/7.
245. Atkinson, R.; Aschmann, S. M.; Arey, J.; Shorees, B. *J. Geophys. Res., [Atmos.]* **1992**, *97*, 6065-73.
246. Atkinson, R.; Aschmann, S. M.; Pitts, J. N., Jr. *Int. J. Chem. Kinet.* **1986**, *18*, 287-99.
247. Becker, K. H.; Spittler, M. *The formation of organic nitrates in gas-phase oxidation of alpha-pinene with hydroxyl radicals*, Fachbereich 9 Physikalische Chem., Bergische Univ. Gesamthochschule Wuppertal, Wuppertal, Germany., 1997, p 1-75
248. Bonn, B.; Moortgat, G. K. *Transp. Chem. Transform. Troposphere, Proc. EUROTRAC Symp., 7th* **2002**, 481-484.
249. Chew, A. A.; Atkinson, R. *J. Geophys. Res., [Atmos.]* **1996**, *101*, 28649-28653.
250. Chuong, B.; Davis, M.; Edwards, M.; Stevens, P. S. *Int. J. Chem. Kinet.* **2002**, *34*, 300-308.
251. Davis, M. E.; Stevens, P. S. *Atmos. Environ.* **2005**, *39*, 1765-1774.
252. Davis, M. E.; Tapscott, C.; Stevens, P. S. *Int. J. Chem. Kinet.* **2005**, *37*, 522-531.

253. Gill, K. J.; Hites, R. A. *J. Phys. Chem. A* **2002**, *106*, 2538-2544.
254. Liu, Z.; Chen, Z.; Wang, X.; Shao, K.; Li, J. *Huanjing Huaxue* **2000**, *19*, 270-276.
255. Noziere, B.; Barnes, I.; Becker, K.-H. *J. Geophys. Res., [Atmos.]* **1999**, *104*, 23645-23656.
256. Van den Bergh, V.; Coeckelberghs, H.; Vanhees, I.; De Boer, R.; Compernelle, F.; Vinckier, C. *Anal. Bioanal. Chem.* **2002**, *372*, 630-638.
257. Van den Bergh, V.; Vanhees, I.; De Boer, R.; Compernelle, F.; Vinckier, C. *J. Chromatogr., A* **2000**, *896*, 135-148.
258. Vanhees, I.; Van den Bergh, V.; Schildermans, R.; De Boer, R.; Compernelle, F.; Vinckier, C. *J. Chromatogr., A* **2001**, *915*, 75-83.
259. Vinckier, C.; Compernelle, F.; Saleh, A. M. *Bull. Soc. Chim. Belg.* **1997**, *106*, 501-513.
260. Vinckier, C.; Compernelle, F.; Saleh, A. M.; Van Hoof, N.; Van Hees, I. *Fresenius Environ. Bull.* **1998**, *7*, 361-368.
261. Finlayson-Pitts, B. J.; Keoshian, C. J.; Buehler, B.; Ezell, A. A. *Int. J. Chem. Kinet.* **1999**, *31*, 491-499.
262. Timerghazin, Q. K.; Ariya, P. A. *Phys. Chem. Chem. Phys.* **2001**, *3*, 3981-3986.
263. Canosa-Mas, C. E.; Hutton-Squire, H. R.; King, M. D.; Stewart, D. J.; Thompson, K. C.; Wayne, R. P. *J. Atmos. Chem.* **1999**, *34*, 163-170.
264. Orlando, J. J.; Tyndall, G. S.; Apel, E. C.; Riemer, D. D.; Paulson, S. E. *Int. J. Chem. Kinet.* **2003**, *35*, 334-353.
265. Bedjanian, Y.; Laverdet, G.; Le Bras, G. *J. Phys. Chem. A* **1998**, *102*, 953-959.
266. Coquet, S.; Ariya, P. A. *Int. J. Chem. Kinet.* **2000**, *32*, 478-484.
267. Ezell, M. J.; Wang, W.; Ezell, A. A.; Soskin, G.; Finlayson-Pitts, B. J. *Phys. Chem. Chem. Phys.* **2002**, *4*, 5813-5820.
268. Fantechi, G.; Jensen, N. R.; Saastad, O.; Hjorth, J.; Peeters, J. *J. Atmos. Chem.* **1998**, *31*, 247-267.
269. Lei, W.; Zhang, R. *J. Chem. Phys.* **2000**, *113*, 153-157.

270. Notario, A.; Le Bras, G.; Mellouki, A. *Chem. Phys. Lett.* **1997**, *281*, 421-425.
271. Stutz, J.; Ezell, M. J.; Ezell, A. A.; Finlayson-Pitts, B. J. *J. Phys. Chem. A* **1998**, *102*, 8510-8519.
272. Wang, W.; Finlayson-Pitts, B. J. *J. Geophys. Res., [Atmos.]* **2001**, *106*, 4939-4958.
273. Ragains, M. L.; Finlayson-Pitts, B. J. *J. Phys. Chem. A* **1997**, *101*, 1509-1517.
274. Nordmeyer, T.; Wang, W.; Ragains, M. L.; Finlayson-Pitts, B. J.; Spicer, C. W.; Plastridge, R. A. *Geophys. Res. Lett.* **1997**, *24*, 1615-1618.
275. Lei, W.; Zhang, D.; Zhang, R.; Molina, L. T.; Molina, M. J. *Chem. Phys. Lett.* **2002**, *357*, 45-50.
276. Orlando, J. J.; Tyndall, G. S. *J. Phys. Chem. A* **2002**, *106*, 312-319.
277. Riemer, D. D.; Apel, E. C.; Orlando, J.; Tanaka, P. L.; Allen, D.; Neece, J. *Conf. Atmos. Chem.: Urban, Reg., Global Scale Impacts Air Pollut., 4th* **2002**, 209-213.
278. Kaiser, E. W.; Donahue, C. J.; Pala, I. R.; Wallington, T. J.; Hurley, M. D. *J. Phys. Chem. A* **2007**, *111*, 1286-1299.
279. Rodriguez, D.; Rodriguez, A.; Notario, A.; Aranda, A.; Diaz-de-Mera, Y.; Martinez, E. *Atmos. Chem. Phys.* **2005**, *5*, 3433-3440.
280. Tyndall, G. S.; Orlando, J. J.; Wallington, T. J.; Dill, M.; Kaiser, E. W. *Int. J. Chem. Kinet.* **1997**, *29*, 43-55.
281. Noziere, B.; Spittler, M.; Ruppert, L.; Barnes, I.; Becker, K. H.; Pons, M.; Wirtz, K. *Int. J. Chem. Kinet.* **1999**, *31*, 291-301.
282. Jenkin, M. E.; Cox, R. A.; Emrich, M.; Moortgat, G. K. *J. Chem. Soc., Faraday Trans.* **1993**, *89*, 2983-2991.
283. Orlando, J. J.; Tyndall, G. S.; Fracheboud, J.-M.; Estupinan, E. G.; Haberkorn, S.; Zimmer, A. *Atmos. Environ.* **1999**, *33*, 1621-1629.
284. Rosado-Reyes, C. M.; Francisco, J. S. *J. Geophys. Res., [Atmos.]* **2007**, *112*, D14310/1-D14310/46.

285. Vereecken, L.; Peeters, J.; Orlando, J.; Tyndall, G. *Transp. Chem. Transform. Troposphere, Proc. EUROTRAC Symp., 6th* **2001**, 460-463.
286. Notario, A. M., A.; Le Bras, G. *Int. J. Chem. Kinet.* **2000**, *32*, 62-66.
287. DeMore, W. B.; Sander, S. P.; Golden, D. M.; Hampson, R. F.; Kurylo, M. J.; Howard, C. J.; Ravishankara, A. R.; Kolb, C. J.; Molina, M. J. *JPL Publication 97-4* **1997**, 1-266.
288. Niki, H.; Maker, P. D.; Savage, C. M.; Breitenbach, L. P.; Hurley, M. D. *J. Phys. Chem.* **1987**, *91*, 941-946.
289. Daele, V.; Poulet, G. *J. Chim. Phys. Phys.-Chim. Biol.* **1996**, *93*, 1081-1099.
290. Daele, V. L., G.; Poulet, G. *Int. J. Chem. Kinet.* **1996**, *28*, 589-598.
291. DeMore, W. B.; Sander, S. P.; Golden, D. M.; Hampson, R. F.; Kurylo, M. J.; Howard, C. J.; Ravishankara, A. R.; Kolb, C. J.; Molina, M. J. *JPL Publication 94-26* **1994**, 1-2.
292. Jungkamp, T. P. W.; Kukui, A.; Schindler, R. N. *Ber. Bunsenges. Phys. Chem.* **1995**, *99*, 1057-1066.
293. Maricq, M. M.; Szente, J. J.; Kaiser, E. W.; Shi, J. *J. Phys. Chem.* **1994**, *98*, 2083-2089.
294. Karlsson, R. S.; Szente, J. J.; Ball, J. C.; Maricq, M. M. *J. Phys. Chem. A* **2001**, *105*, 82-96.
295. Noziere, B.; Lesclaux, R. *J. Phys. Chem.* **1994**, *98*, 2864-2873.
296. Heicklen, J. *Adv. Photochem.* **1988**, *14*, 177-272.
297. Orlando, J. J.; Tyndall, G. S.; Wallington, T. J. *Chem. Rev. (Washington, DC, U. S.)* **2003**, *103*, 4657-4689.
298. Arey, J.; Atkinson, R.; Aschmann, S. M. *J. Geophys. Res., [Atmos.]* **1990**, *95*, 18539-46.
299. Fantechi, G.; Vereecken, L.; Peeters, J. *Transp. Chem. Transform. Troposphere, Proc. EUROTRAC Symp., 7th* **2002**, 434-437.
300. Muller, J. F.; Vinckier, C.; Peeters, J. *Transp. Chem. Transform. Troposphere, Proc. EUROTRAC Symp., 5th* **1999**, *1*, 138-143.

301. Reissell, A.; Harry, C.; Aschmann, S. M.; Atkinson, R.; Arey, J. *J. Geophys. Res., [Atmos.]* **1999**, *104*, 13869-13879.
302. Vereecken, L.; Mueller, J. F.; Peeters, J. *Phys. Chem. Chem. Phys.* **2007**, *9*, 5241-5248.
303. Vereecken, L.; Nguyen, T. L.; Hermans, I.; Peeters, J. *Chem. Phys. Lett.* **2004**, *393*, 432-436.
304. Maricq, M. M.; Shi, J.; Szente, J. J.; Rimai, L.; Kaiser, E. W. *J. Phys. Chem.* **1993**, *97*, 9686-9694.
305. Atkinson, R.; Baulch, D. L.; Cox, R. A.; Crowley, J. N.; Hampson, R. F., Jr.; Kerr, J. A.; Rossi, M. J.; Troe, J. *IUPAC Subcommittee on Gas Kinetic Data Evaluation for Atmospheric Chemistry Web Version December 2001* **2001**, 1-56.
306. Atkinson, R.; Baulch, D. L.; Cox, R. A.; Hampson Jr., R. F.; Kerr, J. A.; Troe, J. *J. Phys. Chem. Ref. Data* **1989**, *18*, 881-1097.
307. Atkinson, R.; Baulch, D. L.; Cox, R. A.; Hampson, R. F., Jr.; Kerr, J. A.; Rossi, M. J.; Troe, J. *J. Phys. Chem. Ref. Data* **1997**, *26*, 521-1011.
308. Cox, R. A.; Tyndall, G. S. *Chem. Phys. Lett.* **1979**, *65*, 357-360.
309. Cox, R. A.; Tyndall, G. S. *J. Chem. Soc., Faraday Trans. 2* **1980**, *76*, 153-163.
310. Helleis, F.; Moortgat, G. K.; Crowley, J. N. *J. Phys. Chem.* **1996**, *100*, 17846-17854.
311. Kenner, R. D.; Ryan, K. R.; Plumb, I. C. *Geophys. Res. Lett.* **1993**, *20*, 1571-1574.
312. Masaki, A.; Tsunashima, S.; Washida, N. *Chem. Phys. Lett.* **1994**, *218*, 523-528.
313. Plumb, I. C.; Ryan, K. R.; Steven, J. R.; Mulcahy, M. F. R. *J. Phys. Chem.* **1981**, *85*, 3136-3138.
314. Sander, S. P.; Watson, R. T. *J. Phys. Chem.* **1980**, *84*, 1664-1674.
315. Simonaitis, R.; Heicklen, J. *Chem. Phys. Lett.* **1979**, *68*, 245-246.
316. Simonaitis, R.; Heicklen, J. *J. Phys. Chem.* **1981**, *85*, 2946-2949.

317. Villalta, P. W.; Huey, L. G.; Howard, C. J. *J. Phys. Chem.* **1995**, *99*, 12829-12834.
318. Wallington, T. J.; Dagaut, P.; Kurylo, M. J. *Chem. Rev. (Washington, D. C.)* **1992**, *92*, 667-710.
319. Zellner, R.; Fritz, B.; Lorenz, K. *J. Atmos. Chem.* **1986**, *4*, 241-251.
320. King, M. D.; Thompson, K. C. *Atmos. Environ.* **2003**, *37*, 4517-4527.
321. Bacak, A.; Bardwell, M. W.; Raventos, M. T.; Percival, C. J.; Sanchez-Reyna, G.; Shallcross, D. E. *J. Phys. Chem. A* **2004**, *108*, 10681-10687.
322. Pun, B. K.; Seigneur, C.; Grosjean, D.; Saxena, P. *J. Atmos. Chem.* **2000**, *35*, 199-223.
323. Aschmann, S. M.; Tuazon, E. C.; Arey, J.; Atkinson, R. *J. Phys. Chem. A* **2003**, *107*, 2247-2255.
324. Ma, Y.; Willcox, T. R.; Russell, A. T.; Marston, G. *Chem. Comm. (Cambridge)* **2007**, 1328-1330.
325. Rickard, A. R.; Johnson, D.; McGill, C. D.; Marston, G. *J. Phys. Chem. A* **1999**, *103*, 7656-7664.
326. Fick, J.; Pommer, L.; Andersson, B.; Nilsson, C. *Atmos. Environ.* **2002**, *36*, 3299-3308.
327. Baker, J.; Aschmann, S. M.; Arey, J.; Atkinson, R. *Int. J. Chem. Kinet.* **2002**, *34*, 73-85.
328. Winterhalter, R.; Van Dingenen, R.; Larsen, B. R.; Jensen, N. R.; Hjorth, J. *Atmos. Chem. Phys. Discuss.* **2003**, *3*, 1-39.
329. Seuwen, R.; Warneck, P. *Int. J. Chem. Kinet.* **1996**, *28*, 315-332.
330. Wegener, R.; Brauers, T.; Koppmann, R.; Bares, S. R.; Rohrer, F.; Tillmann, R.; Wahner, A.; Hansel, A.; Wisthaler, A. *J. Geophys. Res., [Atmos.]* **2007**, *112*, D13301/1-D13301/17.
331. Anglada, J. M.; Crehuet, R.; Maria Bofill, J. *Chem.--Eur. J.* **1999**, *5*, 1809-1822.
332. Bilde, M.; Orlando, J. J.; Tyndall, G. S.; Wallington, T. J.; Hurley, M. D.; Kaiser, E. W. *J. Phys. Chem. A* **1999**, *103*, 3963-3968.

333. Atkinson, R. *Atmos. Environ.* **2007**, *41*, 8468-8485.
334. Vereecken, L.; Peeters, J. *J. Phys. Chem. A* **2000**, *104*, 11140-11146.
335. Iwahama, T.; Sakaguchi, S.; Ishii, Y. *Chem. Comm. (Cambridge)* **2000**, *23*, 2317-2318.
336. Denisov, E. T.; Shestakov, A. F. *Kinet. Catal.* **2006**, *49*, 1-10.
337. Maranzana, A.; Ghigo, G.; Tonachini, G.; Barker, J. R. *J. Phys. Chem. A* **2008**, *112*, 3656-3665.
338. Tonachini, G.; Maranzana, A. *personal communication*; 2008.
339. Jenkin, M. E. *Atmos. Chem. Phys.* **2004**, *4*, 1741-1757.
340. Hooshiyar, P. A.; Niki, H. *Int. J. Chem. Kinet.* **1995**, *27*, 1197-1206.
341. Dobis, O.; Benson, S. W. *J. Am. Chem. Soc.* **1991**, *113*, 6377-6386.
342. Pilgrim, J. S.; Taatjes, C. A. *J. Phys. Chem. A* **1997**, *101*, 5776-5782.
343. Knyazev, V. D.; Kalinovski, I. J.; Slagle, I. R. *J. Phys. Chem. A* **1999**, *103*, 3216-3221.
344. Kaiser, E. W.; Wallington, T. J. *J. Phys. Chem.* **1996**, *100*, 9788-9793.
345. Kegley-Owen, C. S.; Tyndall, G. S.; Orlando, J. J.; Fried, A. *Int. J. Chem. Kinet.* **1999**, *31*, 766-775.
346. Knyazev, V. D.; Bencsura, A.; Dubinsky, I. A.; Gutman, D.; Melius, C. F.; Senkan, S. M. *J. Phys. Chem.* **1995**, *99*, 230-238.
347. Sortino, S.; Petralia, S.; Foti, M. C. *New J. Chem.* **2003**, *27*, 1563-1567.
348. Bauer, D.; Crowley, J. N.; Moortgat, G. K. *J. Photochem. Photobiol. A* **1992**, *65*, 329-344.
349. Patchen, A. K.; Pennino, M. J.; Elrod, M. J. *J. Phys. Chem. A* **2005**, *109*, 5865-5871.
350. Olkhov, R. V.; Smith, I. W. M. *Phys. Chem. Chem. Phys.* **2003**, *5*, 3436-3442.

351. Zhang, J.; Huff Hartz, K. E.; Pandis, S. N.; Donahue, N. M. *J. Phys. Chem. A* **2006**, *110*, 11053-11063.
352. Atkinson, R.; Baulch, D. L.; Cox, R. A.; Crowley, J. N.; Hampson, R. F.; Hynes, R. G.; Jenkin, M. E.; Rossi, M. J.; Troe, J. *Atmos. Chem. Phys.* **2007**, *7*, 981-1191.